6-26-2015

Examining 3D Printed Antennas For Space Based Applications

Katherine Belvin

Katherine Belvin

Candidate

Electrical and Computer Engineering

Department

This thesis is approved, and it is acceptable in quality and form for publication:

Approved by the Thesis Committee:

Dr. Christos Christodoulou , Chairperson

Dr. Mark Gilmore

Dr. Youssef Tawk

EXAMINING 3D PRINTED ANTENNAS FOR SPACE BASED APPLICATIONS

by

KATHERINE BELVIN

BACHELOR OF SCIENCE, MATHEMATICS, UNIVERSITY OF NEW MEXICO, 2012
BACHELOR OF ARTS, ART, UNIVERSITY OF NEW MEXICO, 2012

THESIS

Submitted in Partial Fulfillment of the
Requirements for the Degree of

Master of Science
Electrical Engineering

The University of New Mexico
Albuquerque, New Mexico

May, 2015

ACKNOWLEDGEMENTS

First I must acknowledge Derek Doyle, without whom this project would not be possible. His guidance and knowledge were an invaluable resource, as he often had creative solutions to problems. In addition, he and AFRL funded the entire project. Most importantly Derek allowed me to research areas that I found interesting, giving me essentially no limitations. In addition to Derek's help, I also received help from my peer and good friend, Chris Woehrle. Working with Chris was a huge motivation, as he is a very hard worker and filled with many creative ideas. Chris introduced me to Derek and helped come up with initial concepts for my research.

My committee is made up of Dr. Christos Christodoulou, Dr. Mark Gilmore and Dr. Youssef Tawk. I would like to acknowledge their willingness to donate their time and expansive knowledge of electromagnetics to my project. I would next like to acknowledge the assistance of my fellow students in the antennas lab, particularly Arjun Gupta and Firas Ayoub. Lastly, I would like to acknowledge my incredible support system made up of friends and family.

EXAMINING 3D PRINTED ANTENNAS FOR SPACE BASED APPLICATIONS

by

Katherine Belvin

B.S., Mathematics, University of New Mexico, 2012

B.A., Art, University of New Mexico, 2012

M.S., Electrical Engineering, University of New Mexico, 2015

ABSTRACT

3D printing is attractive for antenna manufacturing for a few reasons including the ability to make complex designs realizable that may have previously been too costly or unmanufacturable and the ability to build conformal designs. The idea of 3D printing antennas is not new and has been researched in recent years. However the possibility of using 3D printed antennas for space applications has been researched very little.

The harsh space environment makes material selection an important factor in designing for space applications. Depending on location of the orbit of interest, there are several factors that must be considered when dealing with space including, high vacuum, magnetic fields, electromagnetic radiation (UV rays, X- ray, and gamma rays), charged electrons and protons, and extreme temperatures. In this project 3 patch antennas were 3D printed out of ABS for use at 5, 10, 25 GHz. The antennas underwent testing to understand how the 3D printed ABS material would react in a space conditions. The materials were exposed to radiation and vacuum environment in order to simulate space conditions.

Table of Contents

Chapter 1: 3D Printing Antennas

1.1 3D Printing Overview

Additive manufacturing, or 3D printing has been around since the mid 1980's, when stereolithography, one method of printing, was patented [1]. A major driver for growth in this area is the low cost of materials, meaning more affordable prototyping and manufacturing and the ability to create complicated designs that are not possible with subtraction processes. In addition, with the growing popularity of 3D printers, there is also the benefit of quick turn-around time and in-office accessibility.

The basic idea of additive manufacturing is to form objects by layering small cross sectional sheets of material. That is essentially 2D printing over and over again to build up to a 3-dimensional object. Three popular methods of additive manufacturing are selective laser sintering, stereolithography, and fused deposition modeling. Selective laser sintering (SLS) employs the use of a powerful laser to selectively fuse powder particles of material together. Stereolitography (SLA) uses a UV laser to expose sections of a photosensitive polymer. The liquid polymer is solidified after it is exposed to the radiation. Fused deposition modeling (FDM) is the process by which the material is heated to melting and then extruded in its semi-molten state through a narrow opening, the material is then layered to build up the object being printed [1].

3D printers can print in a variety of materials. Shapeways has printers that can print porcelain, wax, several resins, several plastics, flexible plastics, sandstone, and several ceramics [2]. In addition, Shapeways offers prints in different metals including steel and silver. The metallic objects are made in 3 steps using a standard cast process. The object is first printed in wax, and then put in a container and surrounded with plaster.

After the plaster is set, the wax is melted and then the mold is filled with the molten material of choice. The plaster is removed, leaving the metal object in the desired shape. There do exist printers that print metals, such as those from Optomec that can print in steel, titanium, nickel, cobalt, and other engineering alloys [3]. Typically metal printers use selective laser sintering technology to fuse together powdered metal. These printers are not as common as plastic and resin printers, as they come at a much higher price point. The printer used in this project is a Stratsys uPrint SE, this printer uses FDM to form objects out of its own proprietary plastic material, ABS*plus* [4] [5]. A second printer is used, for the radiation-testing portion of the project, operated by the Air Force Research Lab (AFRL). The second printer is an iPro 8000, that utilizes SLA to print in a variety of materials, but is primarily used to print in Accura 55 and ABS [6]. Note that ABS and ABS*plus* are not the same material and do vary in some unknown degree at the chemical level.

1.2 3D Printed Antennas

The concept of 3D printing antennas is attractive for a few reasons including making complex designs realizable that may have previously been too costly or unmanufacturable and the ability to build conformal designs. In addition, 3D printing could also save a lot of time. For example, instead of spending several months in the design phase and then sending off for final fabrication, several prototypes could have been printed and tested in order to aid the design process.

There are inherent difficulties associated with 3D printing antennas. One major issue is the surface roughness of 3D printed materials.

Figure 1-1: Surface of FDM 3D Printed ABS*plus*

It can be seen [Figure 1-1] that the surface of 3D printed ABS*plus* is not smooth, but instead made up of diagonal strips of the material. The material can be baked to its glass transition temperature to create a smoother surface. However because FDM printed surfaces have small gaps, baking the material will cause the printed shape to shrink about 5-10% [7]. So this may not be a good option for precise geometries.

Three-dimensional antennas, such as horns have been 3D printed in metal [8]. However these metallic printers often lack the resolution that the plastic printers possess. In addition, fabricating out of metal loses some of the benefits of 3D printing in plastic such as light material weight and low material costs. However, the horns in this study were found to perform similarly to the corresponding standard horns, assuming the surface roughness was sufficiently smooth.

There do exist 3D printers that can simultaneously print the plastic 3D material and sections of conductive ink, such as the Rabbit Proto [9]. The Rabbit Proto is an add-on for an existing 3D printer. It is an additional print head that can print complex conductive traces. This is ideal for printing precise circuits and buried transmission lines. However, the Rabbit Proto is not compatible with every printer on the market, and if the user isn't tech savvy enough to build the open-source head, there is additional costs involved. To avoid installing and building the head, there do exist complete turnkey printers that print both dielectric material and conductive ink. One commercial example

is the Voxel8, however one of those printers costs about $9000 [10]. There are ways around spending additional money and time on purchasing a printer that can print both dielectric material and conductive ink. The University of Texas, El Paso [7], describes a few additional methods of adding conductivity. One method is to print channels for the conductive lines, and then micro dispensing the conductive paste in liquid form using a SmartPump. Afterward the paste is cured using a diode laser. Another method would be to use an Inkjet printer to print the lines, however the design would be very thin and likely less than a skin depth at low frequencies.

Chapter 2: Parameter Extraction

2.1 Introduction

In order to design an antenna using 3D printed ABS*plus*, the material must first be characterized, that is, measure the permittivity, permeability and loss tangent. There are values supplied by the manufacturer [11], however there is no specified frequency and is likely not at a microwave frequency. It is important to measure these quantities over several frequencies. Obviously it is necessary for design purposes to measure at the operating frequencies, but it is also good to know how the material acts at surrounding frequencies. There are several methods of characterizing materials. This chapter will start with an overview of two such methods for characterizing materials at microwave frequencies and then discuss the set-up and results for both methods.

Readily available dielectric materials are typically characterized at multiple frequencies. In the instance of 3D printed materials the material information is either not readily available, or perhaps has not been measured for several frequencies. This is likely due to the fact that 3D printing is still developing to go beyond prototyping. Generally, the approved frequency range for a dielectric material will be where the material properties are relatively stable. However because ABS*plus* was not created with the purpose of being a dielectric at microwave frequencies, it is very likely that the material properties will not be stable. Therefore, the material will be characterized with two different methods and compared. This project is primarily concerned with testing the feasibility of ABS*plus* for high frequency antennas, and as such the material will be characterized from roughly 200 MHz – 90 GHz.

2.2 Nicolson-Ross-Weir (NRW) Method

The Nicolson-Ross-Weir (NRW) method is a classic technique of complex property extraction from scattering parameters. Nicolson and Ross [12] outline a procedure for obtaining material characteristics in the time domain. Later, Weir [13] expands upon the general measurement set up as well as equations for extraction. The NRW method consists of measuring the scattering parameters (S-parameters) of a transmission line section filled with the material of interest and then solving for the permittivity and permeability of the material analytically. The values derived are the complex permittivity and complex permeability.

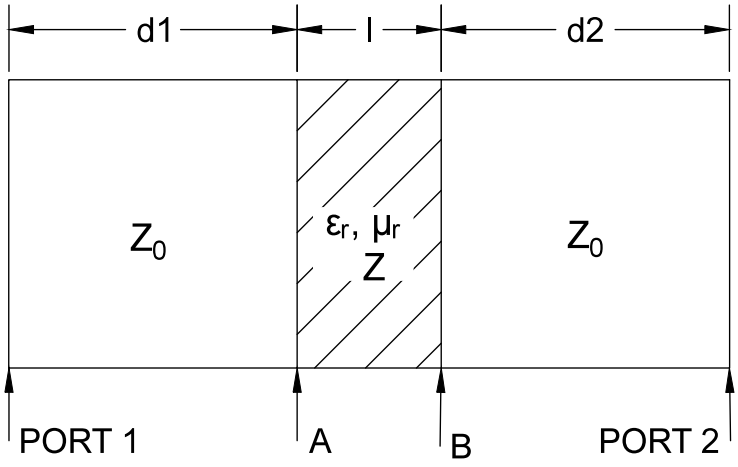

Figure 2-1: NRW Set-Up

The NRW set-up is shown in Figure 2-1, where the material of interest is filled in a transmission line section of length l. Z_0 and Z are the characteristic impedances of each section (air and the material of interest, respectively). Dependent upon calibration method, the calibration plane may not line up with the ends of the sample (planes A and B), but instead with connection planes at Port 1 and Port 2. The S-parameters can be corrected to planes A and B with the following transformation

$$S_{11} = S_{11}e^{j2d_1\beta_0} \tag{2.1}$$

$$S_{12} = S_{12}e^{j2(d_1+d_2)\beta_0} \tag{2.2}$$

$$S_{21} = S_{21}e^{j2(d_1+d_2)\beta_0} \tag{2.3}$$

$$S_{22} = S_{22}e^{j2d_2\beta_0} \tag{2.4}$$

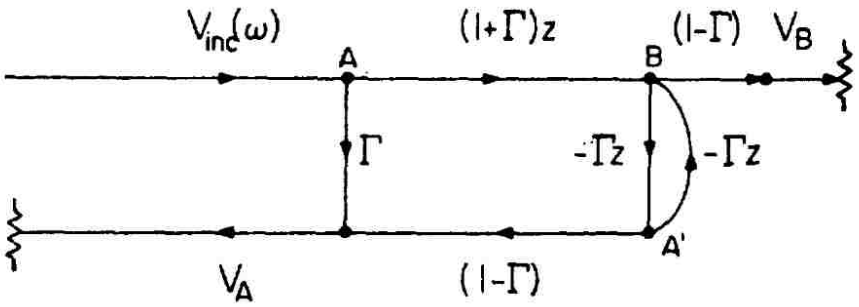

Figure 2-2: Nicolson's Flow Graph [12]

Nicolson's original paper makes use of a signal flow graph [Figure 2-2] to derive the s-parameters of the transmission line by means of functions of reflection and transmission coefficients.

$$S_{11}(\omega) = \frac{V_A}{V_{inc}} = \frac{(1-T^2)\Gamma}{1-\Gamma^2T^2} \tag{2.5}$$

$$S_{21}(\omega) = \frac{V_B}{V_{inc}} = \frac{(1-\Gamma^2)T}{1-\Gamma^2T^2} \tag{2.6}$$

As such, the reflection and transmission coefficient can be written in terms of experimentally obtained s-parameters. First a new variable, X, will be introduced in order to simplify the math involved.

$$\mathrm{X} = \frac{S_{11}^2 - S_{21}^2 + 1}{2S_{11}} \tag{2.7}$$

By combining equations (2.5) through (2.7) , the reflection coefficient can be found in terms of X. After some simplification, Γ can be written as

$$\Gamma = X \pm \sqrt{X^2 - 1} \qquad (2.8)$$

The correct root is chosen by the magnitude of Γ remaining less than 1. Similarly, the transmission coefficient can be found as

$$T = \frac{S_{11} + S_{21} - \Gamma}{1 - (S_{11} + S_{21})\Gamma} \qquad (2.9)$$

The transmission and reflection coefficients, as well as the characteristic impedance are functions of the material's properties. Recall

$$\Gamma = \frac{Z - Z_0}{Z + Z_0} = \frac{\sqrt{\mu_r/\varepsilon_r} - 1}{\sqrt{\mu_r/\varepsilon_r} + 1} \qquad (2.10)$$

$$T = e^{-j(\omega/c)\sqrt{\mu_r \varepsilon_r} l} \qquad (2.11)$$

$$Z = Z_0 \sqrt{\mu_r/\varepsilon_r} \qquad (2.12)$$

Now, combining Equations (2.8) and (2.9) with Equations (2.10), (2.11), and (2.12), the material's permittivity and permeability can be written in terms of the transmission and reflection coefficients; this is best done by introducing two new variables, c_1 and c_2.

$$c_1 = \frac{\mu_r}{\varepsilon_r} = \left(\frac{1+\Gamma}{1-\Gamma}\right)^2 \qquad (2.13)$$

$$c_2 = \mu_r \varepsilon_r = -\left\{\frac{c}{\omega l} \ln\left(\frac{1}{T}\right)\right\}^2 \qquad (2.14)$$

Lastly, the permittivity and permeability can now be written in terms of c_1 and c_2, and as such can be solved with experimentally obtained s-parameters.

$$\mu_r = \sqrt{c_1 c_2} \qquad (2.15)$$

$$\varepsilon_r = \sqrt{\frac{c_2}{c_1}} \tag{2.16}$$

$$\tan\delta = \frac{\Im(\varepsilon_r)}{\Re(\varepsilon_r)} \tag{2.17}$$

The Q-factor can also be solved and is simply the inverse of the loss tangent

$$Q = \frac{1}{\tan\delta} \tag{2.18}$$

The Q-factor determines the selectivity of frequency of the material, the higher the Q-factor the better the frequency selectivity of the material in microwave devices.

It is important to note that Equation (2.14) has an infinite number of roots. Since

$$\ln\left(\frac{1}{T}\right) = j(\theta + 2n\pi) \tag{2.9}$$

where n = 0, ±1, ±2,…,.

This phase ambiguity is the result of the electrical length of the material being a multiple of a half wavelength. The correct value of n must be determined in order for the correct permittivity and permeability values to be obtained. It is possible to correct this ambiguity, as outlined in [14] if the material is known. However, it is not possible to correctly assign an n value to an unknown material. So it is best to make the material samples very thin in order to assume the half-wavelength boundary does not occur within the frequency band of interest.

In order to complete calculations necessary to carry out the NRW method, a MATLAB program was written. The code requires the S-parameters of the material, as

well was the waveguide dimensions and the sample thickness. See Appendix A for the complete code.

2.3 Waveguide Set-Up

In this project, the NRW method was carried out by measuring the S-parameters with a PNA-X utilizing empty waveguides in place of an empty transmission line. So instead of having a transmission line section filled with the material of interest, a waveguide sample holder was filled with the material of interest. The basic set-up of such a measurement is shown in Figure 2-3. The idea is to replace a transmission line with a waveguide, so the calibration planes will be the same as described in Section 2.2. However, one important note to make about using waveguides to take measurements is that the measurement frequencies must correspond to the waveguide frequencies. That is, in order to make measurements in the X-band (8-12 GHz), X-band waveguides must be used.

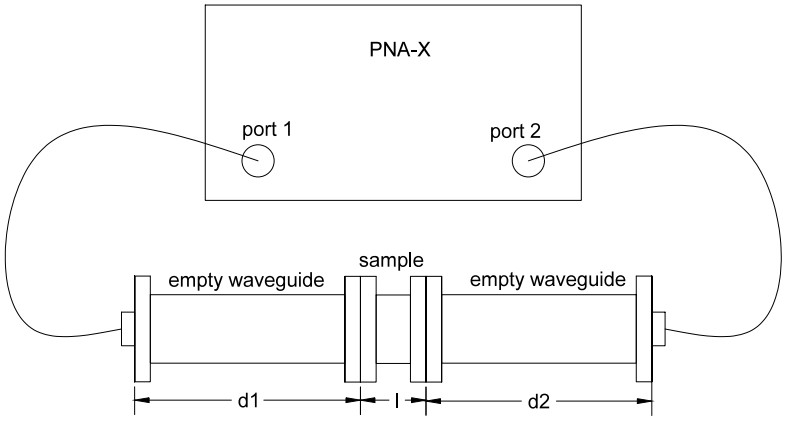

Figure 2-3: Waveguide Measurement Set-up

Calibration of the PNA-X with the waveguide extenders must first be performed before the measurements can be performed. For this experiment the PNA-X was

calibrated with a waveguide calibration kit. There were both E-band (60 – 90 GHz) and Ka-band (26.5 – 40 GHz) waveguides and waveguide calibration kits readily available. As such, ABS*plus* and a few other various materials were characterized for both E and Ka bands. After calibration, the calibration planes were flush with ports A and B, as seen in Figure 2-1. This was achieved by performing a TRL calibration with the waveguides (but not the waveguide sample holder) attached to both ports.

As described in Section 2.2, it is best to keep the material length electrically thin in order to avoid phase ambiguity at multiples of half-wavelengths. The sample holders for this project were constructed out of 0.5 mm copper; so all material samples were 0.5 mm thick. In addition, it is also very important that the material sample fits snugly in the sample holder. If the exact size of the sample is known, it is possible to perform a calculation in order to correct the air gap effects, as described in [15]. However, if a material is not rigid, it is very difficult to get a reliable measurement of the dimensions without squishing the form, and thus changing the measurements. It was determined the sample fit most snugly if the material was cut longer than needed and then cut flush with the sample holder once inserted.

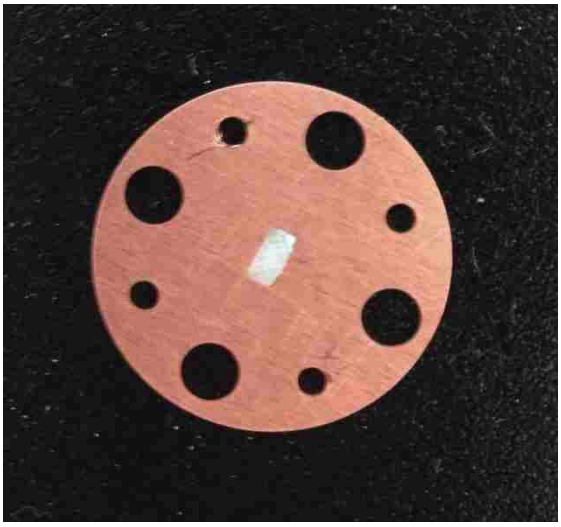

Figure 2-4: ABS*plus* in Waveguide Sample Holder

Materials other than ABS*plus* were characterized for this project in order to serve as controls. It is important to be able to validate experimental results with those obtained by others. This is possible with commercially available materials, such as Rogers. However, there are very few commercially available materials that are rated for the E-band. Therefore, Teflon was chosen to serve as a control material because it is a consistent material that has been characterized for many frequency bands. Teflon was characterized for E-band in [16], the permittivity was found to be 2.05 at 76.5 GHz. For Ka-band, Rogers RO3003, RT5880 and TMM3 were used as the controls and compared to the permittivity given in the specification sheets [17] [18] [19]. Please see Appendix B for a more detailed description of the actual set-up used in this experiment.

2.4 Dielectric Probe

The other method of characterization that will be discussed in the paper is using a dielectric probe, or an open-ended coaxial line probe. The dielectric probe used in this work is located at Sandia National Labs, so many thanks for their collaboration. Dielectric probes are really useful tools because they can characterize materials in a non-

destructive way. That is, the material sample does not need to fit in the waveguide sample holder. In addition to being nondestructive, dielectric probes are also useful for measuring liquids and other materials that may not fit in a sample holder, such as soil. However, the dielectric probe can only measure the permittivity of the material, not the permeability. This is acceptable for this work, since we are primarily interested in antenna design, which does not require the permeability of a material. In this technique, the probe is pressed against the material (or submerged in the liquid) and the reflection coefficient is measured. This measurement is made possible by the probe being attached to a vector network analyzer (VNA). The reflection coefficient is then used to calculate the permittivity of the material. The set up of this method can be seen in Figure 2-5.

Figure 2-5: Dielectric Probe Set-Up

The probe must first be calibrated before measurements can be taken. The calibration algorithm used by the probe is not discussed in the user manual [20]. However there are 3 options for calibration on the machine: air/short/water, load/air/short, and user

defined. The default option is air/short/water, this option is not recommended for low frequency (below 500 MHz) measurements due to the water model not taking ionic effects into account. For this project, the air/short/water calibration will work fine since the frequencies of interest are higher than 500 MHz. The user manual lists the typical accuracies as ±5% and ±0.05 for the dielectric constant and loss tangent, respectively. However, the actual accuracy of the results are dependent upon various factors including the accuracy of the VNA, air gaps between the probe and the material, and the temperature. The probe can operate within the temperature range -40° to +200°C, this project will focus on room temperature measurements.

Although this method of measurement is non-destructive, it does have limitations on the material sizes. This method only works if the material is "infinite" in size relative to the probe and material properties. The user manual gives the following sample size requirements

$$t > \frac{20}{\sqrt{|\varepsilon_r^*|}} mm$$

$$d > 20mm$$

Where t is the material thickness and d is the diameter of the material. The minimum required thickness is dependent upon the material's permittivity. This could potentially be an issue for unknown materials. In the case of ABS*plus*, the material specification sheet [11] listed the permittivity around 2. In order to be conservative, the assumed material permittivity was 1.6, making the minimum required thickness 16 mm. So a 22 x 22 x 17 mm ABS*plus* solid box was printed to measure the permittivity with the dielectric probe.

2.5 Permittivity Measurement Results

The permittivity measurements will be looked at from lowest frequency to highest. This corresponds to looking at the data in the following order: dielectric probe data (200 MHz – 20 GHz), Ka-Band waveguide data (26.5 – 40 GHz), followed by E-band waveguide data (60 – 90 GHz).

ABS*plus* was characterized using the dielectric probe. For this method no additional materials were characterized, as the machine is calibrated to have permittivity error less than or equal to 5%. According to Stratasys [11], ABS*plus* has a dielectric constant between 2.3 and 2.85, however the frequencies of these measurements are not listed. In addition the color of the material is not listed, nor is it specified if the color makes a difference. The dielectric constant of ABS*plus* obtained from the dielectric probe can be seen in Figure 2-6.

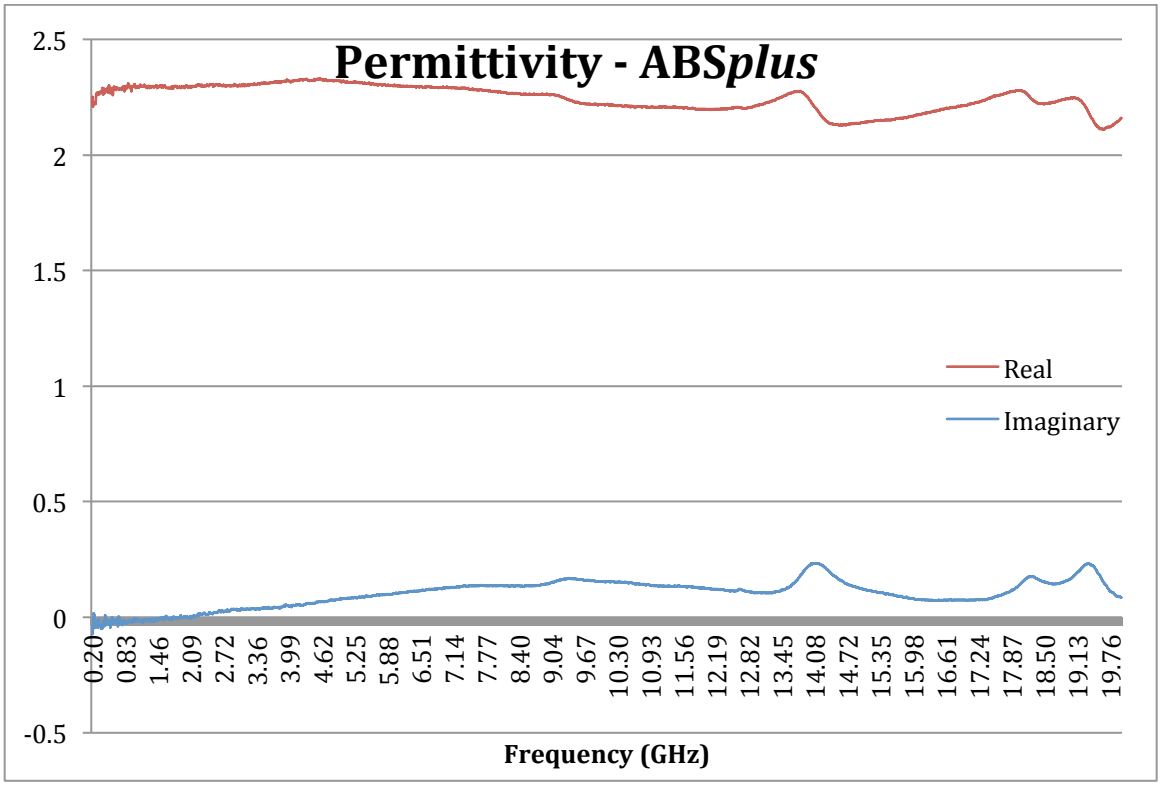

Figure 2-6: Dielectric Constant of ABS*plus* (200 MHz - 20 GHZ)

The manual lists the maximum frequency of the machine at 20 GHz, but also states that the measured permittivity is not accurate at large frequencies. This is dependent upon the material, more specifically

$$f < \frac{110}{\sqrt{|\varepsilon_r^*|}} GHz$$

Using the ABS*plus* specification sheet, this frequency is about 65 GHz, and with the data collected from the probe, about 70 GHz, so the data should be reliable up to the 20 GHz measurable by the dielectric probe. The real permittivity values measured vary from 2.11 to 2.33, the specification sheet states that the values are between 2.3 and 2.85. A value of 2.11 suggests an error of 8%, assuming the actual value is 2.3, this is larger than the typical error value of 5%. This minimum value occurs at 19.7 GHz, however all values at frequencies larger than 19.4 GHz are lower than the 5% accuracy value of 2.185. This could be for a variety of reasons. One reason could be an error with the probe; perhaps its calibration standards are outdated and need to be recertified. Another reason for this error is due to the texture of the 3D printed ABS*plus*, more specifically gaps in-between threads of the material. It's possible that the listed dielectric values on the specification sheet are that of the material, not of the material once it is 3D printed. One final possible reason for the additional error is that the specification sheet measured the dielectric constant at frequencies lower than 20 GHz, as such the value given by the dielectric probe could be within the 5% error for the permittivity at 20 GHz.

The data collected using waveguides and the NRW method was not as easy to understand as that collected from the dielectric probe. The measurements for all of the materials appeared to oscillate, unlike the measurements taken with the dielectric probe,

which were more or less a straight line. The measurements for ABS*plus* seemed to vary dependent upon the sample and the calibration, as can be seen in Figure 2-7.

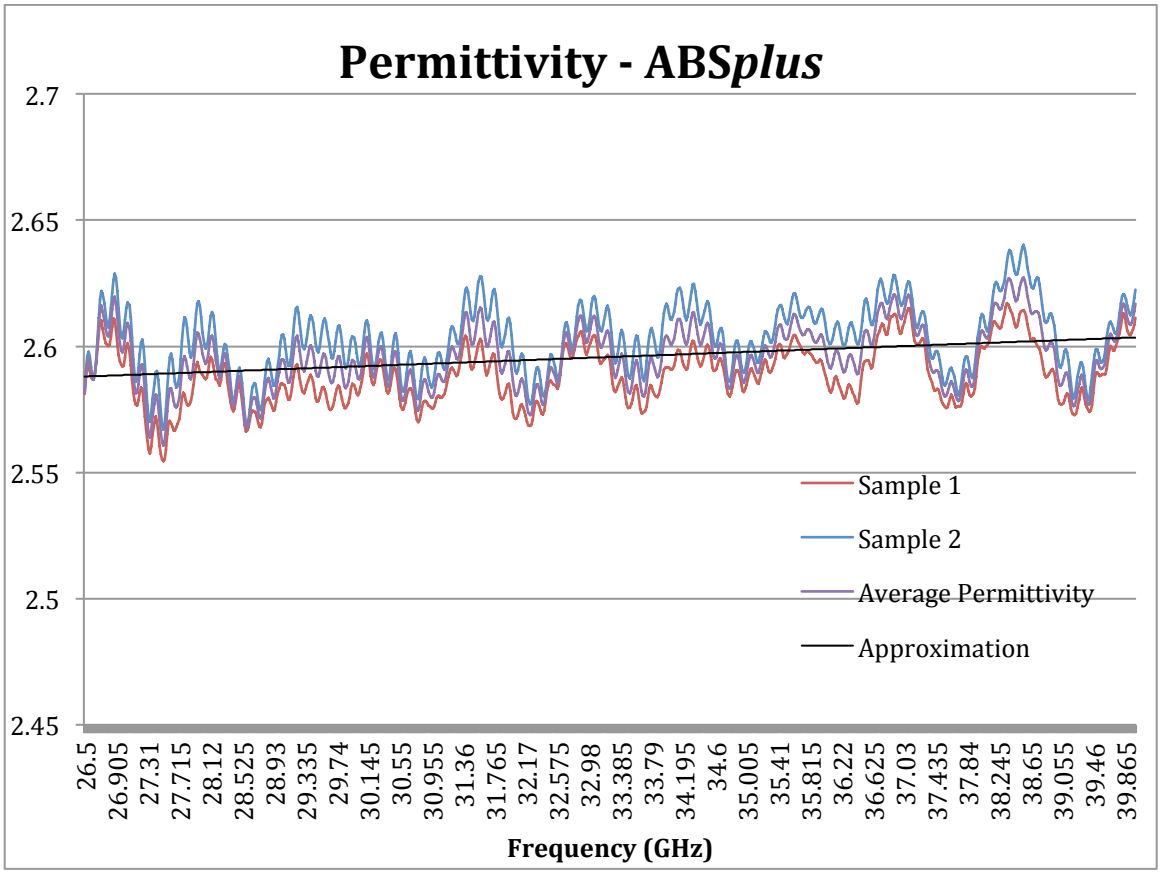

Figure 2-7: Dielectric Constant of ABS*plus* (26.5 - 40 GHz)

In Figure 2-7, the 2 samples measured were measured with different calibrations. The difference between the values at any given frequency can almost be as great as 0.03. The values of the 2 measurements were averaged and can be seen as the purple line in the above chart. The average was then approximated with a few linear approximations in order to minimize the oscillations. This approximation is the black line in the chart above. This is an estimate of the permittivity at the frequencies of interest. However the error in this approximation is unclear, as there is no listed value of dielectric constant of ABS*plus* in the Ka-band.

In the E-band frequency range, there was additional uncertainty, as the difference between samples was typically greater, as can be seen in Figure 2-8. In addition, the E-band samples were very small and particularly difficult to insert in the sample holders. As such, it is very likely that any difference between the dielectric constant of samples was due to the sample not being entirely flush in the sample holder. As stated prior, any air gaps in-between the material and the sample holder changes the measurement, however, this gap becomes much more relevant at these high frequencies. A small air gap, which may not be visible, may be a substantial error because the wavelengths are so small. Because these frequencies are so high, this also makes it difficult to obtain a good calibration of the system. Any dust particles in the system may alter the calibration. So it is also possible that any discrepancy between sample measurements may also be due to calibration error.

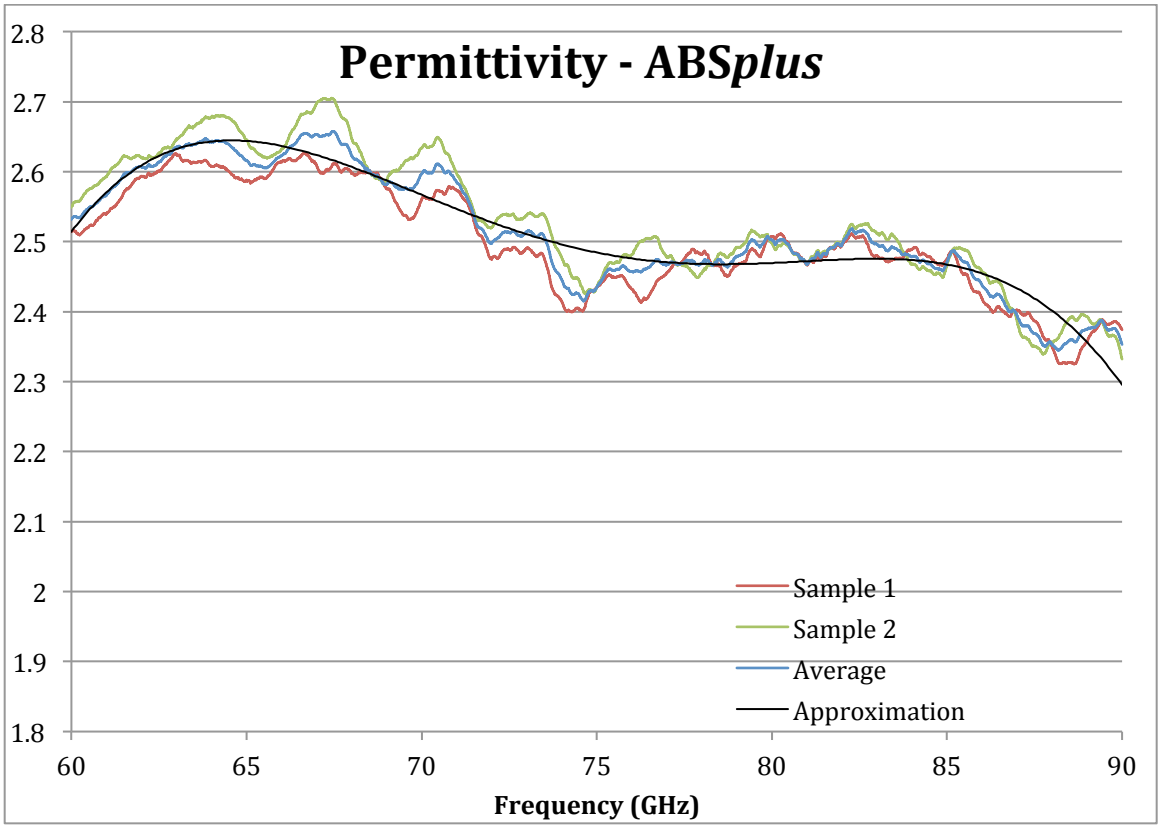

Figure 2-8: Dielectric Constant of ABS*plus* (60 - 90 GHz)

As with the Ka-band data (Figure 2-7), the E-band data was also averaged between the samples (the blue line in Figure 2-8). This average was then approximated. The approximation used was a 4th order polynomial in order to maintain the curvature of the measurements.

A summary of all of the measurements taken of ABS*plus* can be seen in Figure 2-9.

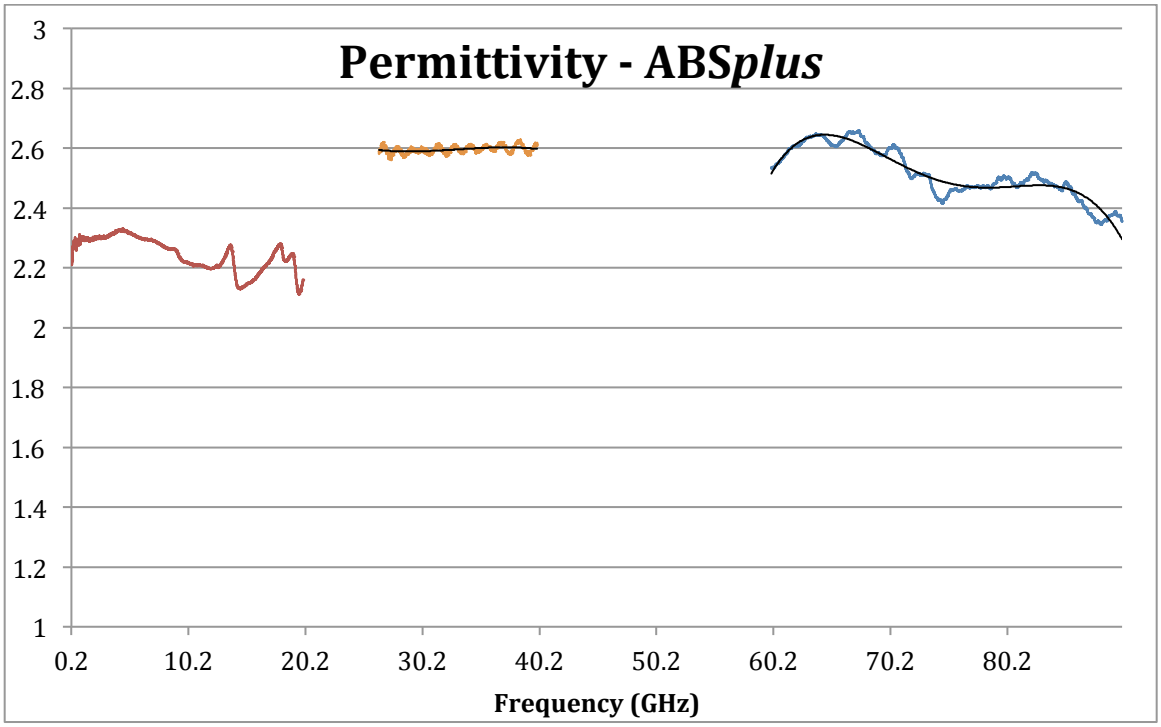

Figure 2-9: Dielectric Constant of ABS*plus* (200 MHz - 90 GHz)

It is apparent that the dielectric constant for ABS*plus* is very stable in the Ka-band range. The measurements are also relatively stable for the dielectric probe. However, the E-band measurements appear to have a "drop off." It is unclear whether this is due to calibration/machine error, or if this is a quality inherent to the material. Either way, the material will not be used for the E-band spectrum in this project.

2.6 Calculated Loss Tangents

The loss was calculated from the real and imaginary permittivity values measured by the dielectric probe. The loss tangent plotted against frequency can be seen in Figure 2-10.

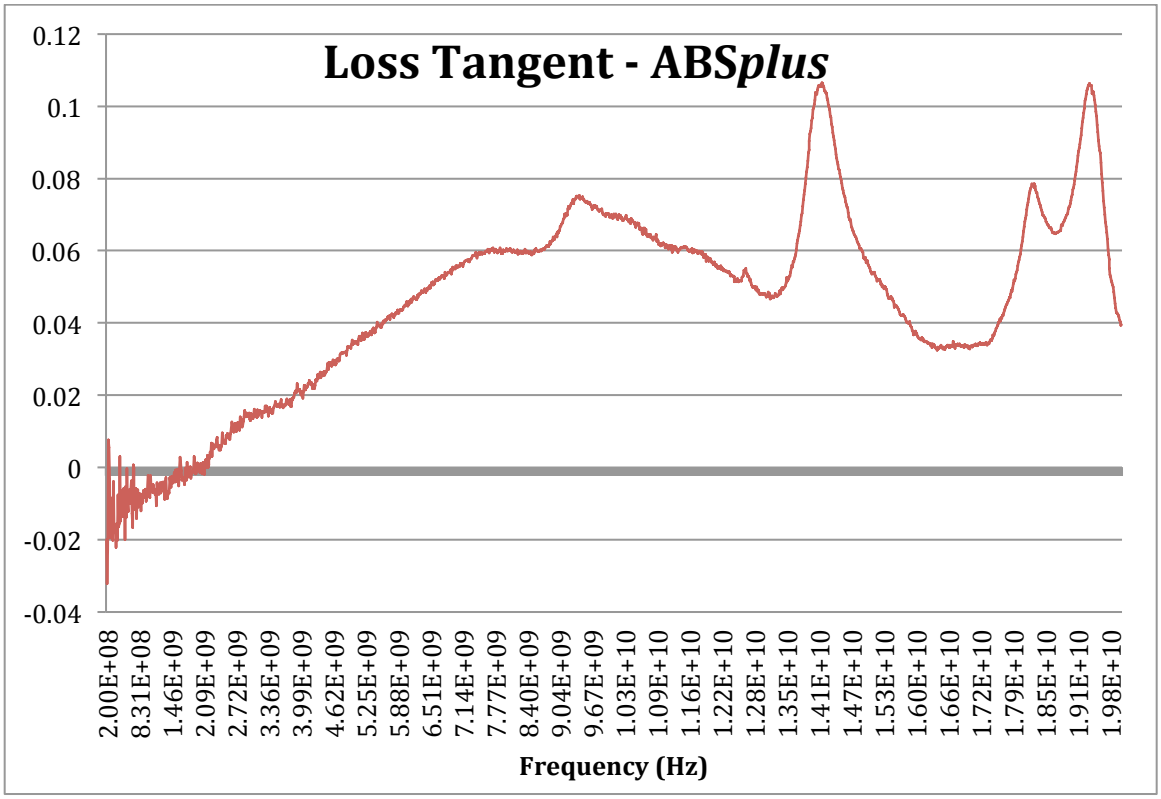

Figure 2-10: Loss Tangent of ABS*plus* (200 MHz - 20 GHz)

As with the dielectric constants, the loss tangents of the measurements taken using waveguides and the NRW method were difficult to determine [Figure 2-11] [Figure 2-12]. The loss tangents also had the oscillations that the permittivity values had. This makes sense since the loss tangent is a function of the dielectric constant. As such, the waveguide measurements for loss were handled the same as the permittivity measurements.

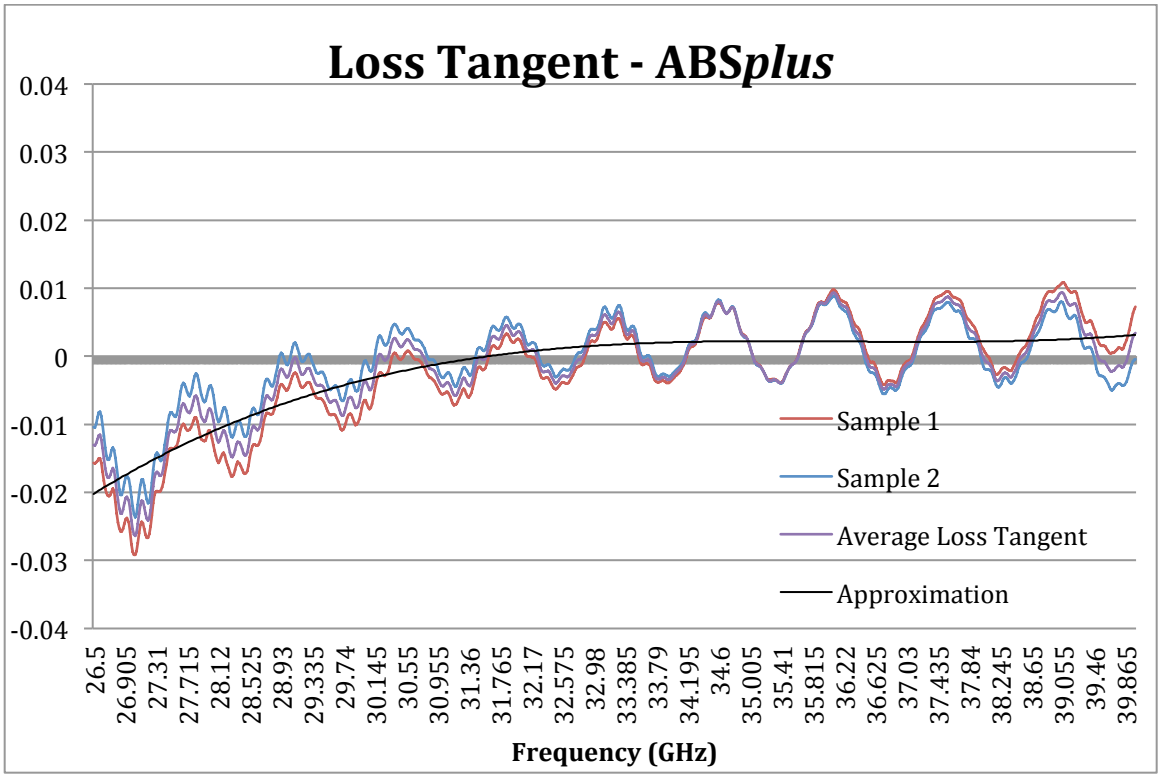

Figure 2-11: Loss Tangent of ABS*plus* (26.5 - 40 GHz)

For the Ka-band, the samples were first averaged (the purple line in Figure 2-11). As with the permittivity, the average was then approximated in order to eliminate the oscillations. Because this loss tangent has a natural curve to it, the approximation was done using a 3rd order polynomial. The black line in Figure 2-11 represents this approximation.

As with the permittivity results, the loss tangent results for E-band were not as clear as those for the Ka-band. The results for the E-band loss tangent also diverged further from each other than those of the Ka-band. This can be seen in Figure 2-12.

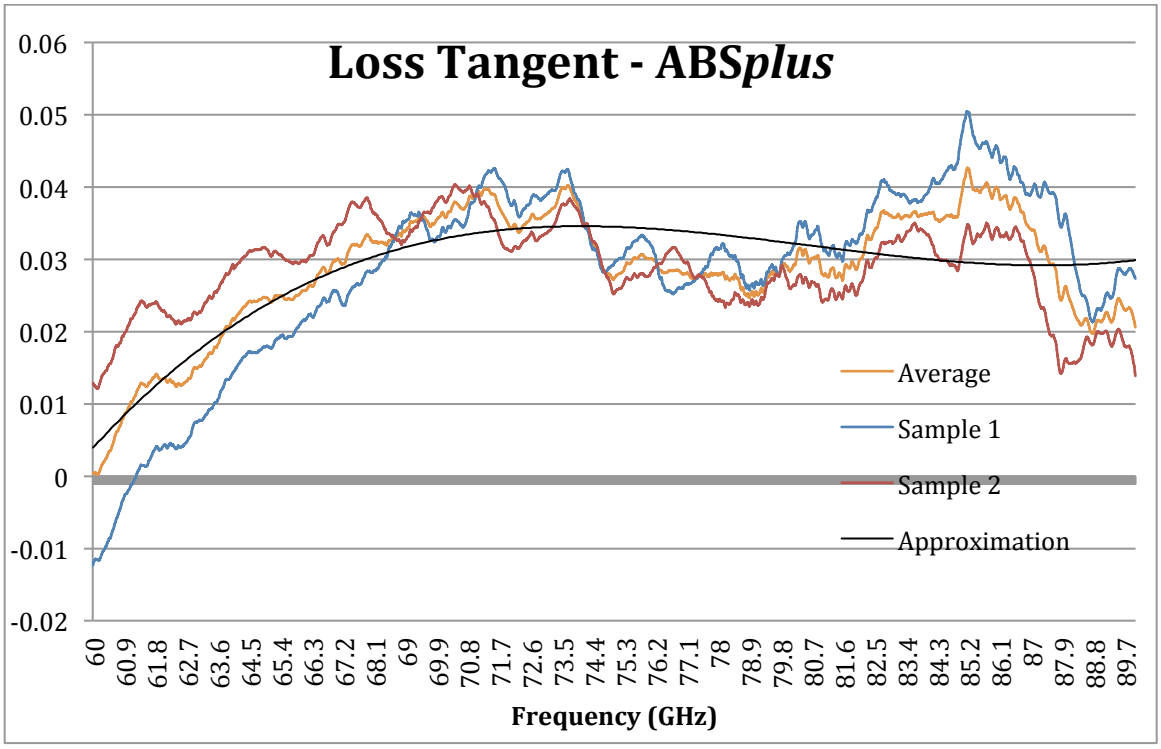

Figure 2-12: Loss Tangent of ABS*plus* (60 - 90 GHz)

The values of the loss tangent were averaged and then the average was then approximated by a 3rd order polynomial. It is unclear if this is a good approximation for the loss tangent of ABS*plus* for the E-band frequencies. Although it is in the middle of the measured values, there is still a great difference between the samples.

All of the calculated loss tangents have some portion of the frequency band in which the value is negative. This, of course, is not physically possible and is an error. It is known that both the dielectric probe as well as the waveguide method have issues with materials with low losses. This measurement can be improved by increasing the PNA sensitivity settings (averaging, number of points, etc.), but would result in substantially longer measurement time, perhaps without better loss tangent measurements [21]. In

addition, the permittivity values are within an acceptable range, making the measurements valid.

2.7 Validation of Waveguide Measurements

As stated prior, waveguide measurements were taken of other materials in order to validate the measurements taken of ABS*plus*. For the Ka-band, Rogers RO3003, Rogers RT5880, and Rogers TMM3 were all measured. The TMM3, RT5880 and RO3003 materials have known dielectric constant in the Ka-band [17] [18] [19]. Each material was measured 2 or 3 times and then the measurement was averaged, as with ABS*plus*. A summary of the measurements can be seen in Figure 2-13.

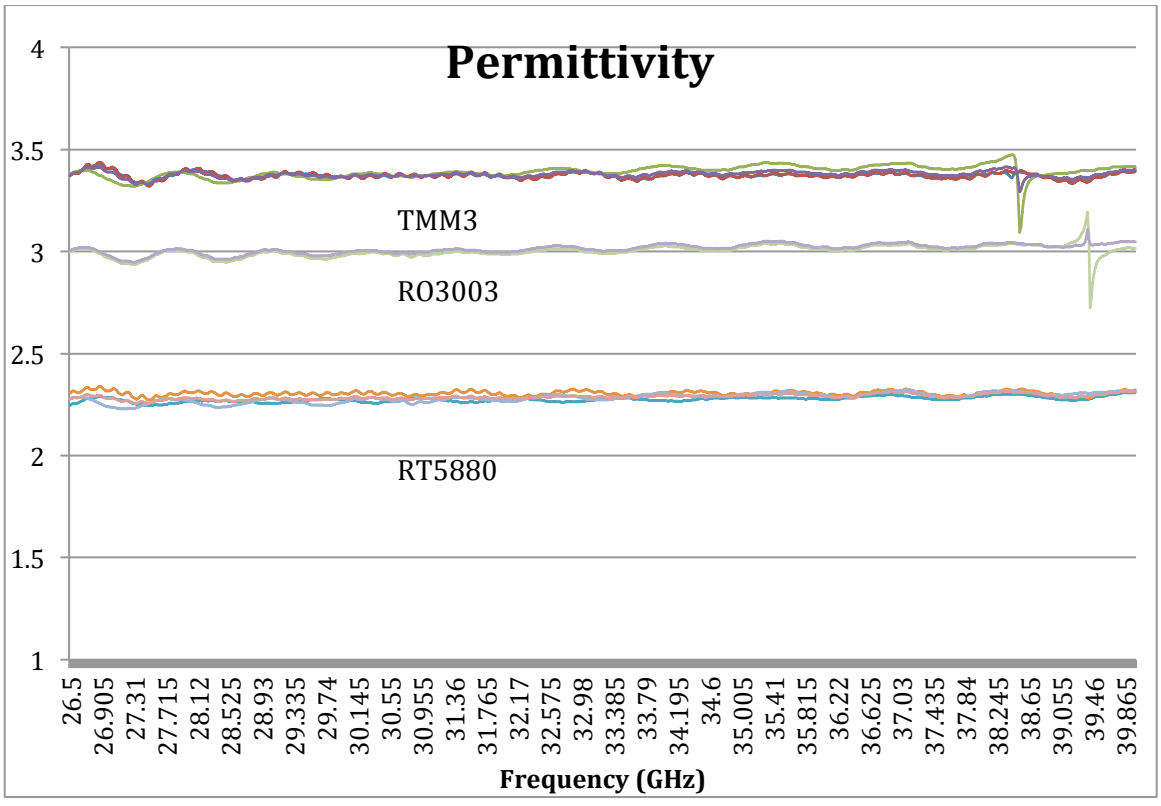

Figure 2-13: Dielectric Constant of Rogers Materials (26.5 - 40 GHz)

According to Rogers, RO3003 has a dielectric constant of 3.00 for 8 – 40 GHz. As can be seen in Figure 2-14, RO3003 oscillates around 3.00 for the majority of the Ka-band.

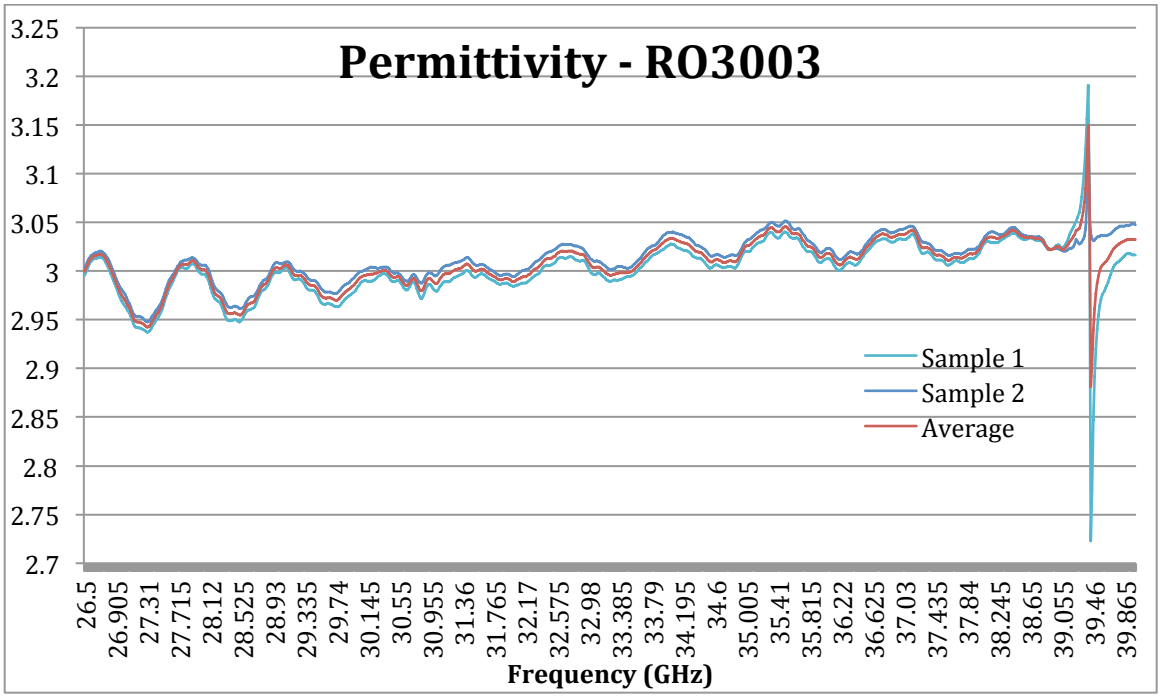

Figure 2-14: Dielectric Constant of Rogers RO3003 (26.5 - 40 GHz)

This is the most accurate of the measurements obtained in this project. The spike near 39 GHz is likely some inherent quality to the material. Although it is rated to 40 GHz, it may not be as well behaved near 40 GHz. The spike may also be due to a calibration error dealing with the system set-up. Each measurement was done on a different calibration, so there would have to be an issue with the system near 40 GHz that affects all calibrations.

Rogers lists TMM3's dielectric constant as 3.45 for 8 – 40 GHz. The results obtained in this project can be seen in Figure 2-15.

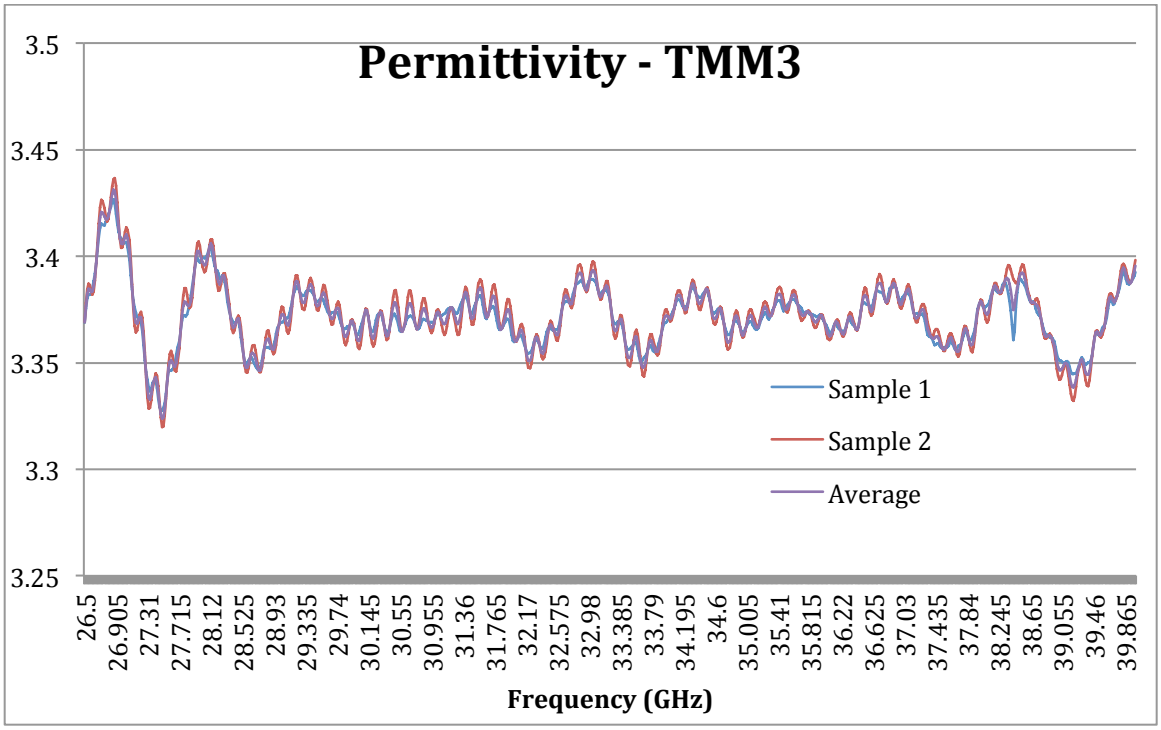

Figure 2-15: Dielectric Constant of Rogers TMM3 (26.5 - 40 GHz)

The measurements obtained are very close to 3.45, but are all shy of 3.45. This could be an issue of again, calibration. However this material was particularly rigid and brittle. This made the material very difficult to cut into the correct size for the sample holder. Even worse, the material was very stiff, so very difficult to insert into the sample holder. There was likely much error due to the sample not fitting completely flush in the holder.

According to Rogers, RT5880 has a dielectric constant of 2.20 for 8 – 40 GHz. The measured dielectric constant can be seen in Figure 2-16.

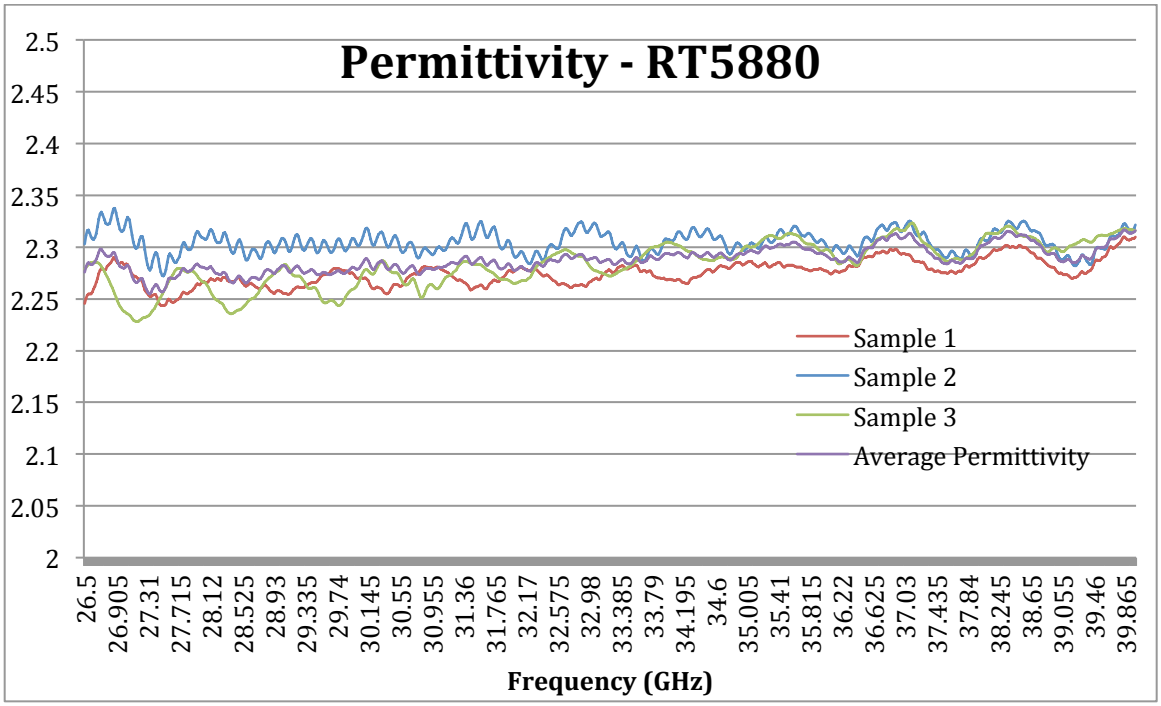

Figure 2-16: Dielectric Constant of RT5880 (26.5 - 40 GHz)

For RT5880 the measured results again did not perfectly match the given dielectric constant values. Another possibility for the measurements not lining up is that it's very likely that RT5880 is not perfectly constant for 8-40 GHz. As such, Rogers just assigned an average or common value of 2.20 for the material. It is possible that this measured data is correct.

For the E-band, Teflon, Rogers RO3003, and Rogers RT5880 were all measured in addition to ABS*plus*. Teflon was measured in a previous study and found to have a dielectric constant of 2.05 at 76.5 GHz [16]. This project found Teflon to have a dielectric constant of 2.10 at 76.5 GHz [Figure 2-17]. The difference between the two results is 0.05, which is very small. This difference could be due to slight differences in calibrations as well as slight differences in the Teflon obtained. In addition, the samples at E-band frequencies are very small, and any error in inserting the samples into the

sample holders could change the results obtained by this amount or more. The found dielectric constant of Teflon for the entire E-band frequency can be seen in Figure 2-17.

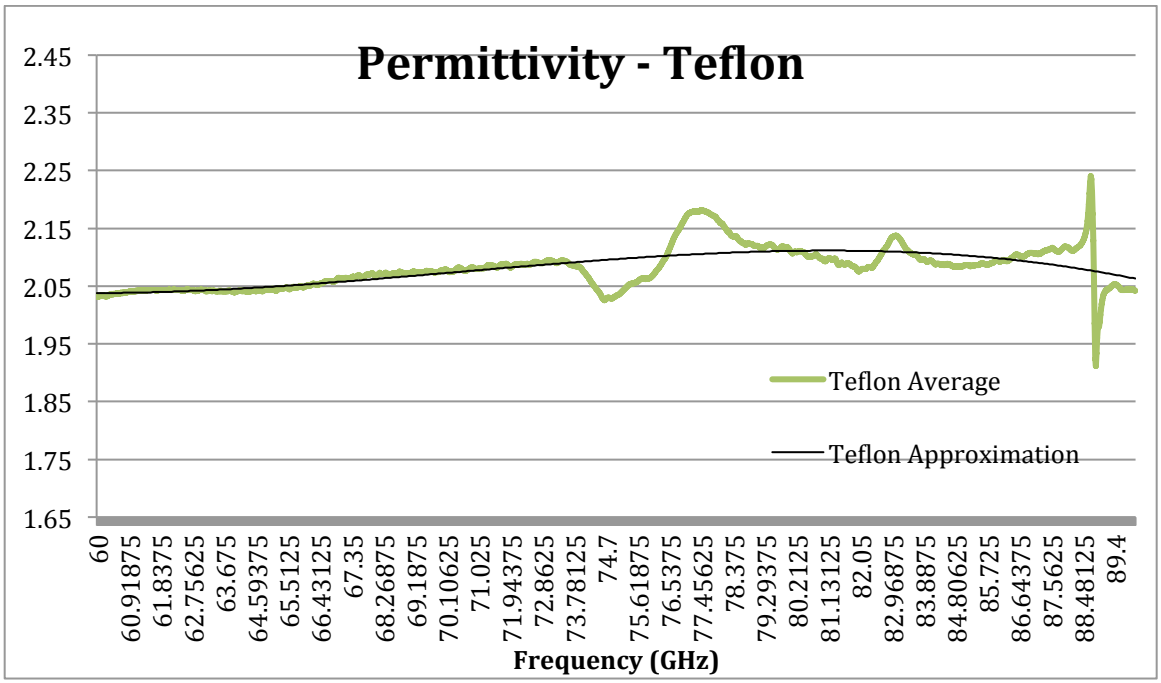

Figure 2-17: Dielectric Constant of Teflon (60 - 90 GHz)

The Rogers materials characterized at E-band frequencies have no other recorded values for comparison. By examining the accuracy of the other materials, it can be said that the dielectric constant obtained for these materials will be relatively close to their actual value. However it is important to remember that this method has its issues, especially at these high frequencies. Mostly dealing with calibration and sample size accuracy. The characterization results of the Rogers materials at E-band frequencies can be seen in Figure 2-18.

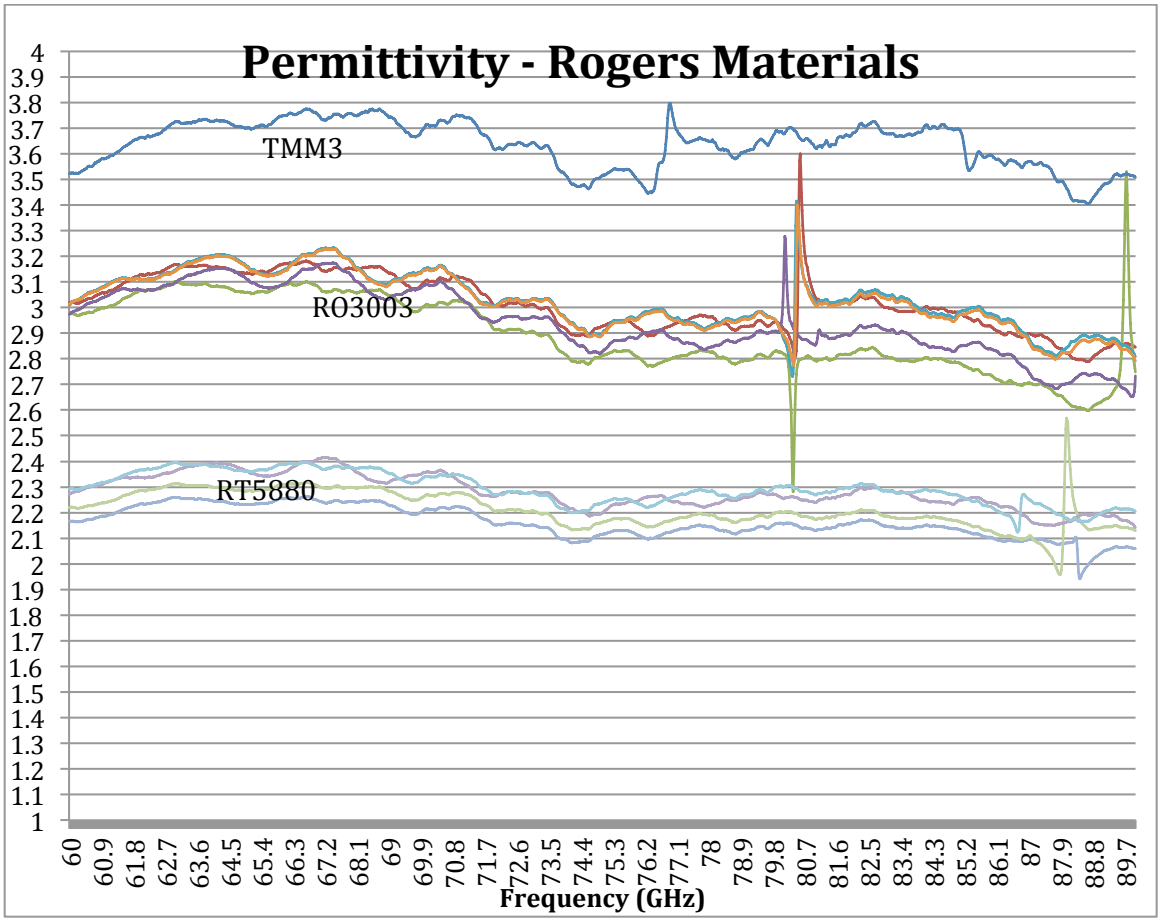

Figure 2-18: Dielectric Constant of Rogers Materials (60 - 90 GHz)

Chapter 3: Antenna Designs

3.1 Purpose

With the material characterized, it is now possible to design an ABSplus antenna for 3D printing. Before an antenna for vacuum testing can be designed, the accuracy of the printer and the method of metalizing the ABS*plus* must be evaluated. Although 3D printing permits for more complication geometry configurations, the main purpose of this study is to examine the feasibility of 3D printing antennas for space applications, as such, a simple antenna design will allow for easier evaluation. The metrics that will be evaluated include physical accuracy and antenna performance repeatability.

3.2 Initial Antenna Design

As a way to examine metallization options and printer accuracy, two pin-fed patch antennas were designed. A rectangular patch antenna was chosen as the design for this project due to its simplicity [Figure 3-1]. The basic geometry of this antenna type allows for a more thorough analysis of 3D printing limitations because the physical dimensions are easily measured. In addition, patches are commonly utilized frequency in space in the form of phased array elements, so this will allow for a more realistic simulation of space vacuum effects on antennas.

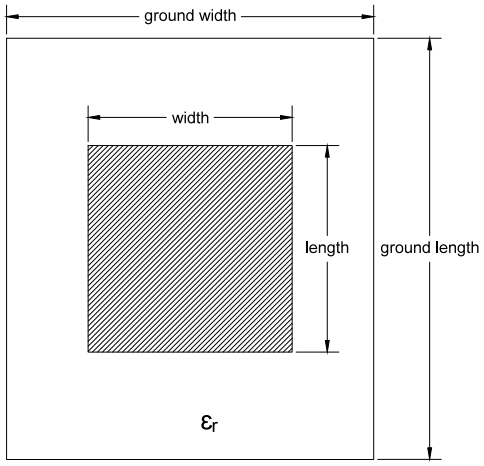

Figure 3-1: Pin-Fed Patch Antenna Design

Before discussing the equations that determine the geometry of patch antennas, it is important to first understand the fringing effects associated with these antennas. The length and width of the patches are finite in length, and as such result in fringing along the edges, as seen in Figure 3-2. The amount of fringing is depended upon the length and width of the patch as well as the height and dielectric constant of the substrate. In the primary E-plane (xy-plane, depending on set-up), the fringing is a function of the ratio of the length of the patch to the height of the substrate and the dielectric constant of the substrate.

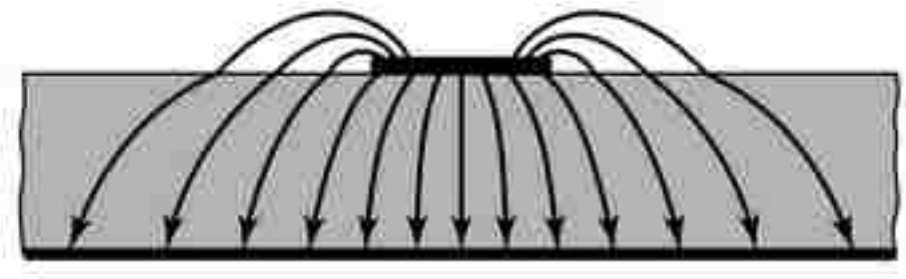

Figure 3-2: Electric Field Lines From Microstrip [22]

The field lines shown in Figure 3-2 lay in two dielectrics (air and the patch substrate), with the majority in the substrate. As the patch width, W, and the patch length, L, increase relative to the substrate height, and as the substrate dielectric constant increases relatively to air, more of the field lines are in the substrate. That is, if $W/h \gg 1$, $L/h \gg 1$, and $\varepsilon_r \gg 1$, then fringing effects are minimized. Because some of the waves travel through air and some travel through the substrate, it is necessary to introduce an effective dielectric constant, ε_{reff}. Using an effective dielectric constant will help account for fringing effects. The same microstrip seen in Figure 3-2 can be redrawn show the effective dielectric constant, as shown in Figure 3-3.

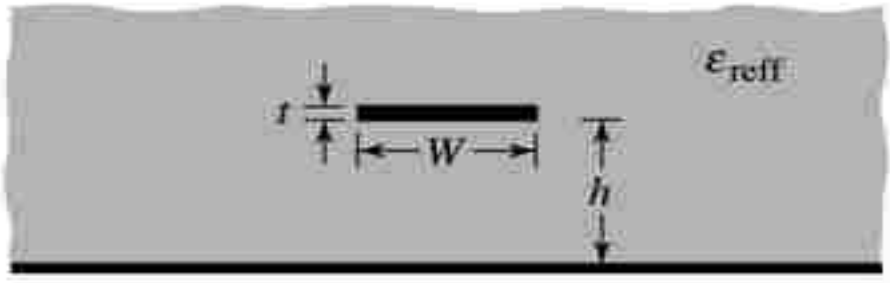

Figure 3-3: Effective Dielectric Constant Model [22]

The effective dielectric constant is constant for low frequencies, but is not for higher frequencies. For higher frequencies, the effective dielectric constant increases until it reaches the value of the substrate's dielectric constant. The initial value of the effective dielectric constant can be calculated with [22]:

$$\varepsilon_{reff} = \frac{\varepsilon_r + 1}{2} + \frac{\varepsilon_r - 1}{2}\left[1 + 12\frac{h}{W}\right]^{-1/2} \qquad (3.1)$$

Of course this is dependent upon the width of the patch, which is given by

$$W = \frac{1}{2f_r\sqrt{\mu_0\varepsilon_0}}\sqrt{\frac{2}{\varepsilon_r + 1}} = \frac{v_0}{2f_r}\sqrt{\frac{2}{\varepsilon_r + 1}} \qquad (3.2)$$

Where ν_0 is the free-space velocity of light, and f_r is the resonant frequency (in Hz).

Due to fringing effects, the patch looks larger than it actually is. In order to account for this in the primary E-plane an effective length is introduced. The effective length is the length of the physical patch plus a difference ΔL on each side of side of the patch, as seen in Figure 3.4.

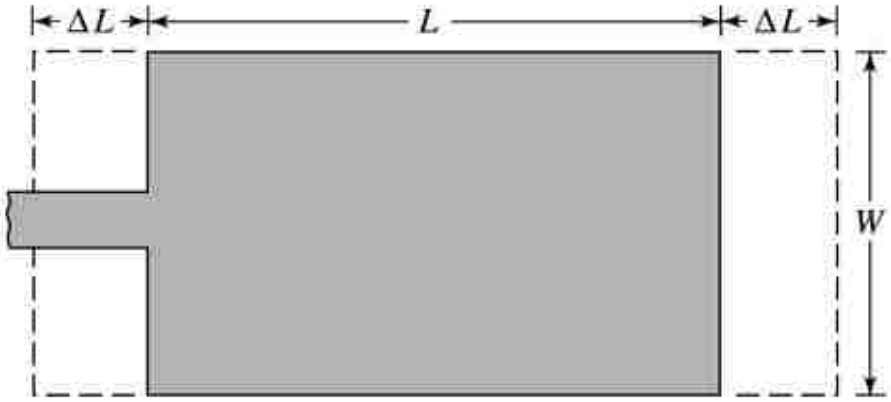

Figure 3-4: Effective Length Of Patch Antenna Compared To Actual Length [22]

The extended length on each side can be approximated by [22]:

$$\frac{\Delta L}{h} = 0.412 \frac{\left(\varepsilon_{reff} + 0.3\right)\left(\frac{W}{h} + 0.264\right)}{\left(\varepsilon_{reff} - 0.258\right)\left(\frac{W}{h} + 0.8\right)} \qquad (3.3)$$

Meaning now the effective length can be computed

$$L_{eff} = L + 2\Delta L \qquad (3.4)$$

For the dominant TM010 mode L is equal to half a wavelength at the resonant frequency. Typically the resonant frequency is a function of the antenna length [22]:

$$(f_r)_{010} = \frac{1}{2L\sqrt{\varepsilon_r}\sqrt{\mu_0\varepsilon_0}} \tag{3.5}$$

However, this equation does not take into account fringing effects. This equation can be modified by using the effective length and effective dielectric constant to take into account fringing [22]:

$$(f_c)_{010} = \frac{1}{2L_{eff}\sqrt{\varepsilon_{reff}}\sqrt{\mu_0\varepsilon_0}} \tag{3.6}$$

Lastly, the actual length of the patch can be determined by solving:

$$L = \frac{1}{2f_r\sqrt{\varepsilon_{reff}}\sqrt{\mu_0\varepsilon_0}} - 2\Delta L \tag{3.7}$$

Using the equations given in Balanis [22] as well as utilizing antenna design tool, Antenna Magus, two patches were designed. The operating frequencies for the antennas were 10 GHz and 25 GHz. Both designs were initially created in Antenna Magus [23] and then exported to the full 3D EM simulator, CST Microwave Studio in order to get accurate simulation results. Both antennas were matched to 50-ohm connections, making the feeding simple, as an SMA connector can be used without a balun.

The initial design for 25 GHz operation had a very small ground plane (about 7 x 7 mm), which would be acceptable for traditional materials, as most milling machines should have no issues with that resolution. However, because the purpose of these initial antenna designs is to test the feasibility of 3D printing antennas, including different methods of metallization, it was best to extend the ground plane to 13 x 13 mm, making the antenna much easier to physically handle. Patch antennas are known for a narrow bandwidth, so this could potentially be an issue for some applications, but useful for secure communications. The bandwidth of the antenna can be increased to an extent by

increasing the height of the substrate. However as the height of the substrate is increased, surface waves are introduced which extract power available for radiation [22]. The height of the substrate used is typically much smaller than λ_0 (usually $0.003\ \lambda_0 \leq h \leq 0.05\ \lambda_0$). A narrower bandwidth can also be a nonissue for some applications where they are typically employed due to their narrow bandwidth, such as secure communications.

The thickness of the dielectric (ABS*plus* in this case) was determined by the limitations of the printer. The minimum layer thickness of the Stratasys uPrint SE printer is 0.254 mm, meaning that the thickness of any print will be a multiple of 0.254 mm. However, with ABS*plus* the layer thickness compatability is 0.330 mm, this is a limitation of the material, not the printer. As such, the 10 GHz patch was designed with 0.990 mm of ABS*plus* (3 layers) and the 25 GHz patch was designed with 0.660 mm of ABS*plus* (2 layers). In order to keep the correct dimensions and placement of the conductive part of the antenna, the conduct part was printed recessed into the dielectric. So this made it important to have the ABS*plus* dielectric be at least 2 layers thick.

3.3 Printer Accuracy

A major concern with 3D printing antennas is the accuracy of the printer being used, and how that affects the antenna performance. Each of the 2 initial antenna designs were printed 15 times (5 per printing pack) in order to have several samples to compare the printed physical dimensions to the dimensions of the original design. The 3D printed antenna designs can be seen in Figure 3-5 and Figure 3-6.

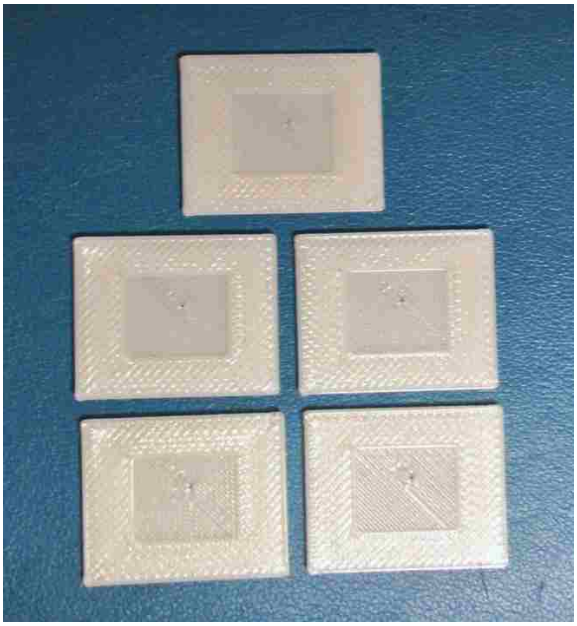

Figure 3-5: Printed 10 GHz Antennas

Figure 3-6: Printed 25 GHz Antennas

The ground plane lengths, widths and depths of all of the antenna prints were measured using a digital caliper. The patch length and widths were not measured, as it was difficult to get an accurate and repeatable measurement since it was an inner dimension. The caliper used has an accuracy of ±0.03 mm, so the measurements taken could be 0.03 mm lower or higher than recorded. Once all of the antennas were sized, the measurements taken were compared to the measurements of the design sent to the printer. The modes

and means of the differences were calculated. These results can be seen in Figure 3-7 and Figure 3-8.

10 GHz Antenna						
Antenna	Length		Width		Depth	
	Actual (mm)	Difference (mm)	Actual (mm)	Difference (mm)	Actual (mm)	Difference (mm)
Design	22.66		17.99		0.99	
1A	22.72	0.06	18.04	0.05	0.90	-0.09
1B	22.75	0.09	18.05	0.06	0.91	-0.08
1C	22.70	0.04	18.00	0.01	0.89	-0.10
1D	22.69	0.03	17.99	0.00	0.91	-0.08
1E	22.82	0.16	18.03	0.04	0.90	-0.09
3A	22.92	0.26	18.04	0.05	0.89	-0.10
3B	22.71	0.05	18.02	0.03	0.90	-0.09
3C	22.76	0.10	18.06	0.07	0.90	-0.09
3D	22.80	0.14	18.04	0.05	0.91	-0.08
3E	22.76	0.10	18.03	0.04	0.89	-0.10
5A	22.73	0.07	18.02	0.03	0.89	-0.10
5B	22.72	0.06	18.08	0.09	0.89	-0.10
5C	22.71	0.05	18.10	0.11	0.89	-0.10
5D	22.66	0.00	18.07	0.08	0.89	-0.10
5E	22.71	0.05	17.99	0.00	0.88	-0.11
Average:		**0.08**		**0.05**		**-0.09**
Mode:		**0.05**		**0.05**		**-0.10**
Maximum:		**0.26**		**0.11**		**0.11**
Minimum:		**0.00**		**0.00**		**0.08**

Figure 3-7: Physical Measurements of 10 GHz Antennas

The largest difference observed between the design and the prints of the 10 GHz antenna was 0.26 mm [Figure 3-7]. This difference corresponds to a 1.15% error.

25 GHz Antenna						
Antenna	Length		Width		Depth	
	Actual (mm)	Difference (mm)	Actual (mm)	Difference (mm)	Actual (mm)	Difference (mm)
Design	13.00		13.00		0.66	
2A	13.11	0.11	13.07	0.07	0.63	-0.03
2B	13.07	0.07	13.08	0.08	0.62	-0.04
2C	13.11	0.11	13.04	0.04	0.62	-0.04
2D	13.09	0.09	13.08	0.08	0.63	-0.03
2E	13.08	0.08	13.04	0.04	0.62	-0.04
4A	13.11	0.11	13.08	0.08	0.63	-0.03
4B	13.10	0.10	13.10	0.10	0.63	-0.03
4C	13.12	0.12	13.07	0.07	0.62	-0.04
4D	13.10	0.10	13.04	0.04	0.63	-0.03
4E	13.08	0.08	13.07	0.07	0.62	-0.04
6A	13.03	0.03	13.03	0.03	0.63	-0.03
6B	13.07	0.07	13.03	0.03	0.65	-0.01
6C	13.08	0.08	13.05	0.05	0.63	-0.03
6D	13.10	0.10	13.07	0.07	0.65	-0.01
6E	13.07	0.07	13.03	0.03	0.62	-0.04
	Average:	**0.09**		**0.06**		**-0.03**
	Mode:	**0.11**		**0.07**		**-0.03**
	Maximum:	**0.12**		**0.10**		**0.04**
	Minimum:	**0.03**		**0.03**		**0.01**

Figure 3-8: Physical Measurements of 25 GHz Antennas

The largest observed difference between the design and the prints of the 25 GHz antenna was 0.12 mm. [Figure 3-8], this is a smaller value than that observed for the 10 GHz antenna. This corresponds to a 0.92% error, which is also less than that of the 10 GHz antenna.

It is also important to note that the hole from the patch to the ground plane used for feeding the antenna was not printed consistently. In the initial round of prints, the hole was specified as 0.09 mm in the design, however only a few had the hole completely formed. In most of the prints there was an irregularity in the patch where the hole should go, as shown in Figure 3-9.

Figure 3-9: Antennas with irregularities instead of holes

Because of this irregularity, the hole diameter was then increased to the printer tolerance value, 0.4064 mm. The increase in diameter was not enough for the printer to consistently print the hole in each antenna. As such, the third batch of antennas was sent to the printer without holes in the design at all. It would still be possible to correctly place the hole by lining up the antenna up with one of the other antennas with the hole printed on it. It is essential that the hole be in the correct position, as this directly affects the impedance of the feed.

The antenna designs were rerun in CST Microwave Studio with the maximum differences observed on the prints in order to better understand how these seemingly small measurement differences will affect the performance of the antenna. Assuming a worst-case scenario, the antenna parameters were swept by their maximum divergence (±0.26 mm for 10 GHz and ±0.12 mm for 25 GHz). The parameters swept were the ground plane length, the ground plane width, the patch width, and the patch length. Even though the path widths and lengths were not physically measured, it can be assumed that the patch dimensions of the prints were different than that of the design. It is essential to sweep the patch dimensions in CST because they greatly affect the resonant frequency of the antenna. So in order to consider the worst-case scenario, the patch measurements

were also swept by the maximum measured divergence (±0.26 mm for 10 GHz and ±0.12 mm for 25 GHz). In the designs it was assume that the hole for the pin was placed in the same spot every time, and did not move. This would assume zero human error; since the holes were drilled by hand it is very likely that the holes are not perfectly placed. This was not taken into consideration for the simulations, as the pin placement greatly affects the impedance of the antenna and an incorrectly placed pin may make the antenna nonfunctional with a 50-Ohm connector.

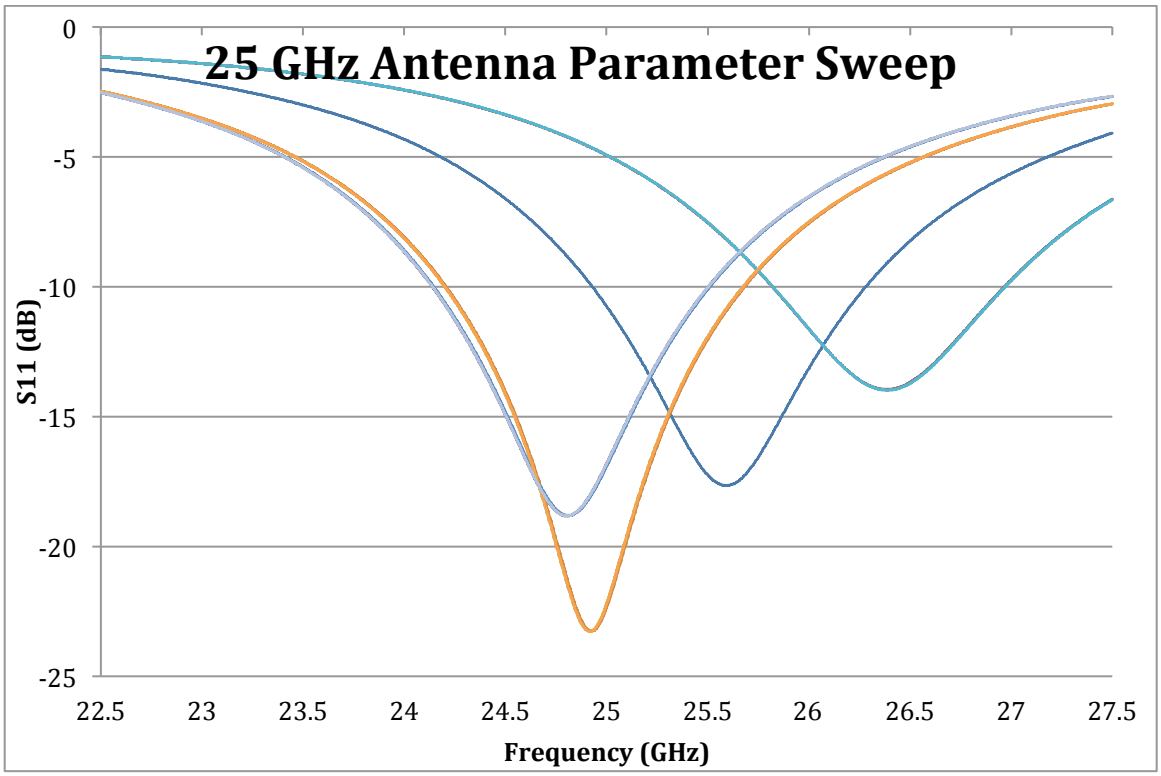

Figure 3-10: Parameter Sweep on 25 GHz Antenna Design

The sweep on the 25 GHz antenna [Figure 3-10] shows that the patch size is very important to the resonant frequency. Even just changed by 0.12 mm, the frequency can shift up to 1.5 GHz, a huge amount for a narrowband antenna like a patch. This is a risk inherent to printing antennas, and as such 3D printing may not be a viable solution for all

antenna designs, such as this one. These results indicate that there will be differences between the printed 25 GHz antenna's resonant frequencies. As such, it is best to make the next antenna design a lower frequency.

3.4 Adding Conductivity

With the antennas now printed, they must be metalized in order to be functional antennas. There do exist 3D printers that can simultaneously print the plastic material and the conductive ink, which would be useful for transmission lines. However this was not an option for this project, so other options were explored. Staying with the same idea of conductive ink, conductive paint was one of the methods of metallization used. Some of the benefits of using conductive paint include the flexibility, ability to apply without special equipment and quick application. For this project the conductive paint selected was MG Silver Print, although there is a large variety of conduct paints available. With paint any section of the printed antenna can be made conductive, no matter how small or awkwardly shaped. In addition, the paint dries quickly, after about 5 minutes to touch, and fully dried within 24 hours at room temperature [24]. However, it is difficult to apply the paint evenly without special equipment, as it does dry quickly. The thickness of the paint does change the sheet resistivity of the paint [24], making it important. Likewise, surface roughness also affects the conductivity of the surface [25], and can also degrade the electromagnetic performance [8].

Although the paint can be applied to any area, it is fairly difficult to control the location and thickness of paint application. For this project painter's tape was applied to the areas of the antennas that were to remain nonconductive. Applying the painter's tape

was time intensive and not exact. That is, it was impossible to insure that the physical dimensions of the conductive patches were exact.

In addition to conductive ink, some antennas were metallized using copper tape. Copper tape was chosen because it is a consistent thickness, unlike the conductive paint. Antennas metallized with copper tape will serve as a control, highlighting the effects of painting the surface. Some benefits of using copper tape include easy application, no curing time, and again no special equipment needed. However, the accuracy of the size of the conductive patch is limited to how accurately the tape can be cut out. To help aid in accuracy, stencils of the antenna patches were printed so that the tape could be cut to fit. However, applying the tape was not very accurate, as it was applied by hand.

3.5 Measuring Resistivity: 4-Point Probe Method

It is necessary to measure the conductivity of the metals to be used for the antennas in order to accurately compare the constructed antennas to the simulated antennas. Typically electromagnetic simulators use perfect electric conductors (PEC's) for the conductive portions of antennas by default. The conductivity value can be changed to simulate how the antenna would perform once actually constructed. For example, if the antenna were to be constructed out of commercially available dielectric material, such as one Rogers, that is copper cladded (0.018 mm or 0.035 mm thick, electrodeposited), the conductivity value in CST can be changed to that of the Rogers' listed value [26]. Therefore, to change the resistivity value in the simulations of these copper taped and painted antennas, it is necessary to measure the resistivity values of the copper tape and various thicknesses of the paint.

A four-point probe was used to measure the resistivity of the materials of interest for this project. This is a very common and simple way to measure the resistivity of a material, particularly useful for low resistance materials. The model used in this project is the Jandel RM3, and it uses four collinear probes. In this method, the four probes are equally spaced into a linear array. The two outer probes are used to source current and the two inner probes are used to measure the voltage. The probe array is usually placed in the center of the material, as seen in Figure 3-11.

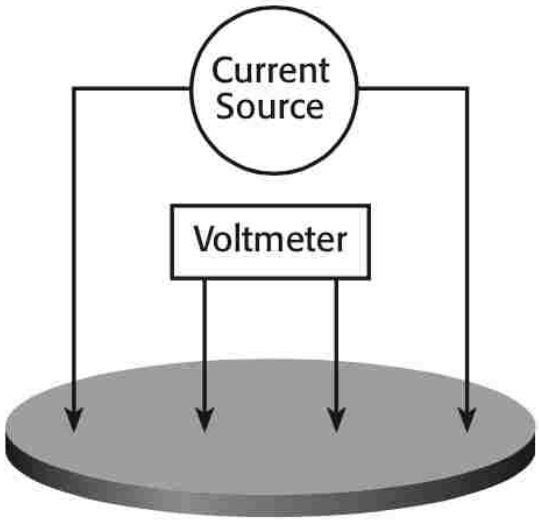

Figure 3-11: Four-Point Collinear Probe Method [27]

The two inner probes measure the resulting voltage drop across the sample. The probe system then uses this voltage drop to calculate the surface resistivity.

$$R_s = \frac{\pi}{\ln 2}\frac{V}{I} \qquad (3.8)$$

Where V is the measured voltage in volts and I is the source current in amperes. This equation is derived by finding the differential resistance given by the area of the conductor. The differential resistance can be solved with the following integral

$$R = \int_{x_1}^{x_2} R_s \frac{1}{2\pi x} \partial x \qquad (3.9)$$

Resistance is given by

$$R = \frac{V}{2I} \qquad (3.10)$$

By substituting Equation (3.10) into Equation (3.9), Equation (3.8) can be obtained.

It is important to note the difference between sheet or surface resistance and volume or bulk resistance. The units of sheet resistance is usually **Ω/□** (ohms per square), this unit is used if the thickness of the conductive material is unknown. Bulk or volume resistance is a constant unit of measure, unlike sheet resistance, which varies with respect to thickness. Bulk resistance measurements can be used to compare different materials. The unit of bulk resistance is **Ω□** m, and is the inverse of the unit of conductivity, S/m. To solve for bulk resistance, the sheet resistance is multiplied by the thickness of the conductive material.

$$\rho = \frac{\pi}{\ln 2} \frac{V}{I} t = R_s t \qquad (3.11)$$

This volume resistivity can be used to solve for conductivity

$$\sigma = \frac{1}{\rho} \qquad (3.12)$$

For this project a 3D printed surface coated in copper tape, a piece of copper tape still attached to the backing, and five MG Silver Print coated 3D-surfaces' resistivities were measured using a 4-point probe. The 3D printed surfaces were some of the antennas printed earlier for the printer reliability measurements. One of the 25 GHz antennas was painted with 1 coat of conductive paint, while one of each of the two antenna types were painted with 2 and 3 coats of paint. Both antennas were used in these

measurements to see if there would be any difference in paint application due to increased surface area. There was indeed a difference in paint application between the two antenna sizes. The 25 GHz antennas were smaller, and therefore difficult to paint, however, it was much easier to obtain a smooth coat, as it only took 2 or 3 brush strokes to cover the entire surface. The 10 GHz antennas were larger and easier to handle, however the increased surface area resulted in more brush strokes, and therefore less even of a painted surface. The 10 GHz antenna was not represented in the 1 coat of paint measurement, as there were no samples with a smooth enough application after 1 coat of paint. In order to check the reliability of the calibration and methodology, a sheet of copper clad Rogers dielectric (0.035 mm cladding) was also measured.

Sample	Voltage	Sheet Resistance	Material Thickness	Bulk Resistance	Conductivity
	mV	mΩ/□	mm	Ω□m	S/m
Rogers	0.003	0.3	0.035	1.05E-08	9.52E+07
Copper Tape	0.005	0.5	0.01	5.00E-09	2.00E+08
3C (Taped)	0.004	0.5	0.01	5.00E-09	2.00E+08
2C (1 coat)	0.788	72.0	0.040	2.88E-06	3.47E+05
1C (2 coats)	0.43	39.0	0.090	3.51E-06	2.85E+05
2E (2 coats)	0.40	37.0	0.060	2.22E-06	4.50E+05
1A (3 coats)	0.35	30.0	0.170	5.10E-06	1.96E+05
2A (3 coats)	0.30	30.0	0.130	3.90E-06	2.56E+05

Figure 3-12: Measured Resistance and Conductivity Values

The data measured can be seen in Figure 3-12, however it does not give values expected. Rogers lists the value of the copper cladding bulk resistivity as 2 μΩ cm [26], which is not the value obtained by the 4-point probe. In order to obtain more realistic values, a correction factor was applied to all of the measurements and can be seen in Figure 3-13.

Sample	Voltage	Corrected Sheet Resistance	Material Thickness	Corrected Bulk Resistance	Corrected Conductivity
	mV	mΩ/□	mm	Ω□m	S/m
Rogers	0.003	0.57	0.035	2.00E-08	5.01E+07
Copper Tape	0.005	0.95	0.01	9.50E-09	1.05E+08
3C (Taped)	0.004	0.95	0.01	9.50E-09	1.05E+08
2C (1 coat)	0.788	136.8	0.04	5.47E-06	1.83E+05
1C (2 coats)	0.43	74.10	0.09	6.67E-06	1.50E+05
2E (2 coats)	0.40	70.30	0.06	4.22E-06	2.37E+05
1A (3 coats)	0.35	57.00	0.17	9.69E-06	1.03E+05
2A (3 coats)	0.30	57.00	0.13	7.41E-06	1.35E+05

Figure 3-13: Conductivity Values With Correction Factor Applied

With the correction factor, it can be noted that 3 of the painted samples now exceed the manufacturer's sheet resistance value of less than 66 mΩ/□. Whereas, without the correction factor, only one of the painted samples exceeded the manufacturer given value. The correction factor did not change much in the final conductivity values of the conductive paint. Perhaps the value listed by Rogers was a not to exceed value, and really just an upper limit. This would make sense because the paint values match the manufacturer's values better without the correction factor.

It can be seen that all corrected values of the painted samples' conductivity are in the same order of magnitude, varying between 1.03 and 2.37. Likewise without the correction factor they vary between 3.47 and 1.96. These are very close values, and as such, it does not seem to make a difference whether 2 or 3 coats of paint is applied. It is best not to apply 1 coat, as it is difficult to apply even and ensure that the entire plastic surface is covered. So all of the painted antennas that will be tested for performance will be painted with 2 coats of conductive paint. It can also be noted that the copper tape was equally as conductive on its initial backing as it was on the 3D printed antenna. The surface texture of the antenna made little difference to the surface resistance.

3.6 Feeding

Both of the initial antennas are designed to be fed with an SMA attached to the bottom of the antenna (the ground plane). This is a very simple connection when using traditional materials, meaning commercially available dielectric that is clad with copper. After drilling a hole from the conductive patch to the ground plane, the SMA pin can be attached with solder. However, it was found with the conductive paint that it was not possible to attach solder. As shown in Figure 3-14, the paint melted away from the solder, making it very difficult to get a clean connection.

Figure 3-14: Conductive Paint Melting Away From Solder

Due to the inability to solder with heat onto the painted surfaces, "soldering" with conductive paint was then tested. That is, using additional paint on top of the dried paint to set the SMA in the correct position. In addition to using conductive paint, conductive silver epoxy (MG Silver Epoxy) was also used as an alternative to traditional solder. This epoxy was applied in the same manner as the conductive paint, on top of the dried paint to set the SMA in the correct position. There were advantages and disadvantages to using both paint and epoxy. The paint tended to dry much quicker than the epoxy, making it

easier to ensure that the connector was securely fit onto the ground plane. However, the epoxy was found to have better adhesion, making the antennas less likely to detach from the connectors. As such the epoxy was used for all of the cold "soldered" antennas. The painted and epoxied antennas can be seen in Figure 3-15 and Figure 3-16.

The conductivity of the MG Silver Epoxy was not measured using the 4-point probe because the epoxy must be mixed each time it is prepared. The epoxy is prepared by mixing a 1:1 ratio of "Part A" to "Part B," this is calculated by the milliliter line marks on the outside of the syringes. However, since this measurement is not done by weight, there is no way to insure that the epoxy mixture is the exact same every time. Because of the uncertainty in the epoxy mixture, the resistivity of the conductive epoxy was not measured with the 4-point probe. The listed value of the epoxy's volume resistivity is 17.4 mΩ-cm, which is low, about the same value as the MG Silver Ink, and should be conductive enough to make an electrical connection.

Figure 3-15: 25 GHz Antenna With Conductive Paint

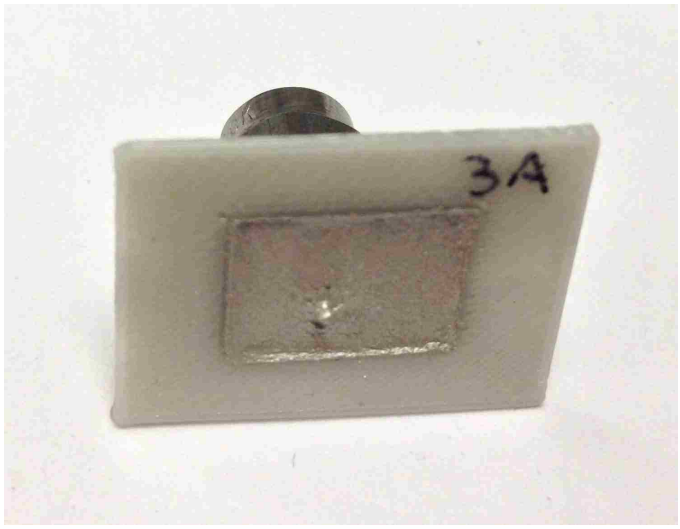

Figure 3-16: 10 GHz Antenna With Conductive Paint

With the copper tape antennas there was less of an issue attaching the SMA pin with solder than compared to the painted antennas using conductive epoxy. The solder successfully bonded with the copper tape, however with heat applied, the ABS*plus* material did tend to warp as seen in Figure 3-17.

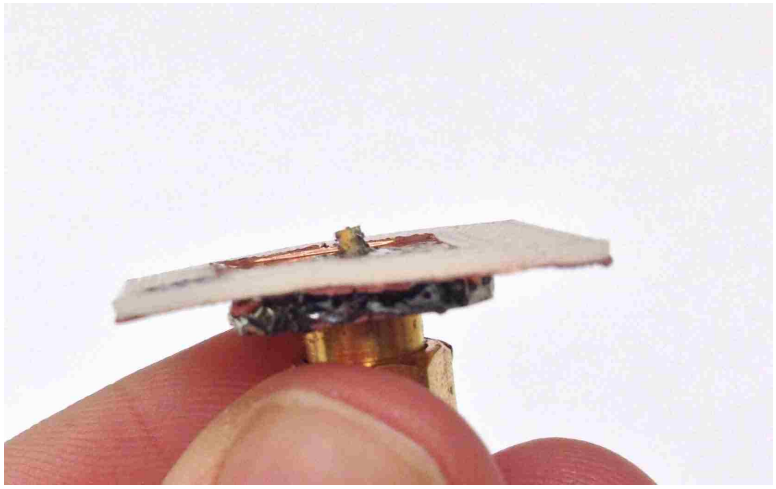

Figure 3-17: 10 GHz Antenna Warped From Soldering Heat

By minimizing the time under heat and contact with the soldering gun, the warping effects were minimized. The minimally warped antennas used for measurements can be seen in Figure 3-18 and Figure 3-19.

Figure 3-18: 25 GHz Antenna Made With Copper Tape And Solder

Figure 3-19: 10 GHz Antenna Made With Copper Tape And Solder

In order to observe how much the ground plane warping affected antenna performance, some of the copper tape antennas were also "soldered" with conductive silver epoxy. The 25 GHz antenna can be seen in Figure 3-20 and the 10 GHz antenna can be seen in Figure 3-21.

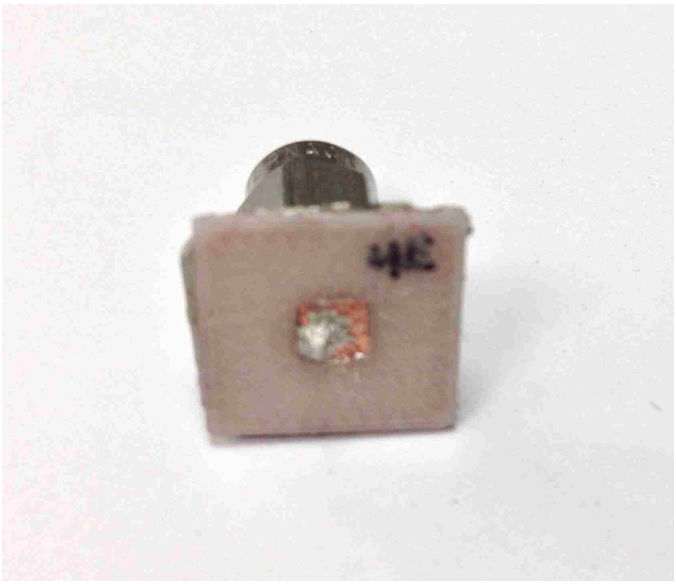

Figure 3-20: 25 Ghz Antenna Made With Copper Tape And Conductive Epoxy

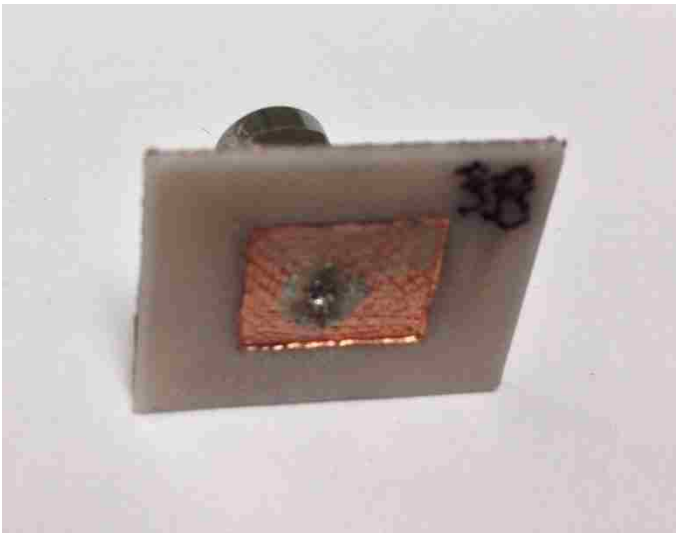

Figure 3-21: 10 GHz Antenna Made With Copper Tape And Conductive Epoxy

Attaching the pins with both the conductive epoxy proved to be a challenge. The first challenge was making sure that the pin was in straight since the adhesives don't set as quickly as solder. It was found to be easiest to apply the epoxy or paint to the backing of connector and then set into place on the antenna using a small clamp (setting the front of the pin into hole cut into another piece of plastic in order to prevent bending the pin).

Another challenge was making sure that the epoxy was thoroughly mixed, since it was packaged in 2 containers. There were a few antennas where the epoxy was not thoroughly mixed and the epoxy was not conductive enough to form an electrical connection.

3.7 Measured and Simulated Antenna Data

After the antennas were made conductive and fed with an SMA connector, their performance was measured using a PNA-X network analyzer. It was discovered that it is very difficult to obtain a good electrical connection between the SMA and the antenna using the conductive epoxy. Three out of four of the antennas connected with conductive epoxy were shorted. The connectors were removed and the holes were re-drilled to insure that there was no conductive paint connecting the ground plane to the patch. The connectors were reattached using the conductive epoxy again. This time, two out of three of the antennas were shorted.

It is believed that the shorts were occurring due to paint or epoxy dripping down the hole that the pin was fed through, connecting the patch to the ground plane. As a method to prevent it, antennas that were printed without holes were painted using the conductive paint. Once the paint was dried, the holes were drilled in the correct position. This insured that paint could not get in the hole during the painting process. Next a small section of the backing of the connector near the pin was coated in non-conductive tape. The idea being that if conductive epoxy or paint happened to drip down the hole, it would not attach to the ground plane but instead this tape. The issue with this is the shortening of the ground plane that occurs by taping off a section of it.

Fabricating these antennas proved that 3D printed antennas are difficult to feed without a dual-head printer that can print conductive paint as it prints the 3D material.

Regardless, this project also showed that it is possible to create these antennas out of hand-applied paint and copper tape. The measured S-parameters of both 10 and 25 GHz antennas can be seen below.

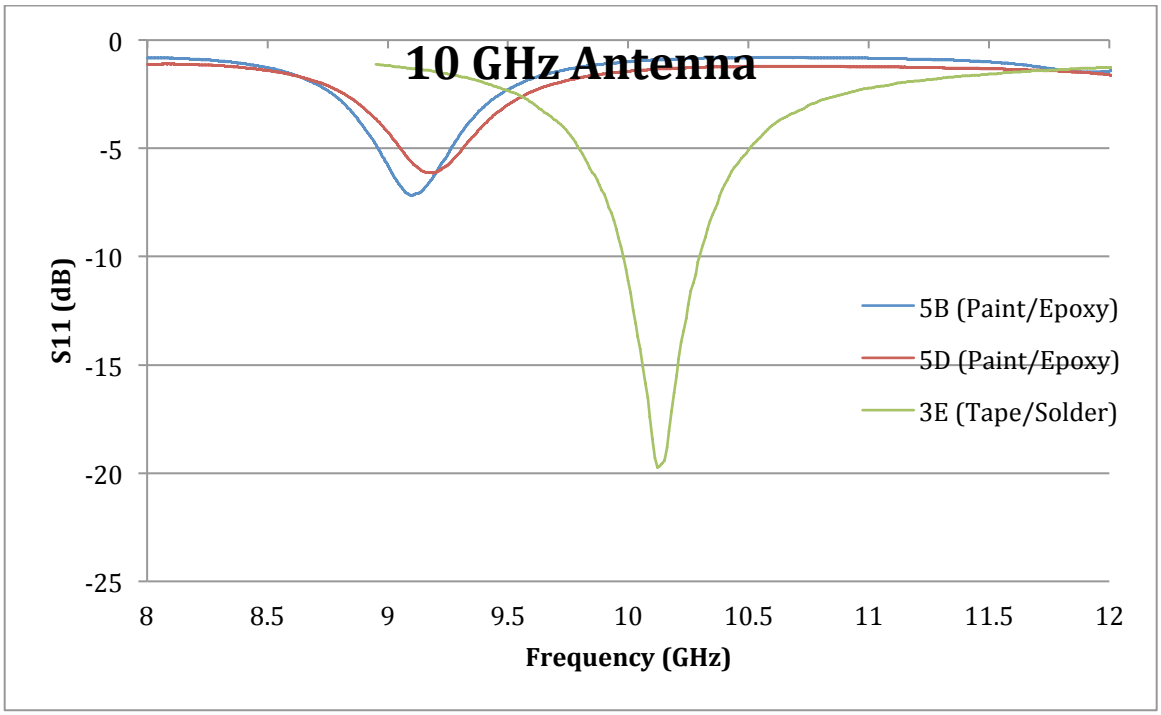

Figure 3-22: Measured S-Parameters of the 10 GHz Antennas

Figure 3-22 shows the measured S-parameters of the 10 GHz antenna created with copper tape and solder, copper tape and conductive epoxy and conductive paint with conductivity epoxy. The 10 GHz antenna was successful when prepared with copper tape and solder. It was difficult to obtain functional antennas with conductive paint and conductive epoxies. Out of the several attempts to create those antennas without having a shorted connection, only one of each was obtained. As can be seen above, neither of those antennas resonate, as the S11 measurement never reaches -10dB.

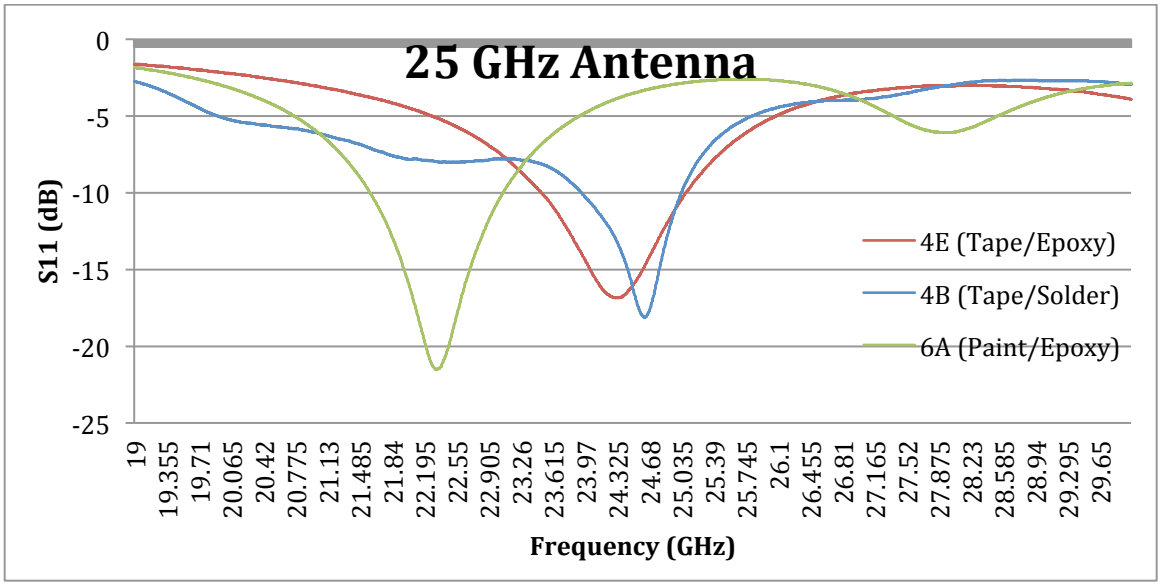

Figure 3-23: Measured S-Parameters of the 25 GHz Antennas

The 25 GHz measurements shown in Figure 3-23 indicate that all 3 antennas resonate. However, the frequency of the painted antenna is unexpected. The resonant frequency value is less than the values given from the parameter sweep in CST. It is likely that this is just a human error maybe painting the patch too large.

Chapter 4: 5 GHz Antenna

4.1 Design

In order to achieve an antenna that is easier to handle, metalize and measure than the initial antenna designs, a 5GH patch antenna was designed. Choosing an operating frequency of 5 GHz gives a much larger ground plane than either 10 or 25 GHz antennas possess, making the antenna much easier to physically handle. In addition to being easier to paint or tape, the 5 GHz design also has more surface area for the vacuum testing, which will be described in a later chapter. The lower frequency will also help in understanding how printer reliability changes the antenna performance with respect to frequency. It was noted that the antenna accuracy shifted the resonant frequency of the 25 GHz antenna more significantly than the 10 GHz antenna. By running the same experiment with a 5 GHz antenna there is a more complete set of data comparing printer accuracy with antenna performance.

Taking note of the difficult pin feeding of the initial antenna designs, the 5 GHz antenna was designed to be side fed. The idea being that the connector could still be attached with either solder or conductive paint, but without the risk of the conductive paint seeping through feed hole to short the patch. In order to feed this antenna with a SMA connector, it was necessary to match this transmission line with a quarter-wave transform. An example of such a design can be seen in Figure 4-1.

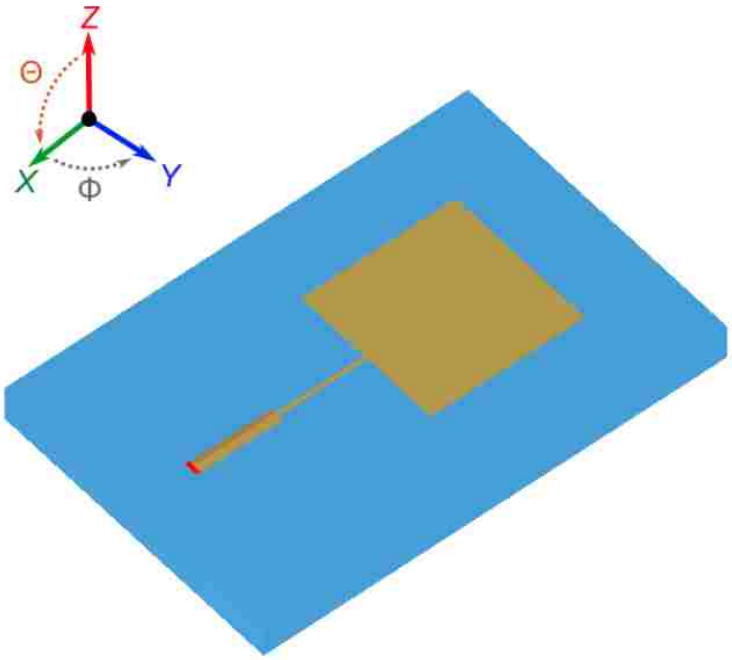

Figure 4-1: Side-Fed Patch Antenna with Quarter-Wave Transform [23]

The side feed will also provide useful data regarding printer accuracy with fine details. This is essential information, as the quarter-wave transform is necessary for the antenna to resonate at all.

4.2 Printer Reliability

As with the 10 and 25 GHz antennas, the 3D printed 5 GHz antennas were all individually measured using a digital caliper. Only the outside measurements were taken because, as observed with the two initial antennas, it is difficult to reliably measure the inner patch dimensions using digital calipers. Again, the caliper used has an accuracy of ±0.03 mm, so these measurements could be 0.03 mm lower or higher. The results of these measurements are summarized in Figure 4-2.

5 GHz Antenna						
Antenna	Length		Width		Depth	
	Actual (mm)	Difference (mm)	Actual (mm)	Difference (mm)	Actual (mm)	Difference (mm)
Design	59.92		46.00		0.66	
7A	59.80	-0.12	45.94	-0.06	0.62	-0.04
7B	59.80	-0.12	46.03	0.03	0.63	-0.03
7C	59.87	-0.05	45.92	-0.08	0.61	-0.05
7D	59.85	-0.07	45.95	-0.05	0.61	-0.05
7E	59.88	-0.04	45.96	-0.04	0.62	-0.04
7F	59.82	-0.10	46.00	0.00	0.61	-0.05
7G	59.85	-0.07	45.91	-0.09	0.62	-0.04
7H	59.87	-0.05	45.91	-0.09	0.61	-0.05
7I	59.86	-0.06	45.96	-0.04	0.62	-0.04
7J	59.87	-0.05	45.99	-0.01	0.61	-0.05
	Average:	**-0.07**		**-0.04**		**-0.04**
	Mode:	**-0.05**		**-0.04**		**-0.05**
	Maximum:	**0.12**		**0.09**		**0.05**
	Minimum:	**0.04**		**0.00**		**0.03**

Figure 4-2: 5 GHz Antenna Physical Measurements

The largest deviation of the 3D printed antennas' measurements from the measurements sent to the printer is 0.12 mm. However the most commonly occurring deviations (the modes of each measurement) is less than 0.10 mm.

Using the measured physical dimensions of the printed antennas, the antenna was re-simulated in the full EM simulator CST Studio Suite. Assuming a worst-case scenario, the antenna parameters were swept by ±0.12 mm. The parameters swept were the ground plane length, the ground plane width, the patch width, and the patch length. Even though the path widths and lengths were not physically measured, the parameter was swept in CST because the patch size greatly affects the resonant frequency of the antenna. Continuing with the worst-case scenario, the patch measurements were also swept ±0.12 mm. The matching line was not swept, as the measurements are critical to the antenna performing at all.

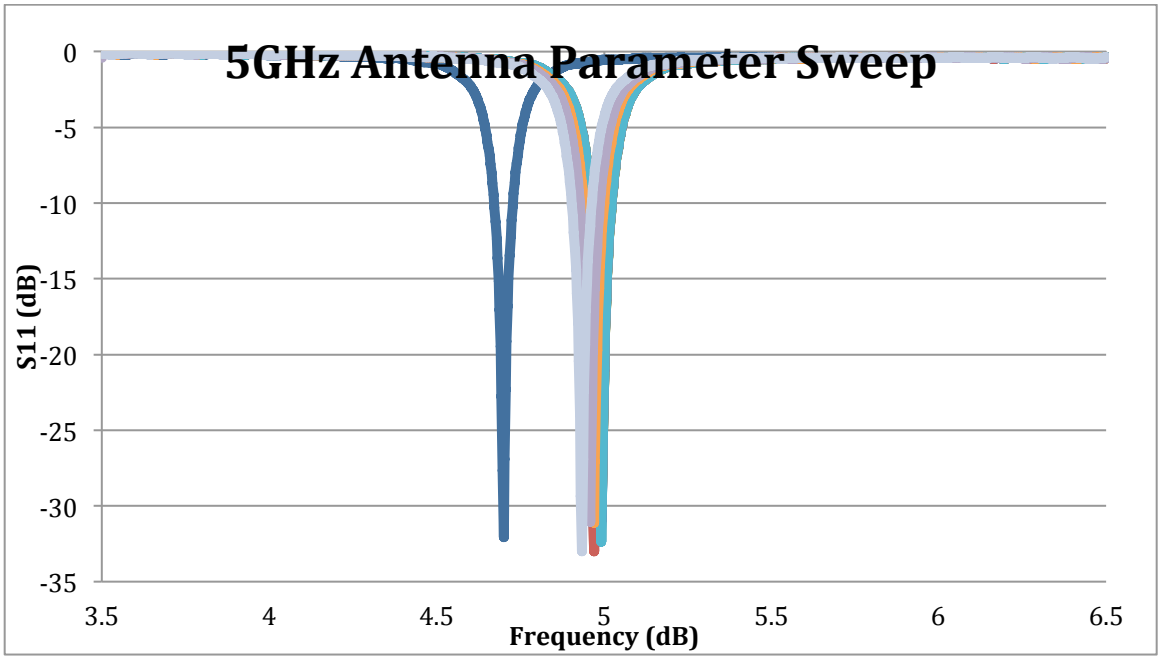

Figure 4-3: Parameter Sweep of the 5 GHz Antenna Design

As can be seen in Figure 4-3, the parameter sweep did not yield nearly as drastic of results as the parameter sweep for the 25 GHz antenna did. The most dramatic shift in resonant frequency was 0.4 GHz.

4.3 Adding Conductivity

As with the 10 GHz and 25 GHz antennas, the 5 GHz antenna was made conductive using both conductive paint and copper tape. It was determined with the 10 and 25 GHz antennas that the pin-fed design was difficult to execute using conductive paint or conductive epoxy, as the liquids would attach the pin to the ground as well as the patch. The majority of those antennas that were painted were shorted. So the 10 GHz antenna was designed with a side feed in order to prevent the antenna shorting out. However, upon measuring the painted 10 GHz antennas it was discovered that all of these were shorted as well. It was finally realized that the reason for the shorting was not due to

the pin-fed design but rather the paint seeping through the printed ABS*plus* pattern, this can be seen in Figure 4-4.

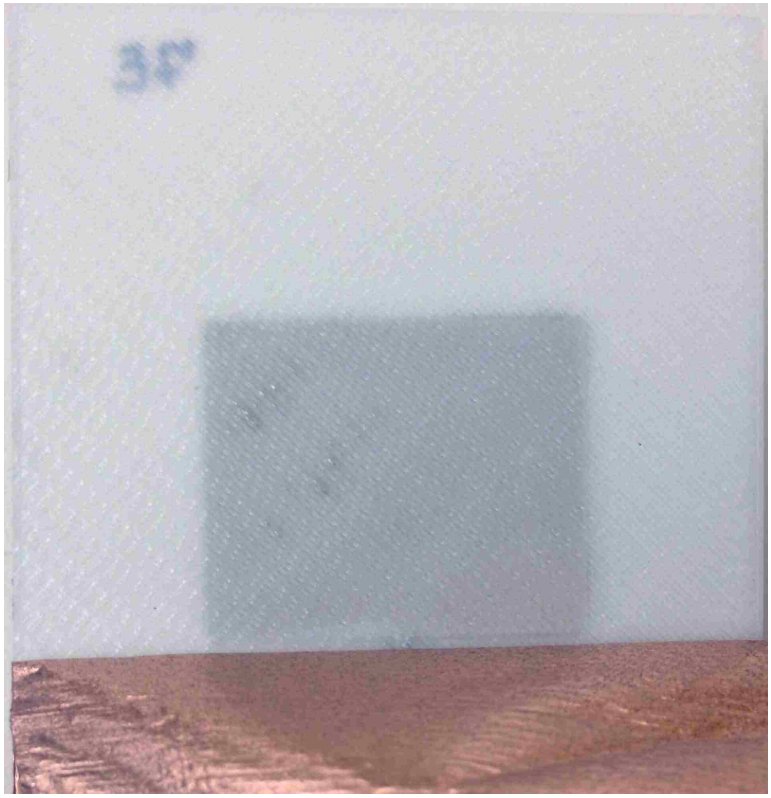

Figure 4-4: Conductive Paint Seeping Through ABS*plus*

The printed ABS*plus* has a distinct surface texture of diagonal lines, which are really individual threads of the material. However the threads aren't completely flush with one another. When the print is thin (1 or 2 material layers thick), there are likely holes in the material from the lines not lying completely flush. An example of these holes with one layer of material can be seen in Figure 4-5.

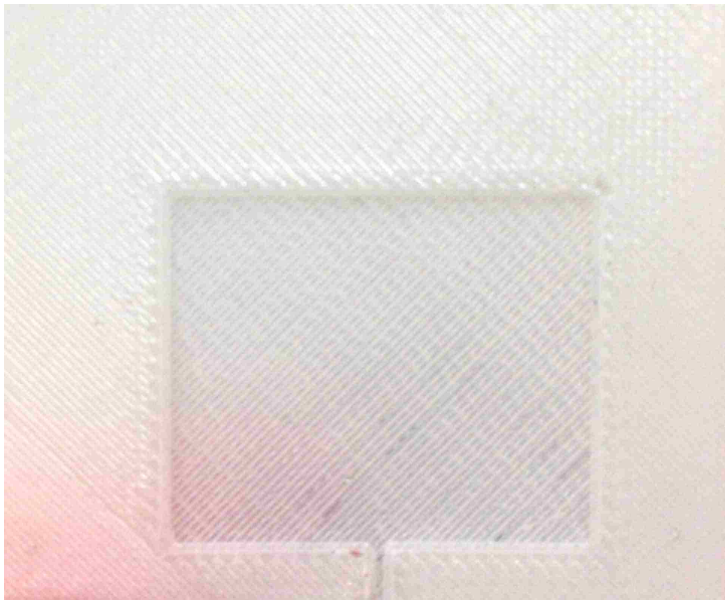

Figure 4-5: 5GHz antenna with holes printed in the material

In order to prevent the patch from connecting with the ground plane on the painted antennas, the backside of the antenna was coated in a thin piece of Kapton tape, as seen in Figure 4-6. The Kapton tape used was 1 mil thick, so the affects on the antenna's bulk dielectric constant should be minimal. Unfortunately the tape did not have a recorded dielectric constant value for high frequencies, so there was no way to re-simulate the model with the additional tape dielectric.

Figure 4-6: The back of a 5 GHz antenna coated with Kapton tape

Now that all of the painted 5 GHz antennas had a layer of Kapton paint on the back, it was now impossible to have a painted ground plane and patch at the same time. So the ground planes on the painted patch antennas were created by adhering copper tape to the Kapton tape.

4.4 S-Parameter Measurements

The S-parameters were measured for three different types of antennas, one made of conductive paint (with added Kapton tape dielectric and copper tape ground plane) and conductive epoxy, one of copper tape and conductive epoxy and one of copper tape and solder.

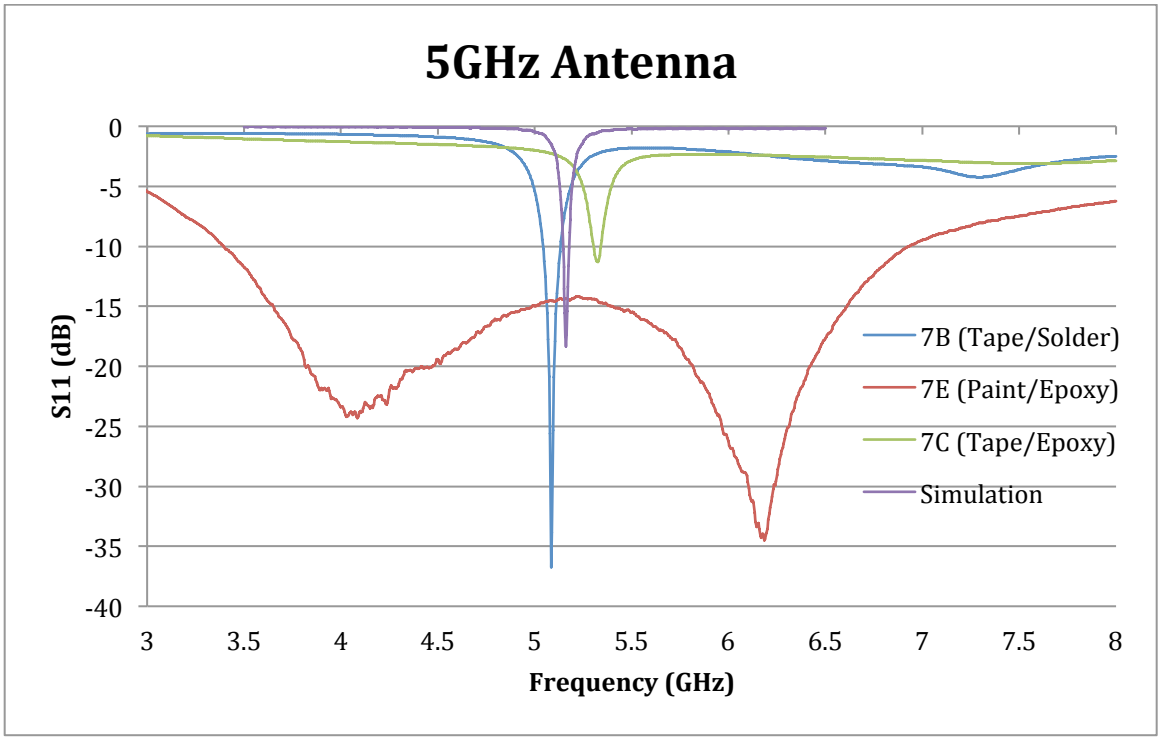

Figure 4-7: Measured S-Parameters of 5 GHz Antenna

As can be seen in Figure 4-7, antenna 7B (created with copper tape and solder) performed very similarly to the CST simulation, the resonant frequencies within 0.1 GHz of each other. The copper tape with the conductive epoxy did not create a very strong electrical connection, just as with the 10 and 25 GHz antennas. After adding Kapton tape to the painted antenna, it was possible to achieve a functioning antenna. However, this antenna does not behave as predicted. This could be due to the Kapton changing the bulk dielectric constant, human error or a poor electrical connection. The human error being that it was very difficult to paint the quarter-wave transform, as it was a very fine line. It is very likely that the line was wider than the required width, causing the antenna to no longer match to 50 Ohms. The difference between the taped and painted quarter-wave transform line can be seen in Figure 4-8.

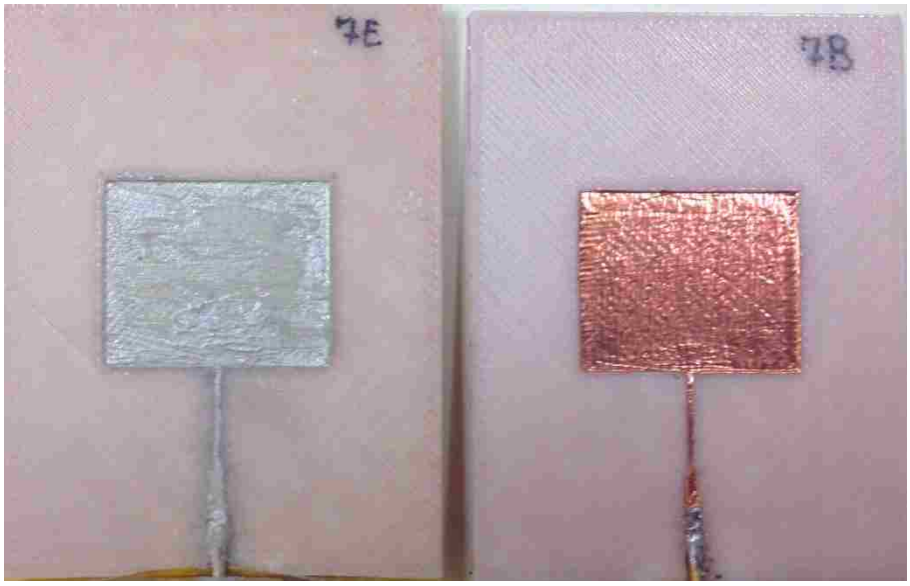

Figure 4-8: Comparison of the Painted and Taped Quarter-Wave Transform

4.5 Radiation Pattern Measurements

The normalized radiation pattern of the functioning 5 GHz antenna was measured in an anechoic chamber at its resonant frequency. The measurement was then plotted and can be seen in Figure 4-9.

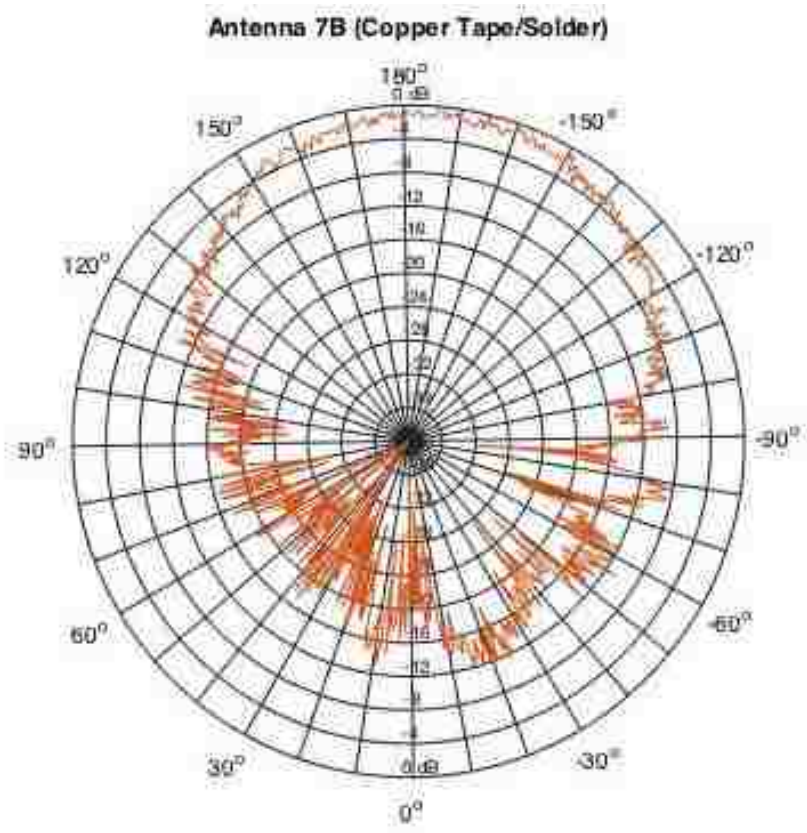

Figure 4-9: Measured Radiation Pattern of Antenna 7B

The radiation pattern matches what a radiation pattern of a patch should be. However, near the 0° area, the antenna is experiencing up to -12 dB radiation. This is greater than expected for a patch. However, this could be due to the antenna itself being somewhat curved. The antenna does not lay perfectly flat, and as such, the patch itself is also curved. This could easily cause the radiation pattern to change in such a manner. A simulation was run in CST with a curved patch antenna, and the radiation patterns obtained for several different radiuses of curvature can be seen in Figure 4-10.

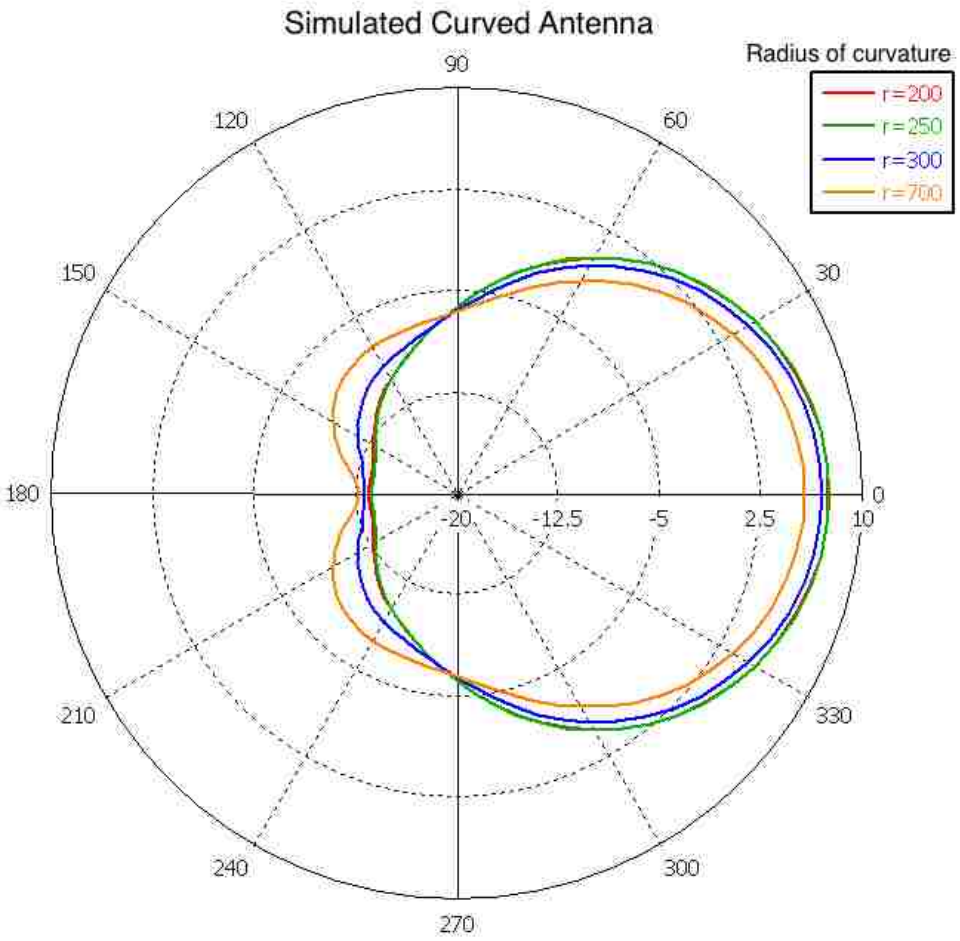

Figure 4-10: Simulated Radiation Pattern of Bent Antenna

As can be seen, the curved antenna also had back lobes at about the same level as the measured 5 GHz antenna.

Chapter 5: Space Effects

5.1 Overview

Material selection is a very important factor in designing for space-based applications. Selecting usable materials requires knowledge of the known space environment of interest. Depending on location of the orbit of interest, there are several factors that must be considered when dealing with space including, high vacuum, magnetic fields, gravitational fields, electromagnetic radiation (UV rays, X-ray, and gamma rays), neutrons, charged electrons and protons, cosmic rays, varying extreme temperature and micrometeorites [29]. In addition, the vehicle may be limited by weight so materials may need to be lightweight as well as tolerant to the above environment factors. Although there are several factors to consider when choosing materials for space, it is not always known how the materials will react in the orbit environment. This is made even more difficult when all of the environmental factors added, yielding non-linear impacts, which is impossible to model exactly. There are several tests that can be conducted to help better understand how the material will behave. However, these tests are expensive and not always conclusive. As such, typically space environment simulations are relied upon heavily, usually analyzed as single variables, not combined as in the actual space environment [29].

One very appealing feature of using 3D printed materials for space applications is the ability to recreate all parts onboard, assuming a manned mission. This is really useful because the reliability of parts over time is not necessarily guaranteed, no matter the quality. Instead of stocking the vehicle with additional components, all 3D printed

components could be recreated as needed. However, minimal research has gone into examining the feasibility of 3D printed materials for space-based applications.

In this project there were 2 tests performed to begin to understand the feasibility of using ABS in space. The first test was placing the 3D printed antennas in a vacuum chamber. The second test was placing 3D printed ABS material under a Sr-90 source for radiation testing.

5.2 Vacuum Testing

It is important to understand how the 3D printed antennas will perform in a vacuum if they are to be considered for space applications. In addition all materials sent into space must pass NASA testing for outgassing and total condensable volatiles (according to ASTM E-595-93, Standard Method for Total Mass Loss and Collected Volatile Condensable Materials from Outgassing in a Vacuum Environment). In order for a material to be considered low outgassing, it must have a maximum total mass loss (TML) value not to exceed 1.0% and a maximum collected volatile condensable material (CVCM) valued not to exceed 0.10% [30].

NASA uses ASTM E-595-90 standard method for calculating TML and CVCM [31]. In this method, the samples are first exposed to a 24-hour pre-conditioning period at 25°C with 50% relative humidity and standard atmospheric pressure. After the pre-conditioning period the samples are weighed. The weighed samples are placed into clean and dry aluminum foil boats. The boats are then loaded into individual compartments within a copper bar. The copper bar is heated to 398 K for 24 hours, meaning the samples are also heated to 398 K by conduction. The TML of a material sample is determined from the mass before and after the 398 K exposure. The CVCM is calculated from the

mass of the clean collector and the mass of the collector with particles after the 398 K exposure.

Plastic materials are typically not used in space-based applications due to relatively high outgassing levels [32]. They tend to outgas for longer periods of times than smooth metals due to the composition of the material. Water inside of the plastic must diffuse to the surface to be pumped away, and as such they take longer to outgas the water contained. In addition, plastics also may contain other chemicals that outgas, such as stabilizers and plasticizers. This is important to note, as these outgassed chemicals can affect the performance of other components. 3D printed ABS*plus* has already been tested for outgassing by NASA. It was found to have a TML of 0.63%, a CVCM of 0.08%, and water vapor regained of 0.25% [31]. This means that ABS*plus* is considered a low outgassing material by NASA's standards. However, it was not specified if this was 3D printed ABS*plus* or just the material prior to printing. This is an important factor, as the gaps in the 3D printed ABS*plus* surface pattern may require longer times to fully release water and other vapors. NASA has not tested the MG conductive epoxy and conductive paint, so their outgassing values are not known. There are several similar products within the NASA database, however some are low outgassing and others are not.

In this project, several 3D printed antennas were placed in a doghouse style vacuum chamber. The chamber has the capability of pumping less than or equal to 10^{-5} Torr. In addition cold plates with temperature ranges of -60 to 100°C can be placed on samples. Some of the antenna samples were not conductive, meaning just the 3D print was placed inside, while some of them were coated in the conductive paint (the same samples used for the 4-point probe measurements). The 5 GHz unpainted antennas were

placed on a cold plate and kept at about 95°C. The added heat helps to speed up the vacuum effects. The painted antennas were not heated, and instead tested without a cold plate at room temperature. This was mainly due to the paint probably not being low outgassing and also having a boiling point of 56°C. In addition, other 10 and 25 GHz antennas were placed in the chamber without a cold plate, in order to compare to the painted ones. All of the samples were kept in the vacuum chamber for one week (with the cold plates only being on during working hours of 8am-5pm for 5 of the 7 days).

After the vacuum testing was completed, the antennas were placed into individual nitrogen filled holding bags, in order to reduce the effects of being reintroduced into atmosphere. This way, the testing could be done as close as possible to vacuum conditions. After vacuum exposure, this project was concerned with antenna performance, conductivity, surface changes and the permittivity of the ABS*plus* and associated conductive paint.

5.3 Vacuum Testing Effects – Resonant Frequency

After the 3d printed portions of the antennas were removed from the nitrogen holding bags, copper tape, an SMA connector and solder were promptly attached, as seen in Figure 5-1.

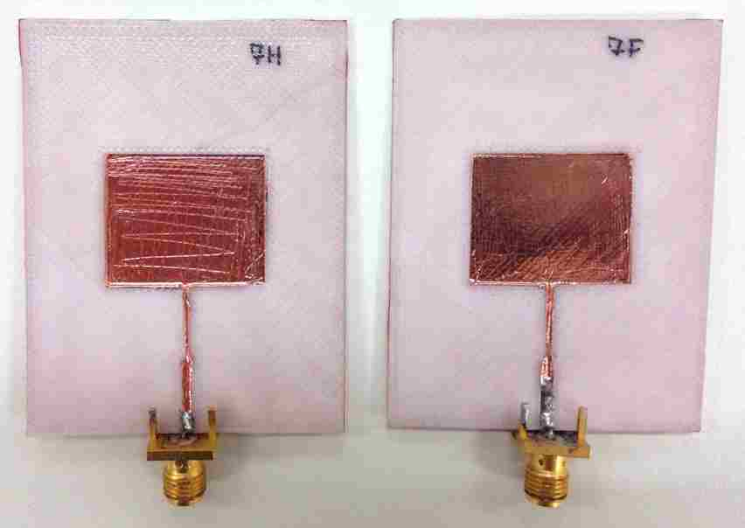

Figure 5-1: Two Post-Vacuum Prepared Antennas

Copper tape was chosen over conductive paint for several reasons, including ease of manufacturing, no setting time, and increased reliability. Adding copper tape to the 3D printed surface is much easier than applying conductive paint, as it is applied in as single sheet. The copper tape is also much more reliable than the paint as described in Chapter 3. The copper tape is more accurate in application than the paint, resulting in antennas closer to the simulated design. The most important factor in the decision to use copper tape instead of conductive paint was time. As described, materials reabsorb water (water vapor regain) after being re-exposed to atmosphere. This absorption happens over time, and in order to really observe the changes caused by the vacuum environment, it is important to be able to take measurements as soon as possible. If conductive paint were used, additional time would be taken in order to wait for the paint to dry. In addition, more time would be taken to wait for the conductive epoxy to dry before being able to take S-Parameter measurements.

After preparing the antennas with copper tape and solder, the S-parameters were taken using the PNA-X. The first set of measurements were taken within an hour of

opening the nitrogen holding bags. The second set of measurements were taken within 2 hours of opening the nitrogen holding bags. After that the measurements were taken approximately every 24 hours for the first 96 hours, and then measured finally after 1 week of being reintroduced to atmosphere. A chart of the measurements taken of antenna 7F can be seen in Figure 5-2.

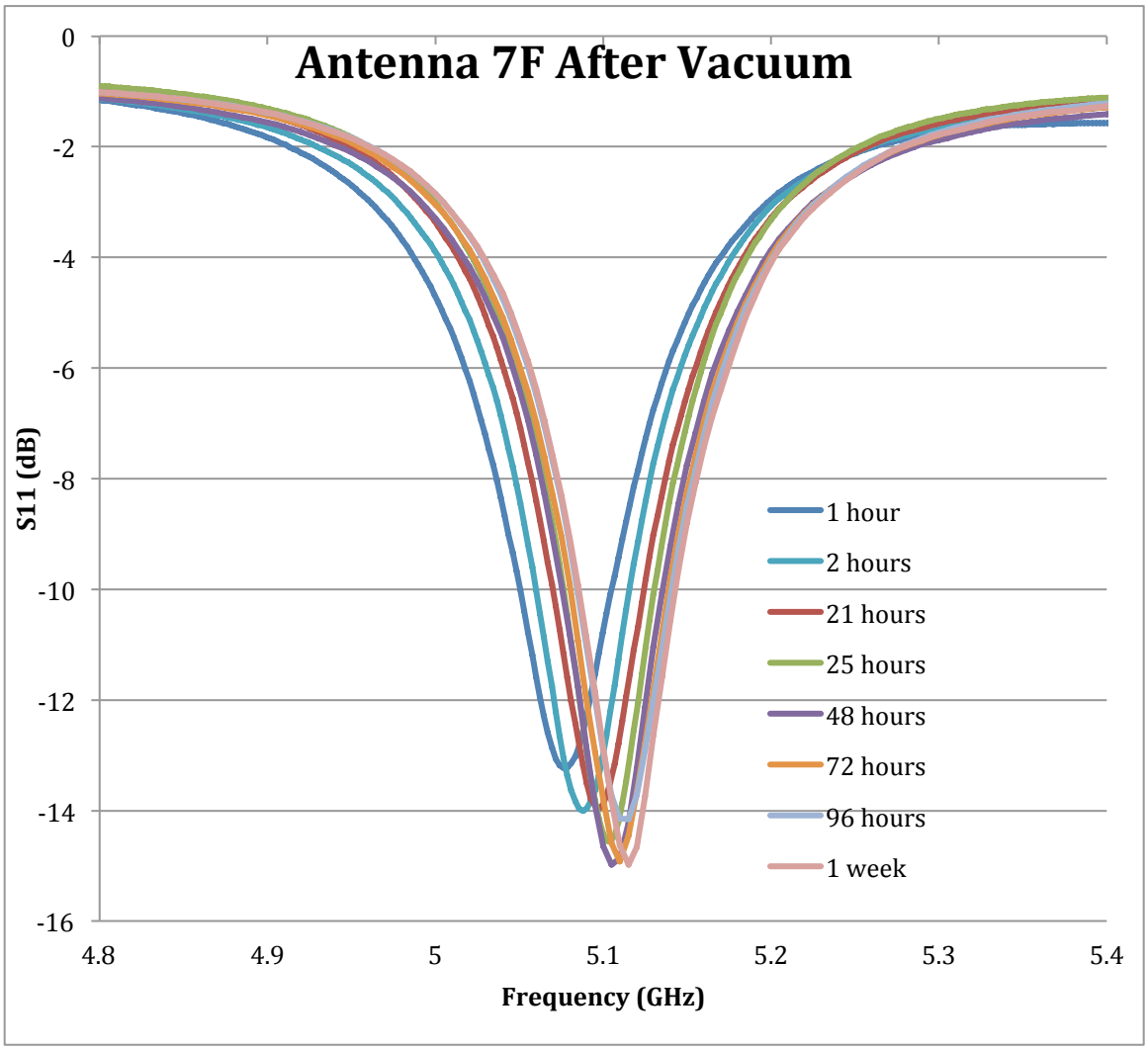

Figure 5-2: S-Parameter Measurement of Antenna 7F After Vacuum Exposure

In Figure 5-2, it is very clear that the resonant frequency shifts as a function of time out of vacuum. The resonant frequency shifts from 5.076 GHz after 1 hour of atmosphere exposure to 5.115 GHz after a week of vacuum exposure. However the resonant

frequency stays pretty constant at 5.115 GHz after 96 hours of atmosphere exposure. In addition, the S11 value also decreases as a function of time out of vacuum, shifting from -13.23 dB after 1 hour to -14.98 dB after 1 week. The measurements for antenna 7H can be seen in Figure 5-3.

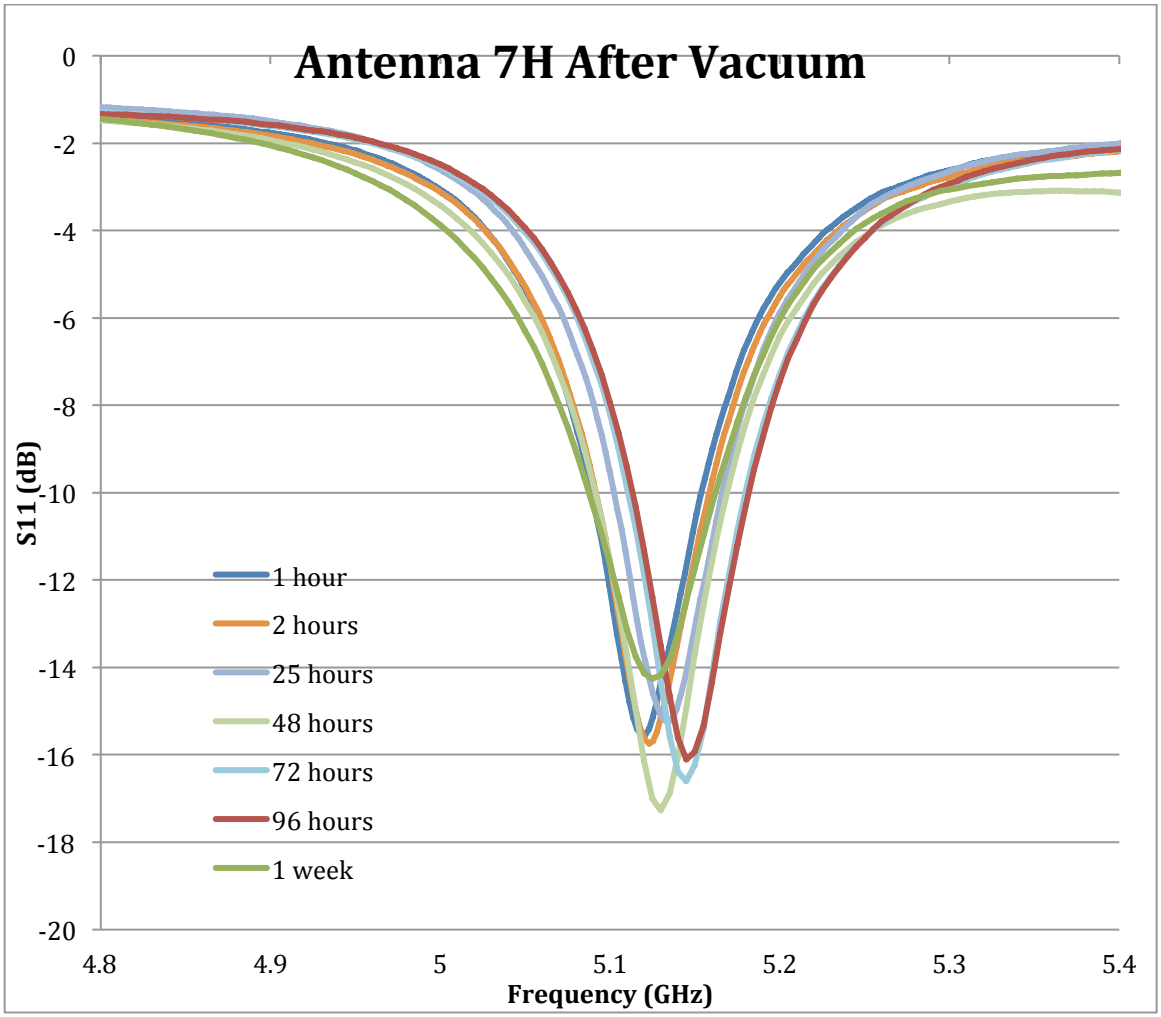

Figure 5-3: S-Parameter Measurements of Antenna 7H after Vacuum Exposure

As with antenna 7F [Figure 5-2], antenna 7H also experiences a resonant frequency shift with respect to time spent out of vacuum, as seen in Figure 5-3. This shift ranges from 5.118 GHz after 1 hour to 5.15 GHz after 96 hours. It is worth noting that the resonant frequency after 1 week is moved back to 5.125 GHz, however this is probably due to a

calibration error, as this is the only value that shifts to a lower frequency. There is less of a difference in minimum S11 value for antenna 7H than antenna 7F. The value appears to be relatively stable.

It can be said that there is a definite shift in the resonant frequency of a patch antenna in vacuum environment. However, this shift is small, (0.039 GHz for one antenna 0.04 GHz for the other) and will only affect very narrow band, secure communications.

5.4 Vacuum Testing Effects – Dielectric Constant

The dielectric constant and loss tangent were measured for samples of ABS*plus* that were exposed to vacuum environment. Due to timing constraints, the samples were measured 2 weeks after having been removed from the nitrogen filled bags. In order to measure the dielectric constant, the PNA must be used. However, in order to measure the S-parameters, the PNA must also be used. The calibration process for measuring the dielectric constant (as described in Appendix B) is very time intensive, as are the measurements themselves. Measuring both permittivity and S-parameters would not have been possible in the same time frame, as both measurements require different attachments and calibrations. The dielectric probe was not used to measure the permittivity of the vacuum exposed samples as the dielectric probe system requires thick samples and the vacuum requires thin samples. It would be possible to use a thick sample in the vacuum, however the results would not be indicative of much, as it would take longer for the air to be released from within the sample It would be necessary to leave the thick sample in the vacuum chamber for longer, which was not an option.

Waveguide samples were cut from the antennas placed in the vacuum chamber. The system was calibrated as described in Appendix B, and the materials measured as in Chapter 2. The results of this measurement can be seen in Figure 5-4.

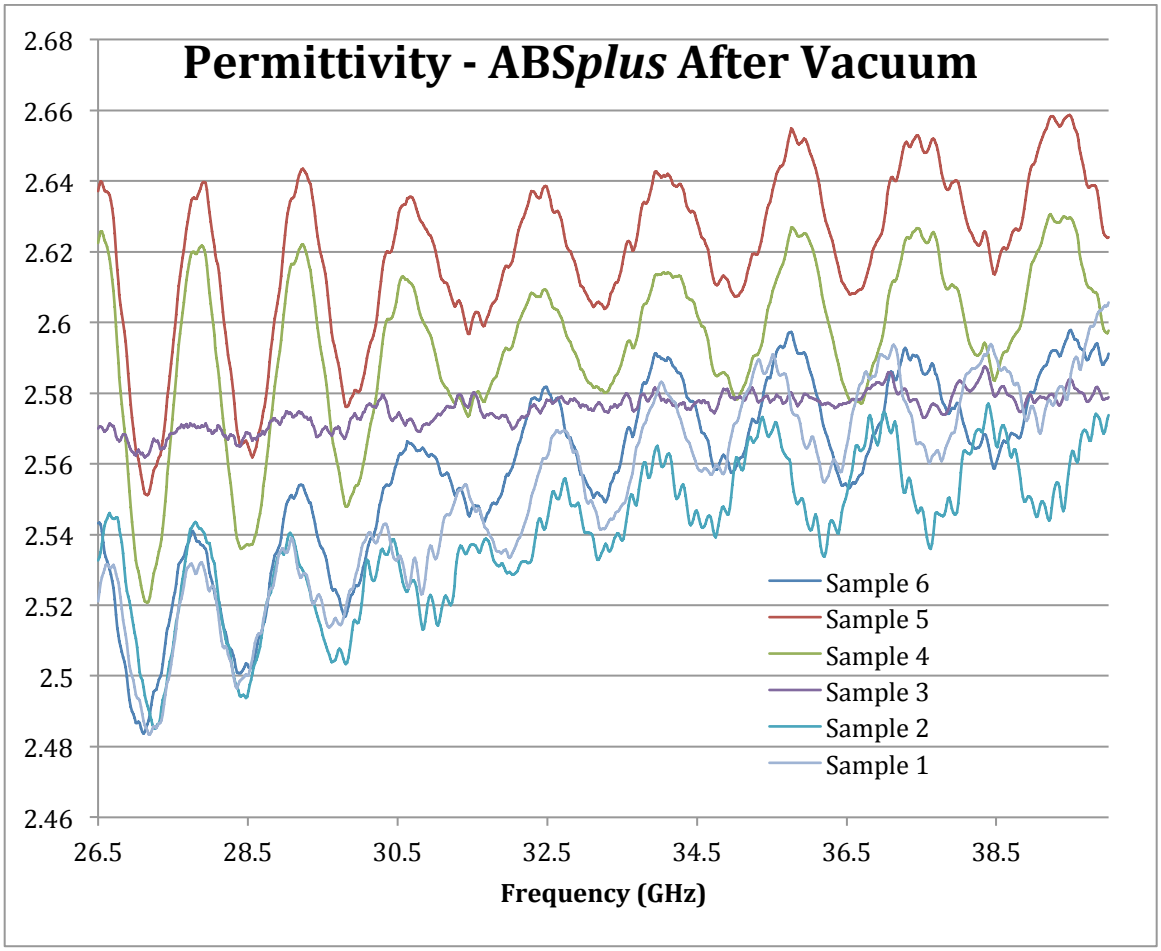

Figure 5-4: Dielectric Constant of ABS*plus* After Vacuum Exposure

The permittivity did not seem to be changed by the vacuum effects. However, these measurements seem to diverge greater from each other than the initial Ka-band measurements [Figure 2-7]. It seemed to make a difference from where the sample was cut from the antenna. The previous measurements used a solid sheet of printed ABS*plus* that was then cut into sample sizes. This used printed antennas that were then cut into sample sizes. It is likely that the printing was not completely uniform within the antenna

compared to the flat sheet of printed ABS*plus*. So the surface print texture of the ABS*plus* could be causing discrepancy between samples.

5.5 Vacuum Testing Effects – Radiation Pattern

The radiation pattern of antenna 7F was measured at its resonant frequency in an anechoic chamber and can be seen in Figure 5-5.

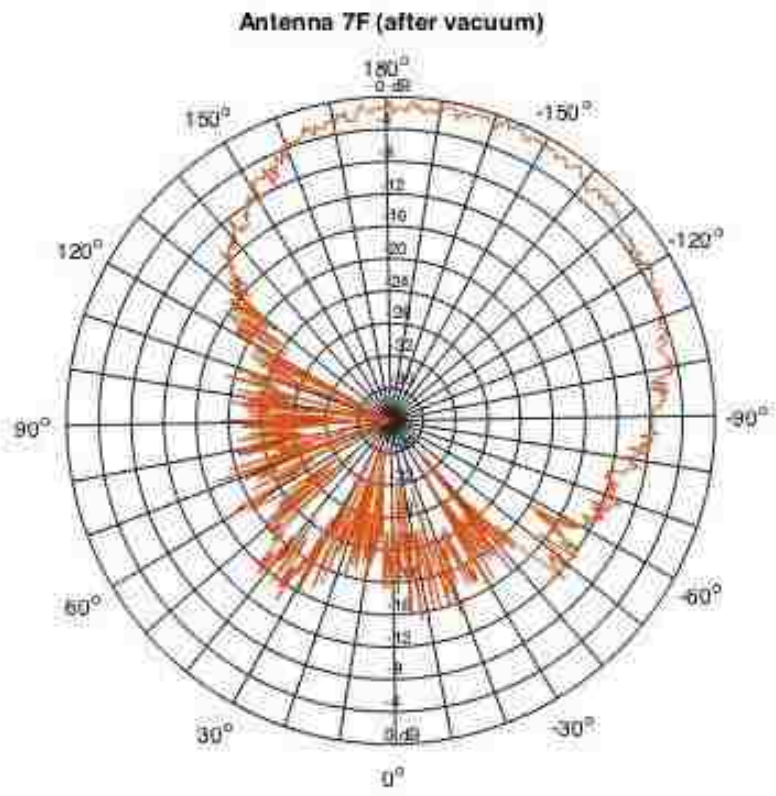

Figure 5-5: Radiation Pattern of Vacuum Exposed Antenna

The radiation pattern is slanted to one side; this is probably due to the fact that the antennas were not perfectly lined up at the start of the measurement. Other than angular shift, there is no notable difference between the vacuum exposed and the non-vacuumed antenna radiation pattern.

5.6 Vacuum Testing Effects – Conductivity/Resistivity

It is unknown whether or not the MG Silver Print conductive ink is low outgassing or not. Therefore, it would be interesting the compare the conductivity measurements after vacuum exposure to those before exposure to see if there were any notable changes. It is important to note that it will not be possible to obtain an accurate conductivity, as it is not possible to know the exact paint thickness after vacuum. Both the ABS*plus* and the conductive paint will likely shrink in the vacuum, so it is impossible to know how much the total depth loss was due to the paint and how much was due to the ABS*plus*. However, sheet resistivity values can still be compared to those values taken before the vacuum exposure.

Upon setting up the 4-point probe and initializing measurements, the same Rogers copper sheet was measured as in previous measurements in order to use as a control. However, once it was time to measure the painted materials, the probe was unable to give a consistent resistivity value. This was found to be the case for each and every painted sample. The samples were moved around in an attempt to find a smoother surface for the probes to make contact with, but no constant measurement was found. As such, it was not possible to re-measure the sheet resistivity for the samples that were exposed to vacuum.

5.7 Vacuum Testing Effects – Material

In order to better understand what happened to the ABS*plus* and MG Silver Print materials in the vacuum chamber, the materials were looked at with an optical microscope. First the non-vacuum exposed antennas were examined, as can be seen in Figure 5-6 and Figure 5-7.

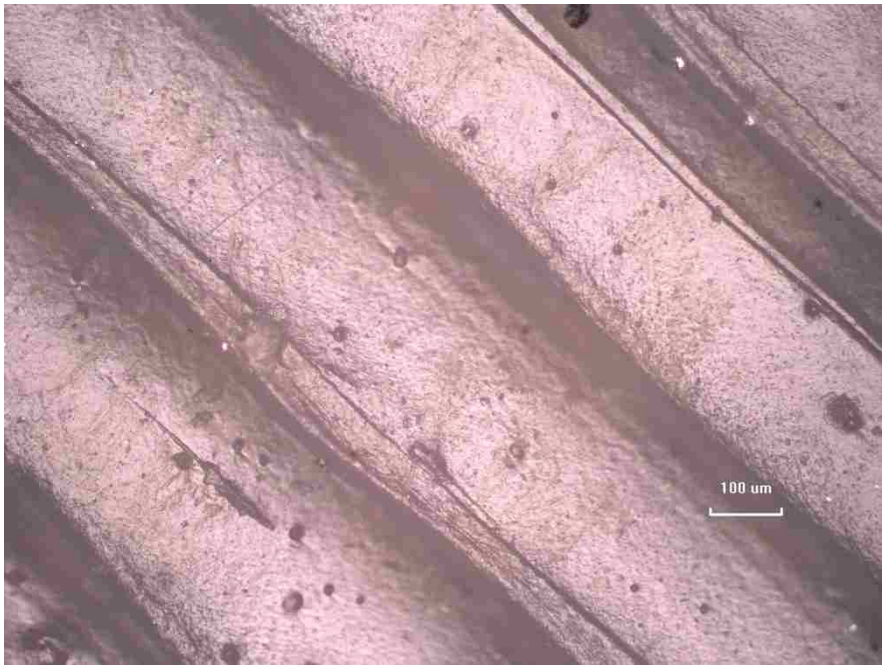

Figure 5-6: ABS*plus* Under Microscope (Antenna 1E, 10x Magnification)

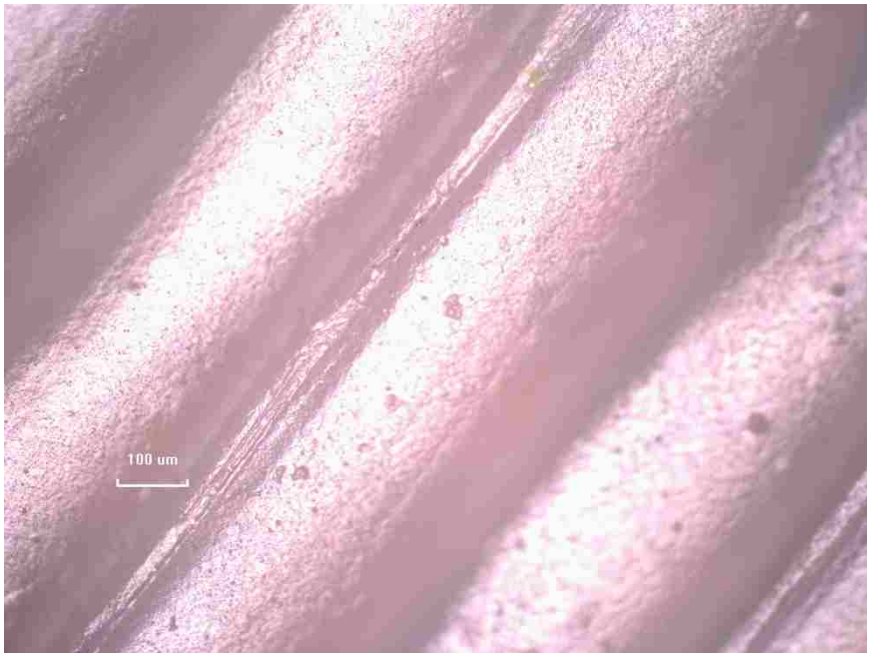

Figure 5-7: ABS*plus* Under Microscope (Antenna 7G, 10x Magnification)

In the 2 figures, note that there a few differences. Figure 5-6 has more scratches and imperfections, however that is expected, as this sample is older and had been moving

around the lab for a few months longer than sample 7G. The white spots in Figure 5-6 are actually specks of conductive paint that seeped through the layers of ABS*plus*, as the reverse side is painted. Note how straight the diagonal lines of ABS*plus* are.

Next the vacuum exposed ABS*plus* was examined under microscope in order to check for differences. Figure 5-8, Figure 5-9, and Figure 5-10 are 10 times magnification images of the ABS*plus* that was exposed to vacuum. The first 2 images are of the same antenna, just different locations.

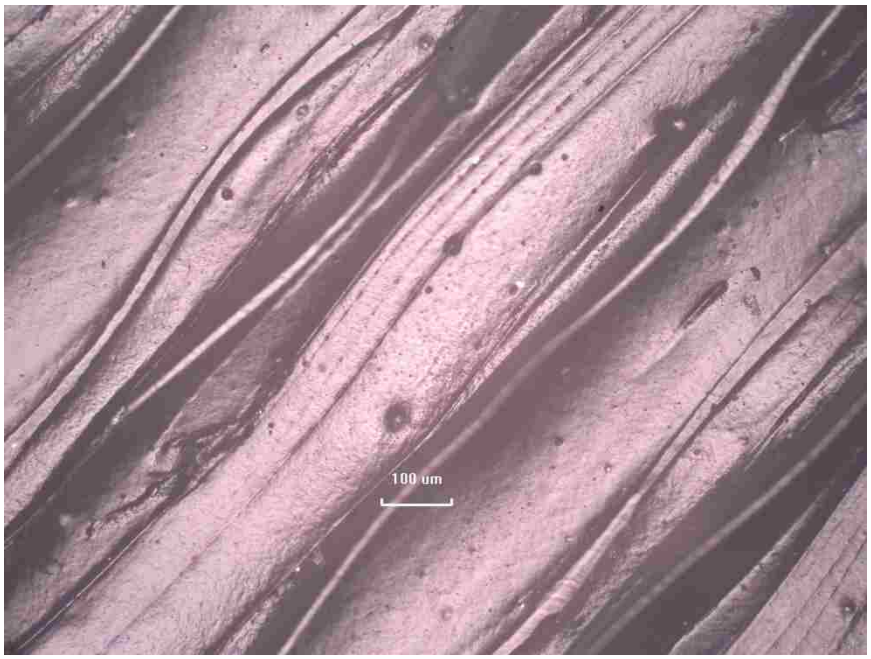

Figure 5-8: Vacuum Exposed Abs*plus* Under Microscope (Antenna 5C, 10x Magnification)

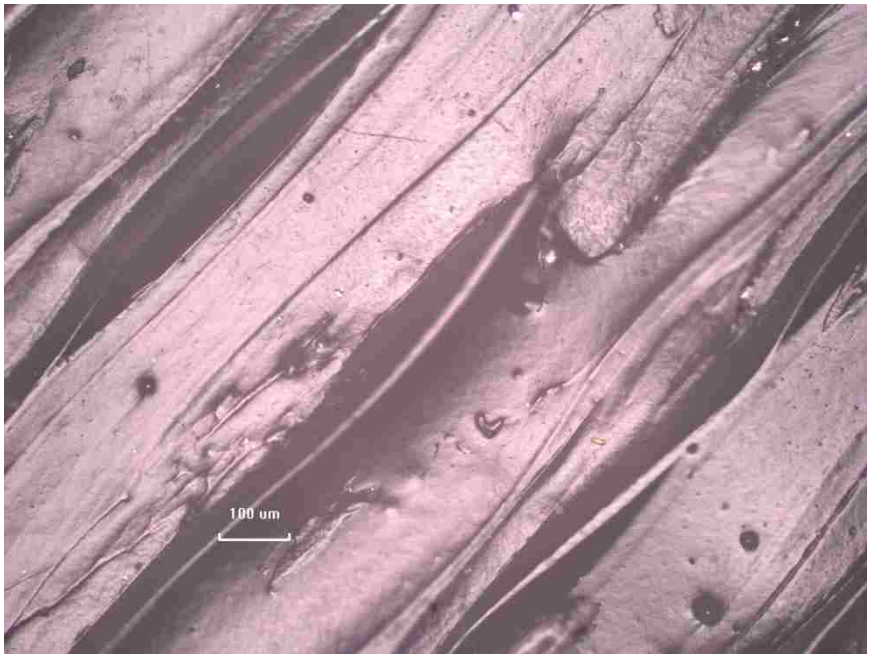

Figure 5-9: Vacuum Exposed Abs*plus* Under Microscope (Antenna 5C, 10x Magnification)

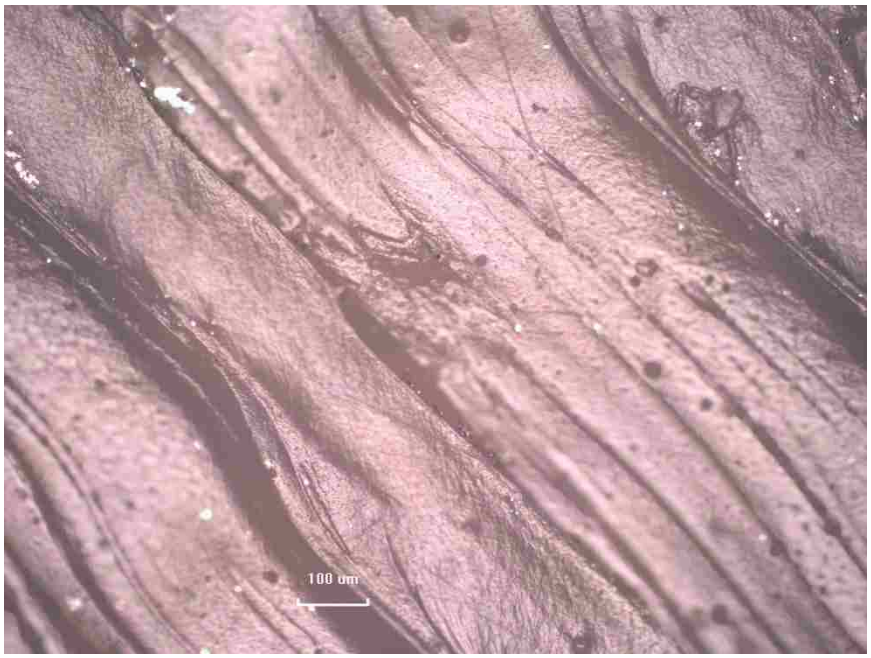

Figure 5-10: Vacuum Exposed Abs*plus* Under Microscope (Antenna 2A, 10x Magnification)

The first notable difference between the vacuum exposed and the non-vacuum exposed ABS*plus* is that the vacuum exposed appears to have warped. The straight diagonal strands of ABS*plus* are now wavy. Another notable difference is that now the spacing

between the strands of ABS*plus* is larger than before. In the photos showing the non-vacuumed samples, the spacing was less than 100 µm (the unit used for reference in all figures). However after vacuum exposure, the spacing appears to be equal to or great than 100 µm. This is particularly interesting information because the samples were only under vacuum conditions for 1 week. If the samples were kept longer, the warping may continue. In addition, the individual strands of the ABS*plus* that the 3D printer lays down appear to be cracking. This could be from water or other gases escaping from the material. This cracking could be the cause of the spacing increases and the warping of the material.

Next the conductive paint was examined under microscope. This is especially important for understanding why the 4-point probe wasn't working with the vacuum-exposed paints. Figure 5-11 and Figure 5-12 show the conductive paint that was not exposed to vacuum conditions under microscope.

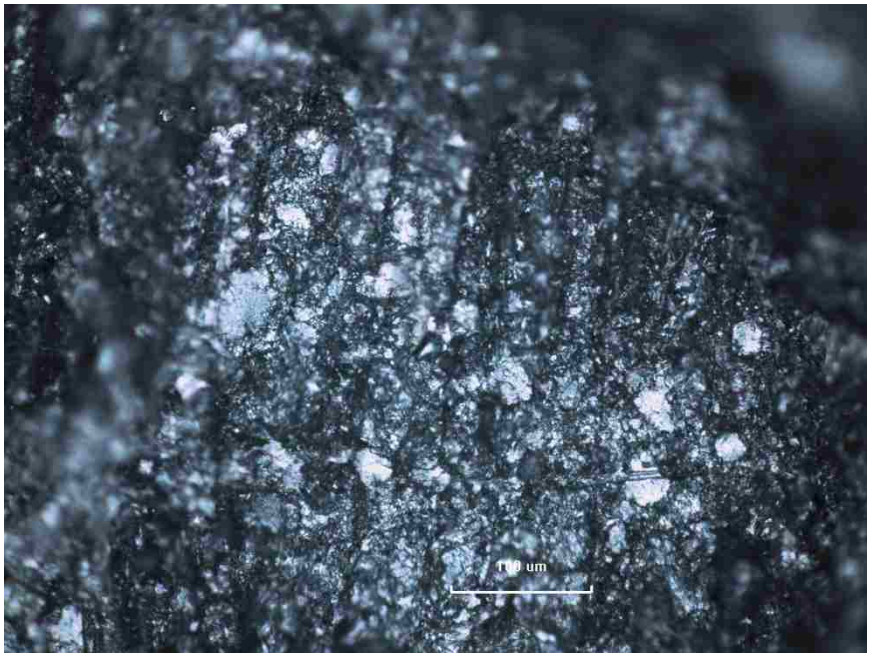

Figure 5-11: Conductive Paint Under Microscope

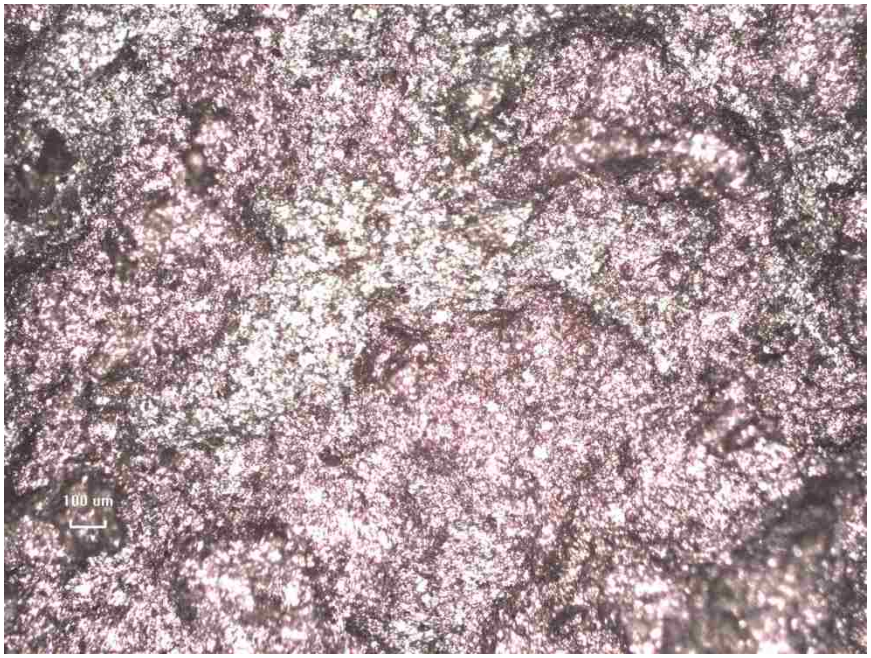

Figure 5-12: Conductive Paint Under Microscope

In these two samples it is worth noting that the surface is not perfectly smooth. Shadows and highlights can be seen from the peaks and valleys of the paint. This is expected since the paint was applied by hand and not by machine, so it would be impossible to achieve a perfectly smooth layer of paint. However, the surface is relatively even giving a smooth enough surface for the 4-point probe to have contact. Next, the vacuum exposed samples of MG Silver Print were examined under microscope. Upon initially looking through the microscope, it was very difficult to get the image in focus. One section would be in focus, while another would not be, this is characteristic of a surface that is not level. It was then discovered that there were indentations on the surface of the paint [Figure 5-13].

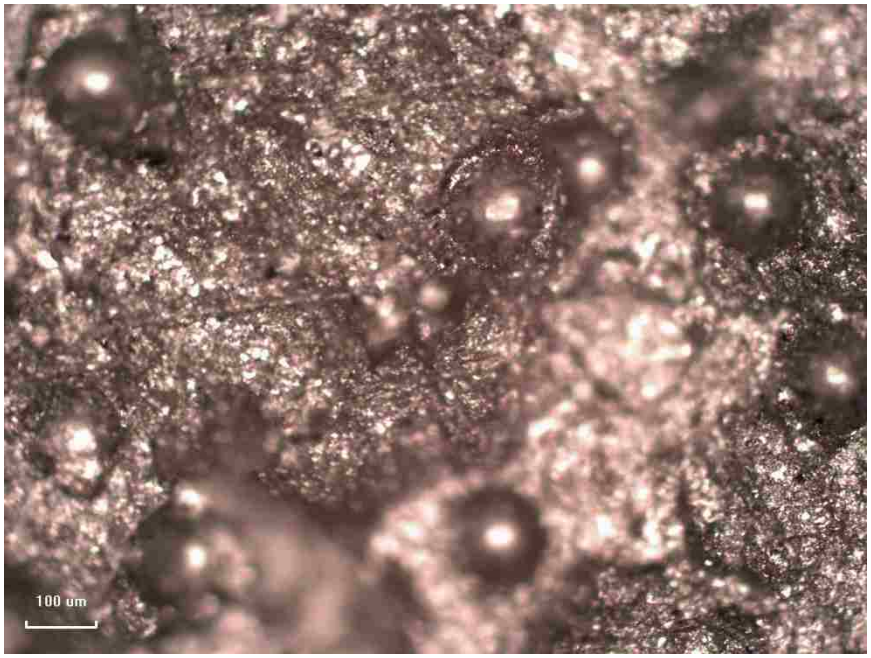

Figure 5-13: Vacuum Exposed Conductive Paint Under Microscope (Antenna 2A, 10x Magnification)

These indentations are likely caused by trapped gases that escaped through the painted surface. However, the actual source of the indentations is unknown. Other vacuum exposed painted samples [Figure 5-14] [Figure 5-15] [Figure 5-16] were looked at under microscope. They were mostly found to also include the strange indentations.

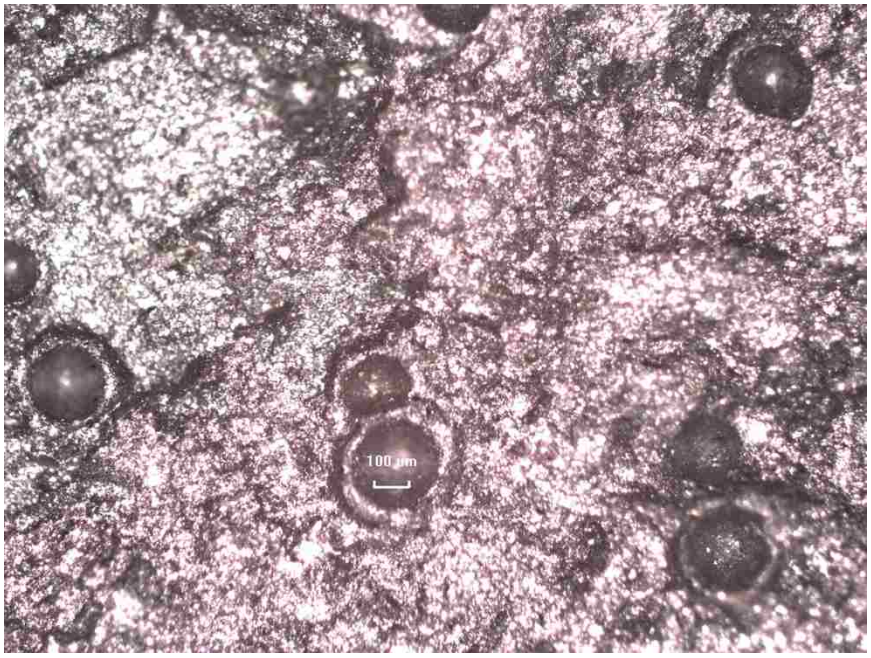

Figure 5-14: Vacuum Exposed Conductive Paint Under Microscope (Antenna 1C, 5x Magnification)

Figure 5-14 is only magnified 5 times, showing that the indentations occur throughout the painted sample. With the frequency of the indents, it makes sense that the 4-point probe would have trouble having a stable connection regardless of location on the sample.

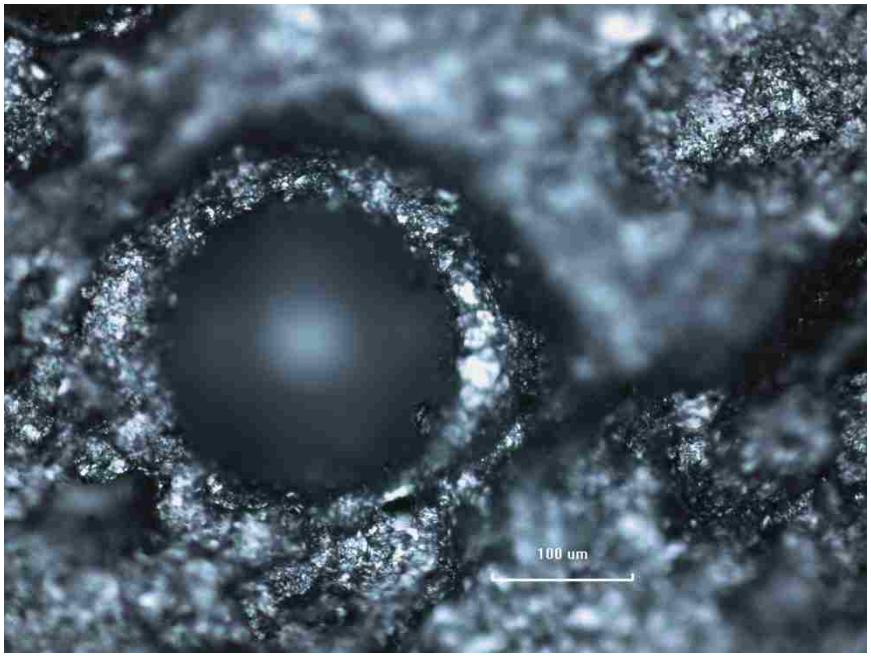

Figure 5-15: Vacuum Exposed Conductive Paint Under Microscope (Antenna 1C, 20x Magnification)

Some of the vacuum exposed painted samples did not have the indentations. However even without the craters, the surface was no longer smooth. Figure 5-16 shows that the surface of antenna 2E did not have any craters, but was very even. This degree of roughness would prevent the 4-point probe from having a secure contact on the material.

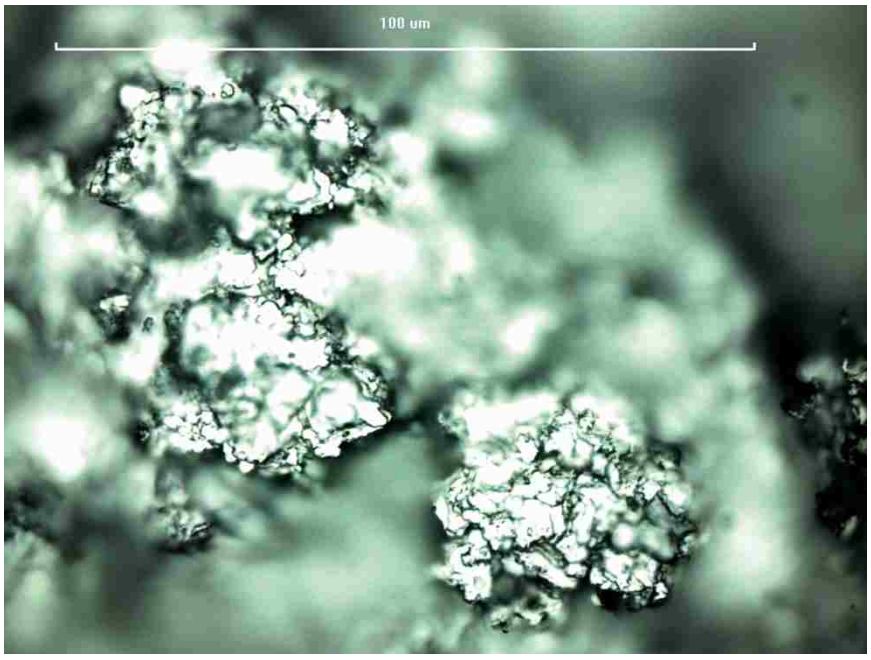

Figure 5-16: Vacuum exposed conductive paint under microscope (antenna 2E, 20x magnification)

5.8 Radiation Testing

The radiation testing reported in this thesis was done in conjunction with another project by Derek Doyle [34]. As such, the ABS used for this portion of the project was not printed with the FDM method utilized by uPrint SE. The ABS used in this portion was instead printed using SLA technology on an iPro 8000 printer. It's important to note that SLA does not utilize strands of ABS, but rather cures powder into a solid sheet of ABS. The printed ABS samples were exposed to radiation from a Sr-90 Beta source. Strontium is a metal that is non-radioactive when naturally occurring. However, there are

12 other isotopes that are radioactive, including Sr-90 [33]. Sr-90 is a by-product of the fission of uranium and plutonium in nuclear reactors, large amounts were produced in the 1950's and 1960's during atmospheric nuclear weapon tests. Sr-90 emits a beta particle, with no gamma radiation.

For higher electron energies ($1x10^6$ eV), the Sr-90 differential flux closely follows those found in geosynchronous equatorial orbit (GEO). This of course is dependent upon the chemical composition of the material undergoing radiation.

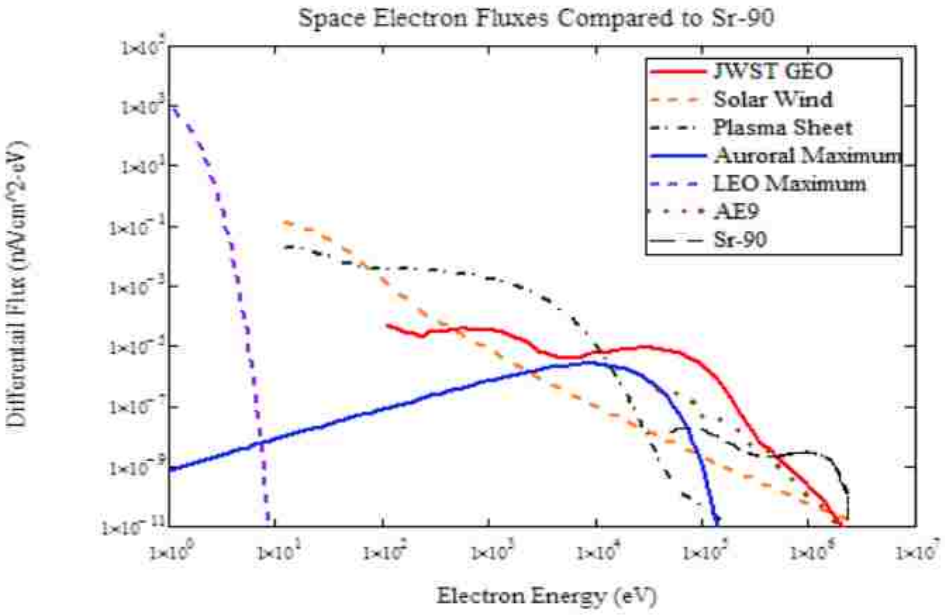

Figure 5-17: Space Electron Fluxes Compared to Sr-90

As can be seen in Figure 5-17, the lower energy spectrum of GEO has much higher flux levels than those of Sr-90. The ABS samples underwent Sr-90 radiation for 2, 3, and 5 day periods. So this would be similar to exposing the ABS samples to 2, 3 and 5 days in GEO orbit, ignoring the lower energy spectrum.

5.9 Radiation Testing Effects – Material

For this project, the SLA printed ABS samples were examined under microscope next to those samples that were radiated with Sr-90.

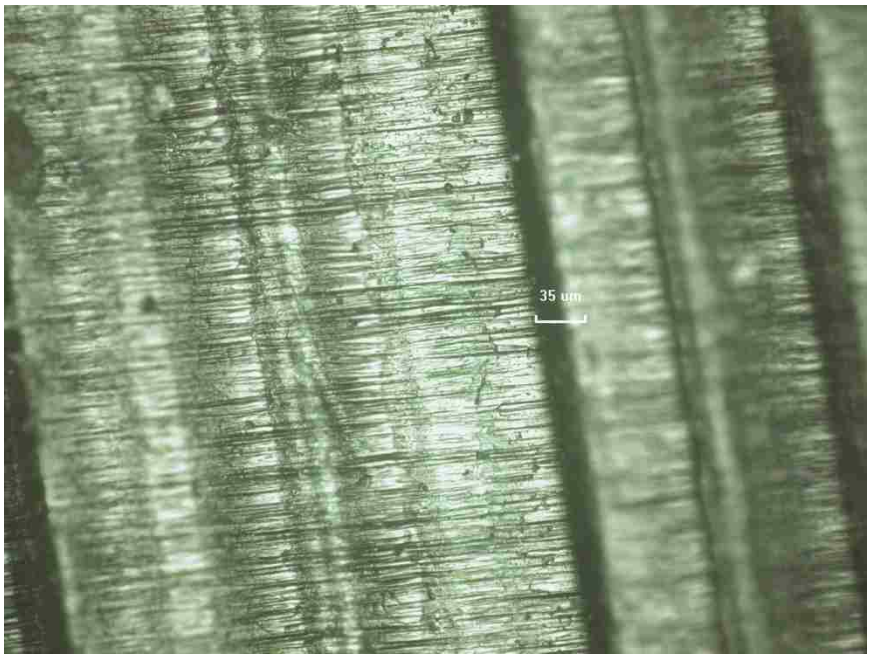

Figure 5-18: SLA Printed ABS Under Microscope

Figure 5-18 shows a SLA 3D printed ABS sample under microscope. There are notable air gaps (less 35 μm wide) in the sample. These fissures are a machining error, having to do with the machine moving during print time. The small horizontal lines are associated with the laser used and typically occur where the material is merged together with the laser.

Figure 5-19: Sr-90 Radiated (2 Days) ABS Under Microscope

Figure 5-20: Sr-90 Radiated (3 Days) ABS Under Microscope

Figure 5-19 and Figure 5-20 show the Sr-90 radiated (2 and 3 days, respectively) ABS under microscope. It can immediately be noted that the vertical fissures seen in the Figure 5-18 have largely increased with radiation. After 3 days of radiation, the fissures

were as wide as 35 μm. This means that the entire print is increasing in size, as these air gaps are growing larger. The horizontal lines created from the laser, appear to be unchanged by the radiation.

Next the ABS samples were looked at from a profile view, that is the sample was cut in half and placed on its side. First the plain ABS sample was looked at under microscope, as seen in Figure 5-21.

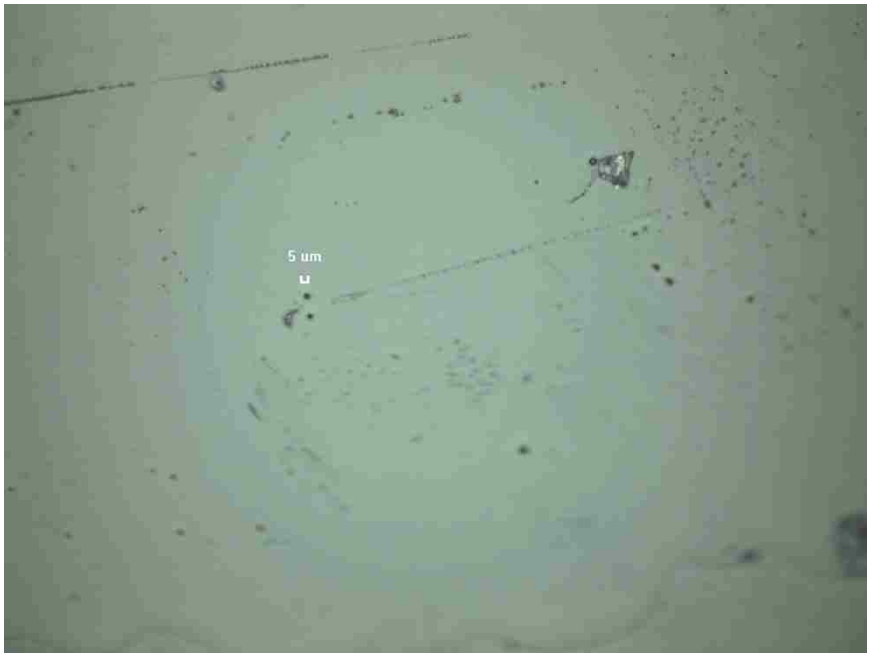

Figure 5-21: ABS Under Microscope (Profile View)

The sample has imperfections throughout. These imperfections are just the result of the printing process and is essentially one of the fissures seen in Figure 5-18. It can be seen that the medium sized imperfections are about 5 μm in diameter. There are a few larger imperfections and several smaller ones. The majority of the imperfections are smaller than 5 μm in diameter. Next the radiated (5 days under Sr-90) sample was examined. This can be seen in Figure 5-22.

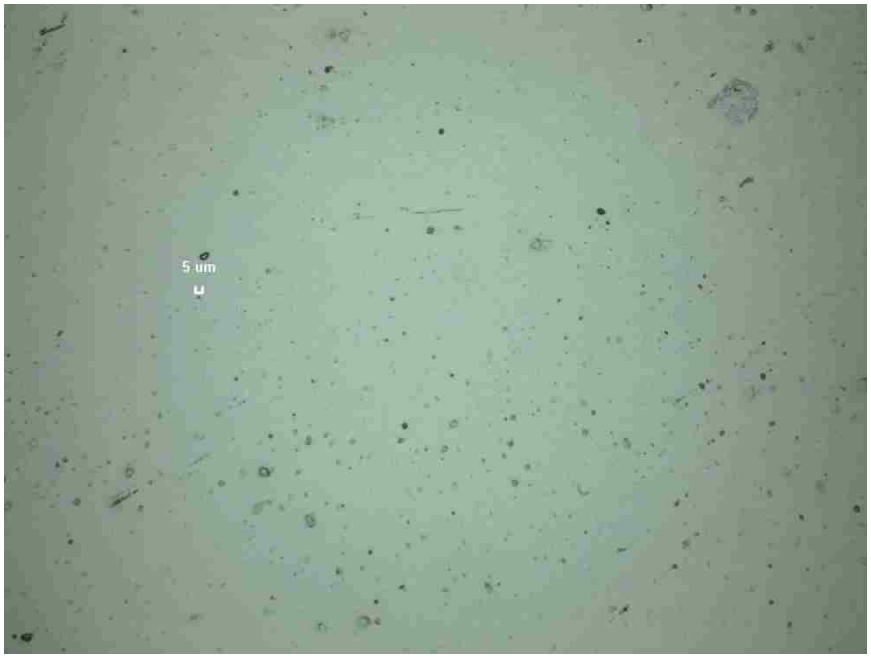

Figure 5-22: Sr-90 Radiated (5 Days) ABS Under Microscope (Profile View)

Immediately it is noticed that there is an increase in the size of the imperfections on this sample, just as the fissures increased in size in Figure 5-19 and Figure 5-20. Most of the imperfections are about 5 μm in diameter, whereas most of them were much smaller in the normal sample. Likewise there appears to be more imperfections on the radiated sample than the normal sample. It is likely that smaller imperfections that were not seen in the control sample were enlarged by the radiation and made visible.

The radiation testing suggests that the ABS material is not suited for GEO radiation, as these tests were only over the course of 5 days. It is likely that if given more time under radiation, the materials would suffer even greater degradation. Similarly, it is unclear how the ABS would perform under radiation in a vacuum environment.

Chapter 6: Conclusions and Future Research

6.1 Conclusions

In this project it was successfully shown that antennas could be 3D printed out of ABS*plus*. These antennas were also functional using conductive paint and copper tape for the metallic portions of the antennas. A parameter sweep EM simulation was run in CST with the physical measurements outputted by the printer. The results were surprising, indicating that not all antenna designs are suitable for 3D printing, of course dependent upon the printer. The 25 GHz patch antenna experienced a resonant frequency shift of 1.5 GHz due to the accuracy of the printer, as such, this design is not suitable for manufacturing with the printer used for this project. Next a 5 GHz antenna was designed and printed; this antenna was more able to handle small dimensional changes caused by the printer.

The antennas were placed under a Sr-90 source and in a vacuum chamber in order to simulate space conditions in GEO. It is inconclusive whether or not ABS*plus* is suitable for space applications. The resonant frequency of the antennas shifted in the vacuum by less than 0.1 GHz. In addition, the material did show extensive surface damage from both the vacuum and the Sr-90. It is likely that the damage would continue to worsen the longer the material was exposed to radiation and vacuum environments. However, there are several more tests that can be run on the material to better understand how the plastic and the antenna will perform in the harsh space environment.

6.2 Future Research

There is much room left for research of 3D printing antennas. There were several lessons learned regarding 3D printing antennas. If antennas are to be printed on any 3D

printer available on the market, it is critical to check printer accuracy, reliability and repeatability. This will greatly determine the type and frequency of antennas that can be printed on a set-up. As shown in Chapter 3, the 25 GHz design was not a viable antenna for creating with the set-up available for this project. After printing several copies of the design, it was shown that the change in parameters due to printer accuracy could change the resonant frequency by up to 1.5 GHz, a dramatic shift for any antenna, but particularly for this narrowband patch design. It is important to test this with every design used by a printer, because the accuracy and tolerances of a printer change depending on the geometry of the design. The change in physical dimensions due to printer accuracy might matter less for a less geometry-sensitive design, such as a horn antenna. However it is important to consider that the printer might experience more of an error in regards to dimensions with geometry like a horn. This is a risk inherent to printing antennas, and as such 3D printing may not be a viable solution for all antenna designs.

It would be very interesting to continue characterizing *ABSplus* for more frequency bands. In the characterization portion of the project, the permittivity and losses could only be calculated for the frequency bands that the lab had waveguide calibration kits available for. The results of the E-band measurements were not the best. Worse yet, there was 20 GHz before the E-band began where the permittivity of ABS*plus* is unknown. A complete characterization of ABS*plus* for microwave frequencies would allow for further antenna design.

There are several future projects that could be completed by repeating the vacuum and radiation testing. For example, it would be advantageous in the future to run the vacuum and radiation testing for several different sets of samples at different times. That

way all of the parameters of interest (permittivity, physical changes, radiation pattern and resonant frequency) could be tested against time out of vacuum. In addition, there are several different radiation tests that can be run on materials, running some of these other tests would help determine whether or not ABS would be a material suitable for space.

Perhaps the biggest limitation in this research was that the uPrint SE printer only printed in ABS*plus*. It would be worth repeating this project for several different 3D printed materials. There are many different types of 3D printed materials, and it would interesting to see which type has the most potential for 3D printed antennas, and which has the most potential for space applications. In particular, there are resin printers with very high accuracy, which may be better suited for a microstrip antenna project than the uPrint SE. Access to a printer that has dual heads for printing conductive ink would also be very useful, or at least a SmartPump as used in [7] to inject the conductive ink. Applying the conductive ink by hand was determined to be ineffective, especially concerning small details.

Appendix A: MATLAB Code

A.1: Parameter Extraction Code

In order to use this code, the S2P file from the PNA must be converted to a Microsoft Excel file type. With this file type, the header is deleted, leaving row 1 as the first row of data. In addition, this code makes use of the S2P files saved in real/imaginary format. The code can be edited to the suit magnitude/phase format, if that is desired.

```
% Katherine Belvin
% ktbelvin@gmail.com
clc
clear all
close all
%% User input
filename = './file.xls'; %location of .xls file
d = 0.0005; % thickness of sample in m;
%a = 0.007112; % Ka-band waveguide broad measurement, m
a = 0.0030988;% E-band waveguide broad measurement, m
%% Import Data
data = xlsread(filename, 1);
f = (data(:,1))/(1e9); % convert frequency to GHz
S11_Real = data(:,2);
S11_Imag = data(:,3);
S21_Real = data(:,4);
S21_Imag = data(:,5);
S11 = S11_Real + (i*S11_Imag);
S21 = S21_Real + (i*S21_Imag);

%% Constants
c = 3*10^8; % speed of light m/s
lambda_0 = c./(1e9*f); %free space wavelength, m
k_0 = 2*pi./lambda_0; % wave number, free space
k_c = pi./a ; % wave number, cut off
lambda_c = 2*pi./k_c;
gamma_0 = (k_c - k_0).^(1/2);

%% Calculations

Chi = (S11.^2 - S21.^2 + 1)./(2*S11);
Gamma_1 = Chi+((Chi.^2)-1).^(1/2);
Gamma_2 = Chi-((Chi.^2)-1).^(1/2);
n = max(size(Gamma_1));
for p = 1:n
%for p = 1
   if abs(Gamma_1(p))<1 && abs(Gamma_2(p))>1
      Gamma(p)=Gamma_1(p);
```

```
    end
    if abs(Gamma_1(p))>1 && abs(Gamma_2(p))<1
        Gamma(p)=Gamma_2(p);
    end
    if abs(Gamma_1(p))<=1 && abs(Gamma_2(p))<=1
        if abs(Gamma_1(p))>abs(Gamma_2(p))
            Gamma(p) = Gamma_1(p);
        end
        if abs(Gamma_2(p))>abs(Gamma_1(p))
            Gamma(p) = Gamma_2(p);
        end
    end
end
Gamma = Gamma';
P = (S11 + S21 - Gamma)./(1 - (S11 + S21).*Gamma); % Propagation Factor
loglog=log(1./P);
Lambda_inv_2=-1*((1/(2*pi*d)).*loglog).^2;
Lambda_inv_a = sqrt(Lambda_inv_2);
Lambda_inv_b = -1*sqrt(Lambda_inv_2);
for p=1:n %condition re(1/lambda) >=0
    if real(Lambda_inv_a(p))>=0 && real(Lambda_inv_b(p))<0
        Lambda_inv(p) = Lambda_inv_a(p);
    end
    if real(Lambda_inv_a(p))<0 && real(Lambda_inv_b)>=0
        Lambda_inv(p) = Lambda_inv_b(p);
    end
    if real(Lambda_inv_a(p))>=0 && real(Lambda_inv_b(p))>=0
        if real(Lambda_inv_a(p))>real(Lambda_inv_b(p))
            Lambda_inv(p) = Lambda_inv_a(p);
        end
        if real(Lambda_inv_a(p))<real(Lambda_inv_b(p))
            Lambda_inv(p) = Lambda_inv_b(p);
        end
    end
end
Lambda_inv = Lambda_inv.';
mu_r = ((1+Gamma)./(1-Gamma)).*Lambda_inv.*2*pi./sqrt(k_0.^2-k_c.^2);
epsilon_r = (Lambda_inv_2+(k_c.^2/(4*pi.^2))).*(lambda_0.^2./mu_r);
%% Calculate loss

loss = (-1*imag(epsilon_r))./real(epsilon_r);
%% Plot comparison

figure (1)
plot (f, real(epsilon_r),'g')
hold on
plot (f, real(epsilon_r_non),'--k')
figure(3)
plot(f,loss,'b')
```

Appendix B: Waveguide Test Set-Up

B.1: PNA Settings

In order to have accurate measurements it is critical to have the PNA set-up with IF bandwidth, number of points and smoothing techniques that are optimum for the measurement. For the Ka-Band measurements, 801 sample points (about 59 points per GHz) were taken and for the E-band measurements, 1601 sample points (about 53 points per GHz) were taken.

The IF bandwidth was chosen such that the data on the screen would be refreshed about every 10 seconds, this worked out to be about 10 kHz. The smaller the bandwidth, the slower the data would be taken, but the more accurate the results would be. 10 kHz was chosen for the majority of the measurements, however, small spikes were noticed in the data. In order to determine weather the spikes were inherent to the material or just a result of the measurement set-up, the measurements were retaken with the IF bandwidth set to 10 Hz. These measurements went very slow, taking about 15 minutes each, as the averaging factor was set to 4 (turned on in case any small movement in the set-up occurred, since this sweep is so slow). The measurements taken with the slow sweep were used to determine which spikes could be replaced with linear approximations and which were inherent to the material and must remain.

Having the IF bandwidth set to 10 Hz is more accurate but also has its drawbacks, mostly related to the time required to take the measurement. For example, the temperature may not remain totally constant within the waveguide extenders for 10 minutes, as they only have 2 small cooling fans. As such, the “fast” measurements were used primarily, with the “slow” measurements being used only for spike elimination.

B.2: Calibration

A proper calibration is essential for accurate S-parameter measurements. For this experiment, a variation of a thru, reflect, line (TRL) calibration method was used. A TRL calibration was selected because it is extremely accurate. TRL is a set of calibration techniques that determine 2-port error coefficients with two transmission standards and one reflection standard. So thru, reflect, match (TRM), line, reflect, line (LRL), and line, reflect, match (LRM) are all considered TRL calibrations [35]. A TRM calibration was used for this experiment, with the following settings:

1. When prompted to select a calibration standard, "reflect" was chosen.
2. For the reflect measurement, the precise short was attached to both waveguide ports.
3. An "isolation" measurement is optional, and was carried out in the calibration. For this measurement the precise load was attached to both waveguide ports.
4. For the line/match standards, both a line and a match measurement were taken. For the line measurement, the quarter-wave offset was placed in-between the two waveguide ports, creating a line of a quarter-wave length. For the match measurement, the precise load was attached to the waveguide port 1.
5. The thru measurement was taken with the two waveguide ports connected directly to each other (no quarter-wave offset).

The calibration should then be check for accuracy. With the waveguides still attached, as in the thru measurement, check that both the phase and magnitude of the S21 measurement are zero. In addition, in a good calibration, the S21 and the S12

measurements should be interchangeable. Next, the calibration can be checked further by attaching the precise shorts (or loads) to both ports and formatting the data as a smith chart and checking to see that the measurement looks like either a short or a load. In addition there are further methods of checking calibration in the Keysight waveguide calibration manual.

Works Cited

[1] Wong, Kaufui V., and Aldo Hernandez. "A Review of Additive Manufacturing." *ISRN Mechanical Engineering* 2012 (2012): 1-10.

[2] "3D Printing Materials: Plastic, Metal, Ceramics and More - Shapeways." *Shapeways.com*. N.p., n.d. Web. <http://www.shapeways.com/materials>.

[3] "Metal 3D Printers LENS Systems - Additive Manufacturing." *Optomec Additive Manufacturing*. N.p., n.d. Web. <http://www.optomec.com/3d-printed-metals/lens-printers/>.

[4] Stratasys. *UPrint SE*. N.p.: Stratasys, 2013. PDF.

[5] Hiemenz, Joe, Stratasys Inc. "3D Printing with FDM." (2014)

[6] 3DSystems, *SLA Production Series, Production 3D Printers*, 2013. PDF.

[7] Deffenbaugh, Paul. "3D Printed Electromagnetic Transmission And Electronic Structures Fabricated On A Single Platform Using Advanced Process Integration Techniques." (2014)

[8] Tsang, H.h., J.h. Barton, R.c. Rumpf, and C.r. Garcia. "Effects of Extreme Surface Roughness on 3D Printed Horn Antenna." Electronics Letters 49.12 (2013): 734-36.

[9] "Electronic Prototyping." *Rabbit Proto*. N.p., n.d. Web. <http://www.rabbitproto.com/>.

[10] "3D Printer Hardware." *Voxel8: 3D Electronics Printing*. N.p., n.d. Web. <http://www.voxel8.co/printer/>.

[11] *ABSplus-P430*. N.p.: Stratasys Inc., 2014. PDF.

[12] Nicolson, A. M., and G. F. Ross. "Measurement of the Intrinsic Properties of Materials by Time-Domain Techniques." *IEEE Transactions on Instrumentation and Measurement* 19.4 (1970): 377-82.

[13] Weir, W.B. "Automatic Measurement of Complex Dielectric Constant and Permeability at Microwave Frequencies." Proceedings of the IEEE 62.1 (1974): 33-36.

[14] Crowgey, Benjamin Reid. "Rectangular Waveguide Material Characterization: Anisotropic Property Extraction and Measurement Validation." Diss. Michigan State U, 2013.

[15] *Application Note: Measurement of Dielectric Material Properties*. N.p.: Rohde & Schwarz, 2014. PDF.

[16] Pfeiffer, Florian, and Erwin M. Biebl. *Determination of Complex Permittivity Using a Scalar Quasi-optical Measurement System in the E-band*. Technische Universitat Munchen, Fachgebiet Hochstfrequenztechnik

[17] Rogers Corporation "RO3003® Series Circuit Materials, RO3003, RO3006, RO3010, and RO3035 High Frequency Laminates Data Sheet" (2014)

[18] Rogers Corporation "RT/duroid ® 5870/5880 High Frequency Laminates Data Sheet" (2014).

[19] Rogers Corporation "TMM® Thermoset Microwave Materials Data Sheet" (2014)

[20] *User's Manual HP 85070B Dielectric Probe Kit*. Santa Rosa CA: Hewlett-Packard Company, 1993. PDF.

[21] Zwick, T., A. Chandrasekhar, C.w. Baks, U.r. Pfeiffer, S. Brebels, and B.p. Gaucher. "Determination of the Complex Permittivity of Packaging Materials at Millimeter-wave Frequencies." *IEEE Transactions on Microwave Theory and Techniques* 54.3 (2006): 1001-010.

[22] Balanis, Constantine A. Antenna Theory: Analysis and Design. 3rd ed. Hoboken, NJ: Wiley Interscience, 2005. Print.

[23] Antenna Magus. Computer software. Vers. 2014. N.p., n.d. Web.

[24] MG Chemicals. *Silver Print*. N.p.: MG Chemicals, n.d. Print.

[25] Ning, Y., and Jiang, W.: 'The electromagnetic characteristics of conducting rough surfaces at millimeter wave frequencies'. IEEE Int. Conf. Microwave and Millimeter Wave Technology, 2008 (ICMMT 2008), Nanjing, China, April 2008

[26] Rogers Corporation. "Thick Metal Copper Cladding on High Frequency Laminates". PDF.

[27] *Application Note Series: Measuring the Resistivity and Determining the Conductivity Type of Semiconductor Materials Using a Four-Point Collinear Probe and the Model 6221 DC and AC Current Source*. N.p.: Keithley, 2005. PDF.

[28] MG Chemicals. *Silver Conductive Epoxy Adhesive, Moderate Cure/High Conductivity*. N.p.: MG Chemicals, n.d. Print.

[29] Lehr, S. N., and V. J. Tronolone. "The Space Environment and Its Effects on Materials and Component Parts." *IRE Transactions on Reliability and Quality Control* RQC-10.2 (1961): 24-37.

[30] Fisher, Aaron and Mermelstein, Benjamin, "A Compilation of Low Outgassing Polymeric Materials Normally Recommended for GSFC Cognizant Spacecraft," NASA TM X-65705, July 1971.

[31] "Outgassing Data for Selecting Spacecraft Materials System." *NASA*. N.p., n.d. Web. <http://outgassing.nasa.gov/>.

[32] "Plastics in Vacuum Applications." Meyer Tool & Mfg. Inc. N.p., 27 Aug. 2010. Web.

[33] "Strontium." *EPA*. Environmental Protection Agency, n.d. Web. <http://www.epa.gov/radiation/radionuclides/strontium.html>.

[34] Doyle, Derek, Tatiana Starr, and Christos Christodoulou. "Dielectric Characterization of 3D Printed Materials with a Confocal Fabry Perot Resonator for Space Utilization." *IEEE* (2014): 223-24.

[35] "TRL Calibration." *Keysight*. N.p., n.d. Web. <http://na.support.keysight.com/pna/help/WebHelp9_9/S3_Cals/TRL_Calibration.htm>.